CHAPTER 1

INTRODUCTION

Alkaline volcanic associations (whose salic members may be either oversaturated or undersaturated) are common and occasionally volumetrically important components of the continents and oceanic islands. These associations are perhaps best developed in continental regions such as east Africa which are characterized by extensional or rift tectonics.

Volcanic activity, resulting in accumulation of significant volumes of eruptives has occurred in eastern Australia since the Late Cretaceous. Individual provinces may be divided into two distinct type of volcanic associations (Wellman and McDougall, 1974a), namely lava field and central volcano provinces. The former are almost exclusively composed of 'basaltic' fissure-type eruptives, whereas the central volcano provinces are generally characterized by an abundance of basic volcanics associated with subordinate volumes of felsic types, most of which were extruded through central vents.

The Nandewar Volcano (Abbott, 1969) located approximately 35 km east of Narrabri in north-eastern New South Wales (Fig. 1.1), is one manifestation of the eastern Australian Tertiary volcanism and it can be broadly categorized as a central volcano province. Abbott (1969) showed that the Nandewar lavas include both sodic and moderately potassic types ranging from *hy*-normative transitional hawaiites and trachyandesites to mildly peralkaline trachytes and rhyolites.

The compositional variation evident in the Nandewar Volcano and many other central-type volcanic complexes is most commonly attributed to fractional crystallization of parental 'basaltic' magmas (e.g. Bowen, 1928; Abbott, 1969; Barberi *et al.*, 1975). However, the predominance of (voluminous) felsic eruptives in some alkaline provinces (e.g. Williams, 1972; Lippard, 1973) has led to alternative proposals based on partial melting of lower crustal or upper mantle source rocks (e.g. Bailey, 1964,1970,1974; Wright, 1969; Macdonald *et al.*, 1970). Accordingly, the efficacy of the fractional crystallization model as

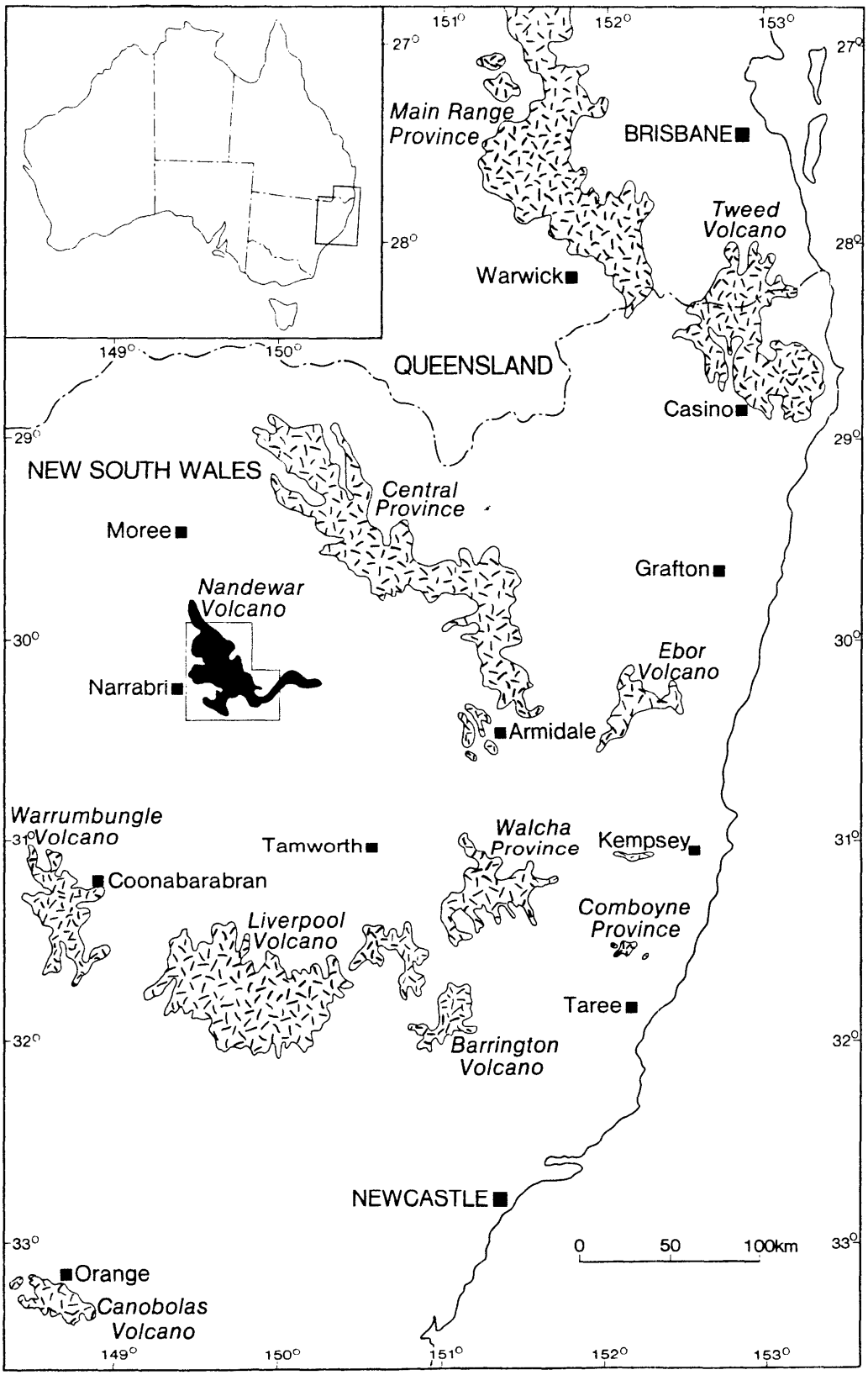

Fig. 1.1: Location of the Nandewar Volcano in relation to the other major Cainozoic volcanic provinces in eastern New South Wales and south-eastern Queensland.

the major genetic control should be carefully reexamined and reassessed for specific provinces with a view to establishing the internal consistencies of the model.

AIMS

The prime aim of this thesis is to evaluate, in some detail, the genesis of the more evolved members of the Nandewar series in the light of newly acquired field, petrographic, mineralogical and chemical data. The Nandewar Volcano was selected for this study because it has been widely quoted in the literature, following the work of Abbott (1969), as a classic example of a fractionation series which derived from a moderately potassic transitional basaltic parent.

CHAPTER 2

FIELD RELATIONS

The products of the Nandewar Volcano crop out in an elongate belt about 50 km long and up to 30 km wide covering an area of approximately 800 sq.km. The present-day maximum thickness of the volcanics is estimated to be approximately 800 metres based on a section from Bullawa Creek towards Mt Kaputar (Fig. 2.1). However, the original thickness of volcanics must have been considerably more than this since the intrusive plug-like body outcropping at the Mt Kaputar lookout is presently one of the highest points in the complex. The spatial relations of the various rock types mapped during this study are presented on the accompanying map.

EXTRUSIVE HISTORY

The oldest volcanic rocks in the complex, dated at 20.5 Ma (Stipp and McDougall, 1968), include a mafic trachyte flow overlying a teschenite sill, 2 km north of Kilarney Gap. This flow forms a prominent bluff and is capped by trachyandesite and intruded by a small comendite plug, indicating that it is older than the latter two rock types. The mafic trachyte flow is not found in contact with alkali rhyolites which are also considered to have been erupted before the main shield-forming volcanism, and hence their relative age relationships are unknown.

The mildly porphyritic and sometimes vesicular rhyolites occurring as domes and flows appear to have been extruded along a NNW-SSE fracture, possibly an extension of the Hunter-Mooki thrust which strikes from the south-east towards the Volcano. They were extruded on to an irregular basement of Palaeozoic sedimentary and volcanic rocks on the eastern side, and Mesozoic sedimentary rocks[1] on the western side of the complex. At present the rhyolites are up to 600 metres thick in the region to the west of Mt Lindesay and occupy much of the central region of the Volcano, having been exposed by erosion of the main shield-forming lavas.

Abbott (1965) argued that many of the rhyolitic domes in the central region were endogenous, and had intruded the main shield-forming

[1] The Triassic sedimentary rocks are intruded by teschenite sills (see geological map) upon which part of the volcano rests unconformably.

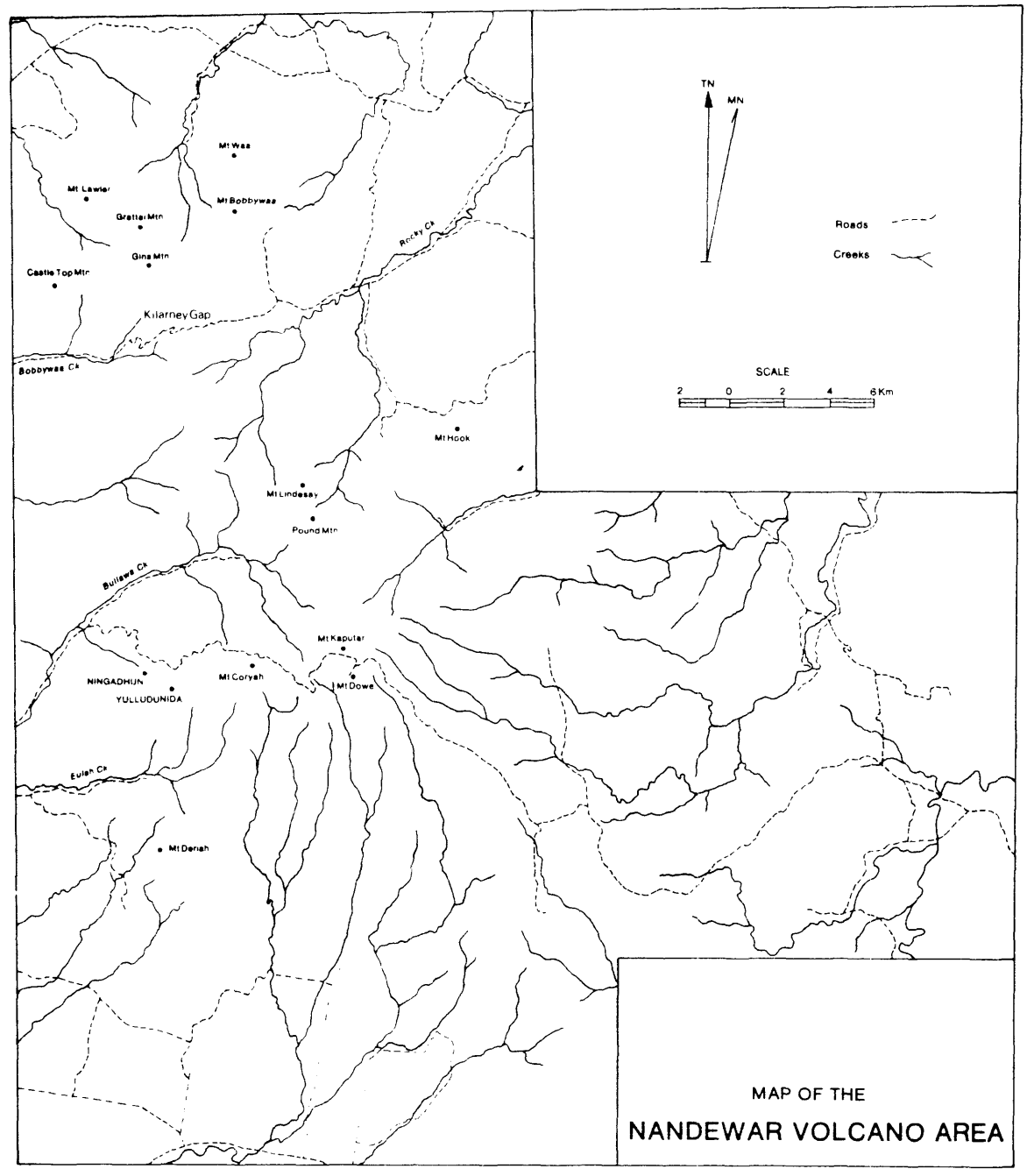

Fig. 2.1: Map of the study area showing the principal localities referred to in the text.

lavas. However, a number of these rhyolites are vesicular and have associated breccias which suggests that they were extruded, possibly as large exogenous domes during the early stages of volcanism. Furthermore, the absence of xenoliths of shield-forming lavas in the rhyolites and lack of evidence of buckling and deformation in the Mesozoic sandstones adjacent to the domes, does not support a model of forceful rhyolite emplacement. Several of the rhyolitic domes in the region between Kilarney Gap and Mt Kaputar (see Fig. 2.1) display a concentric banding, whereas others exhibit a strong NNW-SSE lineation. These features are best observed on aerial photographs and are interpreted as the result of viscous flow of magma through restricted conduits and fissures respectively.

Eruption of the main shield-forming lavas, which range in composition from hawaiite, trachyandesite and tristanite to trachyte and comendites, appears to have been the result of activity largely emanating from a central vent. The location of this vent is considered to be in the vicinity of Mt Lindesay (see Fig. 2.1) because traceable flow boundaries and pyroclastic horizons dip radially away from this general area at about 5 to 10 degrees. The occurrence in the region surrounding Mt Lindesay, of a small high-level monzonitic intrusion and abundant small dykes ranging in composition from trachyandesite to rhyolite, indicates the concentration of intrusive magmatic activity in this area and supports the notion that this is close to the feeder zone for the extrusive rock types.

Extrusion of the main shield-forming lavas occurred over the restricted interval 18.0 to 17.2 Ma (Stipp and McDougall, 1968; Wellman *et al.*, 1969; Wellman and McDougall, 1974b). The earliest of these were hawaiites, followed by trachyandesites, tristanites, trachytes, comendites, then more tristanites and trachytes. The flows vary in thickness from about 2 to 20 metres, the mafic variants commonly occurring in relatively thin flows (2 to 10 metres), whereas the trachytic flow units are typically the thickest (10 to 20 metres). Several of the more massive flow units display considerable lateral persistence and crop out continuously for 6 to 8 km as prominent bluffs in youthful valleys on the southern flank of the Volcano.

In the 500 metres of volcanics exposed from the base to the top

of Mt Grattai in the northern sector, flows of hawaiite, trachyandesite and tristanite are most common, whereas trachytes are relatively scarce compared to the southern sector. Because of the advanced stage of erosion in the intervening area, correlation of individual flows between the northern and southern sectors of the Volcano is not possible.

Relatively abundant pyroclastic rocks have been found intercalated with flows in the southern part of the Volcano. Tuffaceous rocks associated with the hawaiites, trachyandesites and tristanites are usually extensively weathered and typically composed of highly vesicular, lapilli-sized fragments of nearby lava types, crystal debris and ash. On the other hand, the pyroclastics associated with the trachytes are characteristically agglomeratic. They are composed of ejected blocks up to 1 metre in diameter which range in composition from trachyandesite to alkali rhyolite, set in a matrix of smaller clasts, lapilli-sized fragments and ash. These pyroclastic deposits indicate the occurrence of violent eruptive episodes in the development of the Volcano and this is contrary to the relatively passive eruptive history envisaged by Abbott (1965,1969).

Following, and possibly even during the waning stages of eruption of the main shield-forming lavas, alkaline and peralkaline trachyte dykes, ring-dykes and plugs intruded the volcanic pile and surrounding basement rocks. Ages of 17.4 Ma and 17.0 Ma (Stipp and McDougall, 1968) were determined on peralkaline trachytes which intrude basement rocks 10 km west and 12 km south-west of Mt Kaputar, respectively. Rocks of similar composition occurring as ring-dyke (Mt Yulladunida) and plug-like (Mt Kaputar) intrusives into the main shield-forming volcanics must be comparable in age or slightly younger and have clearly cooled and consolidated under very shallow cover. These trachytic intrusives are largely confined to the southern portion of the Volcano. This contrasts with the major occurrence of a younger group of alkali rhyolite and comendite extrusives and intrusives within the northern sector.

Evidence for the existence of two distinct episodes of rhyolitic magmatism is manifest in the occurrence of a comendite plug (18.1 Ma) intruding the older alkali rhyolites at a locality 5 km north-east of Kilarney Gap. This information together with another date of 17.2 Ma determined on an alkali rhyolite from the northern sector (Stipp and

McDougall, 1968) indicates emplacement of these magmas during the main shield-forming episode.

The comendites occur as high-level ring-dykes, dykes and plugs which have intruded both the volcanic pile and basement rocks. Alignment of several small comendite intrusions along a NNW-SSE trend in the eastern part of the complex suggests a strong structural control on their emplacement. The younger alkali rhyolites are typically vesicular and generally more leucocratic than the comendites which are rarely vesicular. The contact relations between the relatively erosion-resistant alkali rhyolites and adjacent rocks are often unclear but their commonly vesicular character suggests that, in general, they were probably extruded as exogenous domes.

VOLUME ESTIMATES

A knowledge of the relative volumes of the major rock types in volcanic provinces is obviously important in petrogenetic considerations. The approximate relative proportions of the main lava types within the Nandewar Volcano (for an estimated total volume of approximately 150 km^3 of extrusive products) are:

	Volume Percent
Hawaiite/trachyandesite/tristanite	70
Alkaline and peralkaline trachyte	3.6
Comendite/alkali rhyolite	2.4
Older alkali rhyolites	24

The virtual absence of volcanics with strictly basaltic compositions and the relatively large volume of the older alkali rhyolite extrusives are the most important aspects of these data.

CHAPTER 3

PETROGRAPHY

NOMENCLATURE

The nomenclature of the volcanic rocks in the compositional range basalt to trachyte is based on chemical and normative criteria, following Coombs and Wilkinson (1969). Their scheme was proposed for the classification of members of mildly undersaturated sodic and potassic series and their more strongly undersaturated equivalents. However, the scheme is also applicable to the transitional and oversaturated volcanic rocks comprising the Nandewar Volcano. The criteria used to distinguish the major rock types of the series are summarized in Table 3.1.

For the most evolved rocks the division between trachyte and rhyolite has been taken as 10 percent C.I.P.W. *qz*, following Macdonald and Bailey (1973). The qualifier peralkaline is applied to trachytes and rhyolites with molecular $(Na_2O + K_2O)/Al_2O_3 > 1$, whereas the mafic trachytes and alkali rhyolites have molecular $(Na_2O + K_2O)/Al_2O_3 \leq 1$. The distinction between comendites and pantellerites in the field of peralkaline rhyolites is based on the discriminant diagram of MacDonald and Bailey (1973), employing the percent of *qz* and femics in the C.I.P.W. norm.

PETROGRAPHY

Hawaiites and Trachyandesites

Applying the normative criteria of Coombs and Wilkinson (1969), none of the mafic volcanic rocks in the Nandewar Volcano can be strictly termed basalt or trachybasalt. Since all the mafic variants have $100\ an/ab+an < 50$ and exhibit a range of Na_2O/K_2O ratios (1.8 to 3.9), they are most appropriately classified as hawaiites and trachyandesites.

The hawaiites are generally non-vesicular porphyritic rocks with 5 to 20 percent variably zoned phenocrysts (up to 5x5 mm) of olivine (Fo_{85} core to Fo_{67} rim), plagioclase (An_{63} to An_{46}) and clinopyroxene ($Ca_{45}Mg_{46}Fe_9$ to $Ca_{45}Mg_{40}Fe_{15}$), set in a groundmass dominated by sub-

TABLE 3.1

Classification scheme for alkaline volcanic rocks

Parameter	Sodic Series ($Na_2O/K_2O > 2$)	Moderately Potassic Series ($Na_2O/K_2O < 2$)
$\geqslant 10$ *Q*	Alkaline or peralkaline rhyolite	Alkaline or peralkaline rhyolite
D.I. $\geqslant 75$		
100 *an*/*ab*+*an* < 10		
$0 \geqslant Q < 10$	Trachyte	Trachyte
$0 > ne < 10$	Feldspathoidal trachyte	Feldspathoidal trachyte
$ne \geqslant 10$	Phonolite	Phonolite
$75 >$ D.I. $\geqslant 65$		
$30 >$ 100 *an*/*ab*+*an* $\geqslant 10$		
$ne < 10$	Benmoreite	Tristanite
$ne \geqslant 10$	Feldspathoidal benmoreite	Feldspathoidal tristanite
D.I. < 65		
$30 >$ 100 *an*/*ab*+*an* $\geqslant 10$		
$ne < 10$	Mugearite	Trachyandesite
$ne \geqslant 10$	Feldspathoidal mugearite	Feldspathoidal trachyandesite
D.I. < 65		
$50 >$ 100 *an*/*ab*+*an* $\geqslant 30$		
* $ne = 0$	Transitional hawaiite	Transitional trachyandesite
$10 > ne > 0$	Hawaiite	Trachyandesite
$ne \geqslant 10$	Feldspathoidal hawaiite	Feldspathoidal trachyandesite
D.I. << 65		
100 *an*/*ab*+*an* $\geqslant 50$		
* $ne = 0$	Transitional basalt	Transitional trachybasalt
$5 > ne > 0$	Alkali olivine basalt	Trachybasalt
$ne \geqslant 5$	Basanite	Feldspathoidal trachybasalt

* Transitional *hy*-bearing basalts and hawaiites can be distinguished from their subalkaline equivalents using the discriminant function proposed by Chayes (1966). When $ne = 0$, mugearites and benmoreites will be *hy*-normative and on occasion benmoreites may be *qz*-normative.

parallel laths of plagioclase (An_{61} to An_{55}), with interstitial subhedral pale-brown to mauve clinopyroxene, and subhedral to euhedral titanomagnetite and ilmenite. Most specimens have abundant apatite needles in their groundmass, whereas olivine, interstitial sanidine, brown glass, pale-green chlorophaeite and carbonate are less common. In some specimens olivine is the most abundant phenocryst type, almost to the exclusion of other phases, whereas in others plagioclase may be dominant, with only subordinate clinopyroxene and olivine phenocrysts.

The trachyandesites are distinguished chemically from the hawaiites by their lower Na_2O/K_2O ratios (<2). Petrographically this is reflected by increases in the amounts of interstitial alkali feldspar, the main mineralogical feature distinguishing the trachyandesites from the hawaiites. The most mafic trachyandesites approach trachybasalt in normative plagioclase composition (100 *an/ab+an* = 49.2). They range from mildly to strongly porphyritic types which contain between 5 and 50 percent phenocrysts (up to 2x1 cm), dominantly plagioclase (An_{61} to An_{50}). Phenocrysts (up to 5x5 mm) of olivine (Fo_{88} to Fo_{58}), sometimes partially pseudomorphed by bowlingite, clinopyroxene ($Ca_{44}Mg_{44}Fe_{12}$) ± euhedral to subhedral microphenocrysts of titanomagnetite and ilmenite are set in a groundmass mineralogically similar to the hawaiites, except for more abundant interstitial alkali feldspar, noted above. Most phenocrysts exhibit evidence of marginal resorption and plagioclase phenocrysts have occasional inclusions of olivine and clinopyroxene. Olivine phenocrysts are usually devoid of inclusions, a rare exception being an inclusion aggregate of tiny prismatic crystals of aluminous clinopyroxene.

Clinopyroxene megacrysts ($Ca_{41}Mg_{47}Fe_{12}$) up to 1 cm are relatively common in several trachyandesite flows. They are typically colourless or pale-brown, devoid of exsolution lamellae, and generally surrounded by a thin low-pressure rim of pale-mauve clinopyroxene ($Ca_{46}Mg_{40}Fe_{14}$). Megacrysts of orthopyroxene ($Ca_3Mg_{77}Fe_{20}$ to $Ca_2Mg_{68}Fe_{30}$), characterized by extensive reaction rims composed of granular olivine and clinopyroxene, range from 1 to 5 mm in diameter and occur in the same hosts with clinopyroxene megacrysts. Rare glomeroporphyritic aggregates (up to 5 mm in diameter) of olivine + clinopyroxene, olivine + plagioclase + clinopyroxene and clinopyroxene + orthopyroxene found in some specimens are examples of small-scale cognate cumulates.

Inclusions in the trachyandesites are very rare; one of the few collected from specimen 49011 is a medium-grained aggregate of euhedral to subhedral titanaugite (1x1 mm), included in larger (3x3 mm) heterad plagioclase crystals which appear to have crystallized from an intercumulus liquid. Anhedral titanomagnetite occurs mainly as inclusions within the pyroxenes. Ultramafic inclusions of either Cr-diopside or Ti-augite type are absent from the Nandewar hawaiites and trachyandesites.

The more evolved trachyandesites (transitional to tristanites) are typically aphyric or contain sparse microphenocrysts of olivine (Fo_{50}), clinopyroxene ($Ca_{44}Mg_{44}Fe_{12}$), titanomagnetite and apatite in a groundmass of flow-aligned laths of plagioclase (An_{40} to An_{31}), calcic anorthoclase ($Or_{20}Ab_{65}An_{15}$) and sanidine ($Or_{45}Ab_{51}An_{4}$), with interstitial subhedral colourless clinopyroxene, subhedral to euhedral titanomagnetite and acicular apatite crystals. A small flow of glassy trachyandesite (49018), similar in composition to the aphyric types, is composed almost entirely of orange-brown isotropic glass. Typically black in hand specimen, the glass is a bright-red colour in specific oxidized zones. Rare partially resorbed microphenocrysts of plagioclase, clinopyroxene and apatite are the only crystalline constituents.

Tristanites

The tristanites are either aphyric or contain up to ~5 volume percent microphenocrysts (up to 0.5x0.5 mm), including olivine (Fo_{60} to Fo_{40}), clinopyroxene ($Ca_{44}Mg_{41}Fe_{15}$ to $Ca_{44}Mg_{37}Fe_{19}$), incipiently resorbed plagioclase (An_{47} to An_{40}), subhedral to euhedral titanomagnetite and pigmented apatite. The groundmass is composed of flow-aligned laths of plagioclase (An_{35}), calcic anorthoclase ($Or_{21}Ab_{69}An_{10}$) and sanidine ($Or_{40}Ab_{55}An_{5}$), with anhedral titanomagnetite and clinopyroxene. Traces of a pale-green to pinkish-brown amphibole and biotite were noted in the groundmass of several specimens.

Inclusions in the tristanites are rare, as indeed they are in all of the volcanic rocks in the area, but several small porphyritic trachyandesite inclusions (probably cognate) were found in tristanite 49081. They contain rare phenocrysts of olivine (Fo_{70}) and plagioclase (An_{50}) in a groundmass of interlocking laths of plagioclase, prismatic clinopyroxene, a yellowish-green to pinkish-brown amphibole, titanomagnetite, abundant needles of apatite and a trace of biotite.

Trachytes

The trachytes can be assigned to two main groups which are mineralogically distinctive but chemically transitional. The least evolved types are termed mafic trachytes which are also transitional in their chemistry to the tristanites, whereas the other variants are peralkaline trachytes with a molecular excess of alkalis over alumina.

The mafic trachytes are aphyric or mildly porphyritic with up to 10 volume percent phenocrysts. Mineralogically they are characterized by microphenocrysts (up to 3x1 mm) of plagioclase (An_{59} to An_{26}), clinopyroxene ($Ca_{46}Mg_{41}Fe_{13}$ to $Ca_{47}Mg_{27}Fe_{26}$), calcic anorthoclase or sanidine ($Or_{24}Ab_{63}An_{13}$ to $Or_{49}Ab_{49}An_{2}$) ± olivine (Fo_{20} to Fo_{10}), euhedral pigmented apatite and titanomagmetite. These are set in a groundmass of sub-parallel laths of sanidine and anorthoclase, with interstitial anhedral grains of pale-green clinopyroxene, titanomagnetite, quartz and a greenish-brown to pinkish-brown amphibole. Plagioclase phenocrysts commonly exhibit evidence of partial resorption and occasionally have a rim of granular opaque oxides or calcic anorthoclase.

The peralkaline trachytes are also typically aphyric or mildly porphyritic with up to 10 percent phenocrysts, dominantly euhedral calcic anorthoclase and sanidine ($Or_{17}Ab_{69}An_{14}$ to $Or_{43}Ab_{55}An_{2}$) which are up to 3x1 mm. Subordinate microphenocrysts (0.2x0.2 mm) which may or may not be present, include euhedral pale-green clinopyroxene ($Ca_{46}Mg_{23}Fe_{31}$), titanomagnetite, ilmenite and olivine (Fo_{13}). Where present, titanomagnetite and ilmenite commonly exhibit a narrow rim of aenigmatite, and Fe-rich olivine microphenocrysts in some specimens are rimmed with pale-green clinopyroxene. The groundmass is composed of flow-aligned sanidine and anorthoclase laths, with interstitial anhedral Ca- and Na-rich pyroxenes, quartz and arfvedsonite ± aenigmatite ± titanomagnetite. Small amounts of atacamite ($Cu_2(OH)_3Cl$) occur in the groundmass of many of the peralkaline trachytes. This mineral was initially misidentified as aegirine and it was subsequently identified by microprobe analysis. Some specimens of peralkaline trachyte have a little interstitial devitrified orange-brown glass instead of the usual mafic matrix minerals and quartz.

One specimen of peralkaline trachyte (49099) contains abundant

irregular felsic segregations (up to several cm in diameter), which have diffuse transitional boundaries with the host and a similar grain size. The major mineralogical differences in the segregations are increase in feldspar and quartz and a decrease in the proportion of mafic minerals, mainly amphibole. An unusual textural relationship involving the segregation of the felsic components into ovoid pods (0.5 to 1.0 cm diameter), with the mafic minerals developed between these pods is apparent in the host but very well developed in the felsic segregations. These ovoid pods are aggregates of anhedral to subhedral sanidine and quartz crystals, and the areas between the pods within the segregations are dominated by anhedral aggregates of aenigmatite and subordinate amphibole.

Rhyolites

On the basis of geochronology, field relations and mineralogy, the rhyolitic rocks are divided into 2 major groups. The first comprises the older rhyolites which represent the first manifestations of alkaline volcanism in the area. The second group includes those alkali rhyolites and comendites that were either extruded during the main shield-forming activity, or were subsequently intruded into the volcano proper, or into nearby basement.

The older rhyolites occur as vesicular or compact mildly porphyritic lavas, with restricted mineralogical variation. The abundance of phenocrysts (3x1 mm) varies between 5 and 15 volume percent and these are almost exclusively subhedral anorthoclase or sanidine ($Or_{35}Ab_{63}An_2$ to $Or_{44}Ab_{55}An_1$), commonly glomeroporphyritic. Subordinate euhedral iddingsite pseudomorphs (0.5x0.5 mm) possibly after (?)clinopyroxene, are evident in some specimens, set in a groundmass of sanidine, anorthoclase or rarely albite (Or_1Ab_{99}) laths, with interstitial anhedral quartz and oxidized iron-rich glass. Analogous trachytic lavas from Kenya (Jones, 1981) contain ferroaugite phenocrysts which are partially altered to a mineraloid resembling iddingsite. A feature of this group of rhyolites is the absence of unaltered mafic minerals (relict pyroxene is absent) and the extensively oxidized nature of the rock with the retention of clear, essentially unaltered feldspar. It appears that the alteration must have been a late-magmatic effect resulting from a relatively high fO_2 in the melt, rather than post-crystallization

alteration. Rounded zircons, occasionally included in feldspar phenocrysts of some specimens may be noted, because their presence implies the early crystallization of zircon and later magmatic resorption. Alternatively, the zircons may represent a refractory phase from the source material. The early crystallization of zircon appears inconsistent with the behaviour of zirconium as a 'residual' element in these alkaline lavas.

Only one inclusion was found within these rhyolites, a mildly porphyritic micromonzonite (49074), chemically similar to the tristanites occurring in the main shield-forming lava sequence. It is composed of large (6x4 mm) tabular crystals of sanidine ($Or_{50}Ab_{45}An_5$) and plagioclase (An_{34}) rimmed with sanidine. These are sieved with inclusions of euhedral pigmented apatite and titanomagnetite, which also occur as aggregates of microphenocrysts. The finer-grained groundmass is composed of subhedral tabular to anhedral crystals (up to 1.0x0.5 mm) of anorthoclase and sanidine, with interstitial pale-green clinopyroxene and titanomagnetite.

The second group of rhyolitic rocks include mildly peralkaline, metaluminous and mildly peraluminous variants. Applying the normative criteria of MacDonald and Bailey (1973), the mildly peralkaline types are termed comendites. The metaluminous and peraluminous variants are chemically and mineralogically transitional to the peralkaline rhyolites and are termed alkali rhyolites.

The alkali rhyolites are typically vesicular and mildly porphyritic with about 5 volume percent anorthoclase and sanidine ($Or_{36}Ab_{63}An_1$ to $Or_{38}Ab_{62}$) phenocrysts (3x1 mm), in a fine-grained groundmass of tabular sanidine and anorthoclase crystals with interstitial quartz. Variants transitional to the comendites have small amounts of interstitial arfvedsonite and large (3x1 mm) euhedral arfvedsonite crystals that project into open spaces within vesicles. Similar occurrences of arfvedsonite and aenigmatite protruding into vesicles of comendites from Naivasha, Kenya (Sutherland, 1974) and trachytes from Victoria, have been ascribed by Ferguson (1978) to crystallization from a volatile-rich liquid phase in the process of being expelled from a partly crystallized lava.

With the exception of specimens 49160 and 49161, which are

chemically transitional to the peralkaline trachytes and occur as flows in the southern portion of the Volcano, the comendites are restricted to the northern sector. The more mafic comendites are mineralogically very similar to the peralkaline trachytes, whereas those from the northern section are more leucocratic. The more evolved comendites are typically aphyric or contain sparse microphenocrysts of sanidine ($Or_{38}Ab_{62}$ to $Or_{41}Ab_{59}$) in a groundmass of subparallel anorthoclase laths, with interstitial anhedral arfvedsonite, aegirine, quartz and subhedral to euhedral zircon. Several samples contain two generations of tabular sanidine crystals. The larger crystals (0.8x0.3 mm) sit in a finer-grained aggregate (0.1x0.03 mm), with interstitial quartz, aegirine, arfvedsonite, minor zircon and micrographic intergrowths of quartz and alkali feldspar. The larger generation exhibits evidence of mild cataclasis in the form of strain extinction and fracturing, suggesting that the small pluton was forcefully emplaced as a crystal mush.

Several small inclusions found within the comendites have unusual compositions. They are composed of medium-grained aggregates of deformed subhedral biotite crystals, tabular sanidine ($Or_{46}Ab_{54}$) and calcic anorthoclase ($Or_{28}Ab_{66}An_{6}$) with subordinate anhedral ilmenite.

Pyroclastic Rocks

The pyroclastic rocks range from quite coarse volcanic breccias associated with the trachytic lavas to finer-grained ash-fall tuffs that are associated with the trachyandesites. The latter are heterogeneous accumulations of crystal debris and highly vesicular rock fragments, ranging from <0.5 mm up to several cm in diameter. They are similar in composition to the associated volcanics. The volcanic breccias associated with the trachytes have a wide size range of material from fine ash up to rock fragments 1 metre in diameter. The rock fragments in the breccia are predominantly trachyandesite to tristanite in composition.

Breccias are also associated with the older group of alkali rhyolites. These are composed of angular blocks of leucocratic alkali rhyolite up to 20 cm in diameter, disaggregated fragments of alkali feldspar and single euhedral crystals of alkali feldspar set in a hematite matrix. This textural relationship, plus the unusual nature of the matrix material, suggests that iron in hydrothermal solutions has

permeated the matrix of the breccia and fractures in the fragments, and has subsequently been precipitated as hematite.

Monzonite

A small monzonite pluton intrudes basement rocks near the central area of the volcano. The monzonite is composed of tabular crystals (3xl mm) of plagioclase (An_{37}) and sanidine ($Or_{55}Ab_{43}An_2$); clinopyroxene ($Ca_{44}Mg_{35}Fe_{21}$) with marginal overgrowths of a brown amphibole, in turn rimmed by a yellowish-green to blue-green amphibole, subhedral titaniferous biotite, titanomagnetite and ilmenite, with interstitial quartz, apatite and minor sphene. Patches of leucocratic schlieren occur throughout the monzonite and are characterized by diffuse contacts with the host. They are trachytic in composition and are essentially finer-grained aggregates of the same phases but characterized by more sanidine and less plagioclase, Ca-rich pyroxene, amphibole, biotite, titanomagnetite, ilmenite and apatite.

CHAPTER 4

MINERALOGY

A detailed knowledge of the mineralogy of the Nandewar alkaline series is essential in order to evaluate whether liquid compositions are functions of fractionation controls. Application of appropriate geothermometers and geobarometers based on mineral compositions may also reflect the physical conditions under which crystallization occurred. Microprobe techniques are outlined in Appendix I. In discussions of all mineral groups the tabulated analyses cover the range of compositions encountered in the Nandewar rocks. However, plots of mineral chemical data (Figs 4.1 to 4.11) incorporate all available analyses. A complete listing of mineral analyses and structural formulae is available from the author on request.

OLIVINE

Occurrence

Olivine is a common constituent of hawaiites and trachyandesites. It is less common in the tristanites, rare in the trachytes and is absent from the rhyolites. Olivine exhibits a wide compositional range across the series, from Fo_{88} in the trachyandesites to Fo_{10} in the trachytes and it displays a variety of forms.

In hawaiites, trachyandesites and tristanites the olivine usually occurs as euhedral to subhedral phenocrysts 1-2 mm in diameter or as microphenocrysts 0.2-0.4 mm in diameter, and it generally displays considerable compositional zoning from core to rim. Inclusions in olivine phenocrysts and microphenocrysts are rare. However, some phenocrysts do contain inclusions of apatite and titanomagnetite and in one specimen there occurs an aggregate of tiny, exceptionally aluminous (Al_2O_3 = 13 wt. percent) clinopyroxene.

Some phenocrysts (3-5 mm) occurring in hawaiites and trachyandesites which exhibit marginal resorption may be more precisely called megacrysts. This implies that they may represent liquidus or near-liquidus phases that were precipitated at elevated pressures and

subsequently transported rapidly to lower-pressure regimes.

Euhedral to subhedral olivines 1-3 mm in diameter in some of the hawaiites and trachyandesites which generally exhibit marginal resorption and are devoid of significant zoning or deformation lamellae have been termed xenocrysts. These xenocrysts can be distinguished from phenocrysts and megacrysts on the basis of compositional data that suggest they were not liquidus phases in their hosts.

Olivine is occasionally found within the trachyandesites and hawaiites associated with medium-grained aggregates of clinopyroxene, plagioclase, apatite, and titanomagnetite. These aggregates are interpreted as cognate cumulates. Less frequently, olivine is found in porphyritic inclusions that are coarser-grained than the enclosing lava and closely associated with plagioclase, amphibole, skeletal titanomagnetite and apatite.

Very fine-grained granular olivine occurs associated with clinopyroxene in reaction rims around orthopyroxene megacrysts.

In the more evolved rocks the olivine is present as microphenocrysts 0.1-0.3 mm in diameter, and in the peralkaline trachyte 49103 the microphenocrysts of fayalitic olivine have a granular rim of pale-green clinopyroxene similar in composition to the groundmass pyroxene.

The most common form of alteration of olivine, observed generally around grain boundaries or along internal fractures, is to a reddish-brown fibrous material best termed iddingsite, following Baker and Haggerty (1967). They suggest that such alteration products are formed under oxidizing conditions at temperatures probably less than 140°C. Less commonly, olivine is pseudomorphed by a bright orange-red alteration product and partly altered to a mass of skeletal opaque crystals (probably hematite) which contain interstitial tiny grains of a colourless, high-relief, highly birefringent phase. This style of alteration may be analogous to that discussed by Haggerty and Baker (1967) which is apparently the result of high-temperature (600-1000°C) deuteric alteration under oxidizing conditions. Initially the olivine breaks down to magnetite + orthopyroxene, and on further oxidation, to hematite + forsterite.

Compositional Variation

Analyses of olivines depicting the compositional variation in the Nandwar alkaline rocks are presented in Table 4.1 together with structural formulae calculated on the basis of 4 oxygens, 100Mg/Mg+ΣFe ratios (*mg*-values), and a value for K_D (the exchange partition coefficient relating the partitioning of iron and magnesium between olivine and melt; Roeder and Emslie, 1970).

$$K_D = \frac{(X_{FeO}^{Ol})}{(X_{FeO}^{Liq})} \Big/ \frac{(X_{MgO}^{Ol})}{(X_{MgO}^{Liq})}$$

The range in composition of olivine phenocrysts and microphenocrysts from the hawaiites and trachyandesites including zonal variation from core to rim is Fo_{82} to Fo_{50}. Cumulate olivines have a composition similar to the accompanying microphenocrysts, whereas crystals considered to be xenocrysts are distinctly more Mg-rich than associated phenocrysts and have quite a limited compositional range (Fo_{88-85}). Olivine phenocrysts in the tristanites range from Fo_{60} to Fo_{46} and microphenocryst compositions (Fo_{44}) are comparable to phenocryst rim compositions. The mafic trachytes contain somewhat more Fe-rich microphenocrysts than the tristanites (Fo_{21} to Fo_{10}).

In addition to the substantial variation in Fe and Mg, olivine displays considerable variation in the abundance of the minor elements Ca, Mn and, to a lesser extent, Ni. The variation of these as a function of 100Mg/Mg+Fe olivine ratios is shown in Fig. 4.1. As olivine 100Mg/Mg+Fe decreases, Ca and Mn increase regularly and Ni decreases. Bizouard *et al.* (1980) noted similar trends in Mn, Ca, and Ni with increasing Fe content in olivines from the Erta Ale and Boina volcanic centres, Ethiopia.

The increase in Mn with increasing Fe content is in accord with the observations of Simkin and Smith (1970) who suggest that the Mn contents of olivines are functions of olivine Fe content and this in turn is a function of the bulk chemistry of the host. Experimental data in the system $MgO-CaO-Na_2O-Al_2O_3-SiO_2$ (Watson, 1977) indicate

TABLE 4.1

Analyses of Olivines

	Hawaiites												
Rock Number	49000 PC	49000 PR	49000 MPC	49001 PC	49001 PR	49001 MPC	49002 PC	49002 PC	49002 PR	49002 MPC	49003 PC	49003 PR	49003 MPC
SiO_2	39.31	37.24	37.08	37.30	38.49	39.12	39.61	37.73	36.42	36.20	39.17	37.96	38.81
FeO*	17.29	26.16	27.79	26.33	21.87	17.82	14.55	24.22	29.22	33.12	18.06	23.35	21.66
MnO	0.17	0.29	0.44	0.30	0.28	0.18	0.17	0.31	0.40	0.61	0.15	0.30	0.16
NiO	0.24	-	-	-	-	0.33	0.27	0.15	0.34	-	-	-	-
MgO	42.73	35.63	34.10	35.67	39.26	41.94	45.14	37.44	32.98	29.65	42.17	38.00	39.49
CaO	0.23	0.35	0.42	0.20	0.30	0.38	0.26	0.14	0.33	0.42	0.39	0.33	0.29
Total	99.97	99.67	99.83	99.80	100.20	99.77	100.00	99.99	99.69	100.00	99.94	99.94	100.41
Structural Formulae on the Basis of 4 Oxygen Atoms													
Si	0.999	0.993	0.995	0.993	0.998	1.000	0.995	0.992	0.988	0.997	0.999	0.994	1.001
Fe^{2+}	0.368	0.583	0.624	0.586	0.474	0.381	0.305	0.533	0.663	0.763	0.385	0.512	0.467
Mn	0.004	0.007	0.010	0.007	0.006	0.004	0.004	0.007	0.009	0.014	0.003	0.007	0.004
Ni	0.005	-	-	-	-	0.007	0.005	0.003	0.007	-	-	-	-
Mg	1.619	1.415	1.364	1.415	1.516	1.598	1.689	1.468	1.334	1.217	1.603	1.484	1.519
Ca	0.006	0.010	0.012	0.006	0.008	0.010	0.007	0.004	0.010	0.012	0.011	0.009	0.008
Sum	3.001	3.008	3.005	3.007	3.002	3.000	3.005	3.007	3.011	3.003	3.001	3.006	2.999
100Mg/Mg+Fe	81.5	70.8	68.6	70.7	76.2	80.7	84.7	73.4	66.8	61.5	80.6	74.4	76.5
K_D	0.37	0.67	0.75	0.78	0.59	0.45	0.27	0.55	0.76	0.95	0.35	0.50	0.45

	Hawaiite		Trachyandesites										
Rock Number	49004 PC	49004 PR	49005 PC	49005 PR	49005 MPC	49007 XC	49007 PC	49008 XC	49008 PC	49008 PR	49009 XC	49009 MPC	49009 C
SiO_2	37.76	37.48	38.62	36.24	35.70	39.78	36.22	40.08	38.45	38.39	39.95	36.11	35.56
FeO*	23.77	25.80	19.36	31.82	32.20	13.97	31.81	11.86	19.14	22.68	13.22	32.87	33.44
MnO	0.35	0.21	0.18	0.55	0.63	0.14	0.53	0.18	0.10	0.34	-	0.61	0.43
NiO	-	-	0.37	-	-	0.17	-	0.42	0.29	-	-	0.21	-
MgO	37.93	36.28	41.23	30.93	30.62	45.74	31.05	47.25	41.60	38.31	46.89	28.76	29.72
CaO	0.19	0.23	0.16	0.32	0.36	0.20	0.31	0.17	0.24	0.21	0.17	0.58	0.26
Total	100.00	100.00	99.92	99.86	99.51	100.00	99.92	99.96	99.82	99.93	100.23	99.14	99.41
Structural Formulae on the Basis of 4 Oxygen Atoms													
Si	0.991	0.993	0.993	0.993	0.986	0.995	0.992	0.995	0.989	1.001	0.992	1.004	0.988
Fe^{2+}	0.521	0.571	0.417	0.729	0.744	0.292	0.728	0.246	0.412	0.495	0.275	0.764	0.776
Mn	0.008	0.005	0.004	0.013	0.015	0.003	0.012	0.004	0.002	0.008	-	0.014	0.010
Ni	-	-	0.008	-	-	0.003	-	0.008	0.006	-	-	0.005	-
Mg	1.484	1.432	1.581	1.263	1.260	1.706	1.267	1.748	1.595	1.489	1.736	1.192	1.231
Ca	0.005	0.007	0.004	0.009	0.011	0.005	0.009	0.005	0.007	0.006	0.005	0.017	0.008
Sum	3.009	3.008	3.007	3.007	3.016	3.004	3.008	3.006	3.011	2.999	3.008	2.996	3.013
100Mg/Mg+Fe	74.0	71.5	79.1	63.4	62.9	85.4	63.5	87.7	79.5	75.1	86.4	60.9	61.3
K_D	0.42	0.48	0.28	0.61	0.63	0.17	0.57	0.13	0.23	0.30	0.16	0.63	0.62

* Total Fe as FeO

XC - xenocryst core
PC - phenocryst core
PR - phenocryst rim
MPC - microphenocryst core
MPR - microphenocryst rim
C - olivine from cumulate aggregate
Inc. - olivine from inclusion

TABLE 4.1 (continued)

Analyses of Olivines

	Trachyandesites				Tristanites					
Rock Number	49010 PC	49012 MPC	49056 PC	49056 PC	49075 PC	49075 PR	49076 PC	49076 PR	49078 PC	49078 MPC
SiO_2	35.87	34.88	35.65	35.79	35.08	34.28	35.42	34.55	35.98	33.97
FeO*	35.76	40.67	34.25	36.19	39.16	43.52	36.85	43.02	34.07	44.38
MnO	0.55	0.98	0.66	0.66	0.73	1.15	0.75	1.04	0.79	1.44
MgO	28.07	22.90	28.93	27.61	24.48	20.85	26.31	21.31	28.84	19.77
CaO	0.29	0.57	0.30	0.24	0.34	0.40	0.33	0.38	0.31	0.35
Total	100.54	100.00	99.79	100.49	99.79	100.20	99.66	100.30	99.99	99.91
	Structural Formulae on the Basis of 4 Oxygen Atoms									
Si	0.995	1.001	0.991	0.995	1.000	0.998	0.999	1.001	0.996	0.998
Fe^{2+}	0.829	0.976	0.796	0.842	0.933	1.059	0.869	1.042	0.789	1.091
Mn	0.013	0.024	0.015	0.016	0.018	0.028	0.018	0.026	0.019	0.036
Mg	1.160	0.980	1.198	1.144	1.040	0.904	1.106	0.920	1.190	0.866
Ca	0.009	0.018	0.009	0.007	0.010	0.013	0.010	0.012	0.009	0.011
Sum	3.006	2.999	3.009	3.004	3.001	3.002	3.002	3.001	3.003	3.002
100Mg/Mg+Fe	58.3	50.1	60.1	57.6	52.7	46.1	56.0	46.9	60.1	44.3
K_D	0.45	0.67	0.23	0.26	0.40	0.53	0.34	0.49	0.24	0.45

	Tristanites			Trachytes						
Rock Number	49081 MPC	49081 C	49081 Inc.	49085 MPC	49085 MPC	49088 MPC	49088 MPC	49089 MPC	49089 MPR	49103 MPC
SiO_2	33.51	33.15	37.43	31.91	30.03	31.27	31.23	30.90	30.63	30.58
FeO*	47.13	48.44	26.78	57.24	62.90	58.79	60.18	59.74	60.82	60.16
MnO	1.27	1.40	0.29	2.25	2.49	2.36	2.37	2.34	2.42	2.68
MgO	17.50	16.81	35.43	8.26	3.83	6.89	6.23	6.27	5.45	5.11
CaO	0.43	0.36	0.18	0.65	0.52	0.65	0.61	0.57	0.52	0.61
Total	99.84	100.16	100.11	100.31	99.77	99.96	100.62	99.82	99.84	99.14
	Structural Formulae on the Basis of 4 Oxygen Atoms									
Si	1.000	0.994	0.995	1.008	0.992	1.003	1.002	0.999	0.997	1.003
Fe^{2+}	1.176	1.214	0.595	1.513	1.738	1.578	1.614	1.616	1.656	1.649
Mn	0.032	0.036	0.007	0.060	0.070	0.064	0.064	0.064	0.067	0.074
Mg	0.778	0.751	1.403	0.389	0.189	0.330	0.298	0.302	0.265	0.250
Ca	0.014	0.012	0.005	0.022	0.018	0.022	0.021	0.020	0.018	0.021
Sum	3.000	3.007	3.005	2.992	3.007	2.997	2.999	3.001	3.003	2.997
100Mg/Mg+Fe	39.8	38.2	70.2	20.5	9.8	17.3	15.6	15.8	13.8	13.1
K_D	1.14	1.22	-	1.35	3.21	1.09	1.23	1.26	1.48	1.63

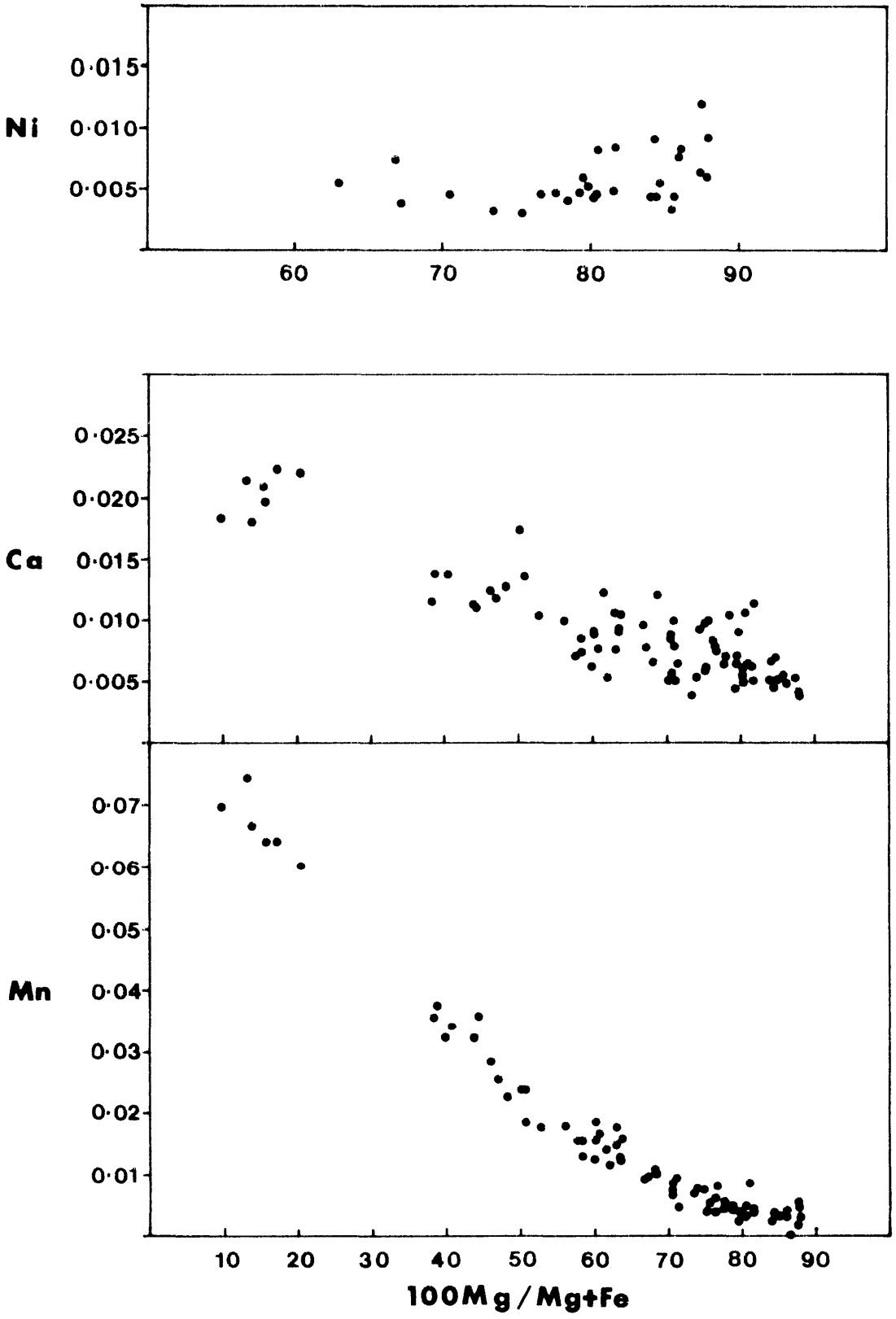

Fig. 4.1: Variation of Ni, Ca and Mn (atoms per formula unit) in olivine relative to 100Mg/Mg+Fe ratio.

that partitioning of Mn between forsteritic olivine and liquid is dependent on both temperature and liquid composition, $K_{Mn}^{Ol/liq}$ increasing with SiO_2. Takahashi (1978) confirmed the dependence of $K_{Mn}^{Ol/liq}$ on silica content of the host liquid and showed that for several basaltic compositions, as well as a variety of liquid compositions in the system Mg_2SiO_4-Fe_2SiO_4-$K_2O.4SiO_2$, a similar relationship holds for Fe, Ni and Co.

Although Ni exhibits a positive correlation with 100Mg/Mg+Fe ratio of the olivine there is considerable scatter in the data which may reflect the precision of the analytical technique employed when concentrations approach the detection limit.

A regular increase in Ca content with decreasing 100Mg/Mg+Fe ratio, apparent in the Nandewar olivines, was not observed by Simkin and Smith (1970) for olivines from a wide variety of host rocks and crystallization environments. They concluded that entry of Ca into the olivine structure was pressure dependent because olivines from the majority of plutonic rocks studied contained very low CaO (<0.1 wt. percent), whereas those from volcanic rocks generally contained greater than this amount. Stormer (1973) and Watson (1979a) confirmed the negative pressure dependence of Ca substitution in olivine, although other factors considered important include silica activity (Stormer, 1973) as well as temperature and Ca content of the melt (Watson, 1979a). However, effects of the latter two variables were determined in a Fe-free system and a further possible compositional dependence on the Fe content of the system is acknowledged by Watson (1979a). While low Ca contents in possible high-pressure xenocrysts and megacrysts indicate the effects of pressure, the Ca content of the more Fe-rich varieties does not appear to be explained by the available experimental data, and further data are clearly required on more Fe-rich compositions to explore other compositional effects of the host liquid.

The variation of K_D values for olivines within each rock and the suite as a whole is quite considerable, some of which is undoubtedly due to subliquidus Fe-Mg fractionation of other ferromagnesian phases, particularly when considering phenocryst rim and microphenocryst compositions. Among the phenocrysts, some which may be of high-pressure origin, as indicated by inclusions of aluminous clinopyroxenes, core

compositions often have K_D values close to the ideal value of 0.3[1] which Roeder and Emslie (1970) found to be constant for olivine/basalt-liquid over a wide range of temperature and oxygen fugacity (fO_2) conditions. However, K_D values for the xenocrysts are consistently less than this value which requires an alternative explanation.

Firstly, these crystals may represent liquidus phases that have precipitated under different conditions to those used in the experiments by Roeder and Emslie (1970). Mysen (1975) proposed that K_D increases with increasing pressure and decreasing temperature and also that oxygen fugacity may significantly affect K_D values. However, a number of studies (Green and Hibberson, 1970; Nicholls, 1974; Takahashi, 1978) have generally confirmed the work of Roeder and Emslie (1970) for a broad range of P, T, fO_2 conditions and a range of basaltic compositions. For example, megacrysts of olivine (Fo_{87}), clinopyroxene and orthopyroxene occurring in an olivine basalt (hawaiite, $100Mg/Mg+Fe^{2+}$ (M) = 66, $K_D^{Ol/liq}$ ~0.3) from Auckland Island were found by Green and Hibberson (1970) to be liquidus phases at temperatures of approximately 1200°C and pressures of 14-16 kb under 'wet' conditions (2-3 wt. percent H_2O). Such studies indicate that the olivine xenocrysts (Fo_{88-85}) in this study are unlikely to be liquidus phases under similar conditions in rocks with M = 47.6 to 60.3.

A second possibility is that the xenocrysts represent fragments of disaggregated lherzolite inclusions. However, their common euhedral form, low Ni contents, and the lack of composite aggregates with tschermakitic clinopyroxene, orthopyroxene and Al-spinel argue against this interpretation.

A third alternative is that the xenocrysts represent liquidus phases from a more magnesian liquid which has subsequently been modified by mixing with a less magnesian liquid, the resultant 'hybrid' being erupted before reequilibration of the olivines with the modified host could occur. This proposal is very difficult to prove unequivocally, although it may be noted that other evidence to support such a model should possibly include the presence of a second population of relatively Fe-rich phenocrysts with more Mg-rich (reverse-zoned) rims. The presence of highly magnesian olivine xenocrysts, together with compositions of glass inclusions in basalts from DSDP legs 45 and 46, were interpreted

[1] The 'ideal' K_D values are based on bulk melt-liquidus olivine compositions.

by Dungan and Rhodes (1978) as evidence of magma mixing.

Values of K_D for the Fe-rich olivines occuring in the trachytic rocks range from 1.09 to 3.01. Even if it is assumed that all of the Fe in the rock is present as FeO, the range in K_D is still from 0.59 to 1.97. If these crystals represent liquidus phases, it seems that K_D is not constant for more Fe-rich compositions, as suggested by Roeder and Emslie (1970).

PYROXENES

Occurrence

The pyroxenes in the Nandewar volcanic rocks exhibit a wide range in composition. Monoclinic Ca-rich varieties are dominant although several flows of trachyandesite carry megacrysts of low-Ca aluminian bronzite. The pyroxenes have four modes of occurrence and these are distinguished on the basis of compositional and textural criteria.

1. Pyroxene megacrysts of inferred high-pressure origin
2. Pyroxene-rich cumulates
3. Low-pressure Ca-rich pyroxene phenocrysts
4. Groundmass pyroxenes (Ca-rich to acmitic types)

Pyroxene Megacrysts

Orthopyroxene and clinopyroxene megacrysts are restricted to the trachyandesites where they are readily identified by textural and chemical disequilibrium with their hosts. Orthopyroxene megacrysts are generally anhedral, 1-5 mm in diameter, devoid of exsolution lamellae or inclusions, and commonly surrounded or, more rarely, completely replaced by fine granular aggregates of olivine and clinopyroxene. Clinopyroxene megacrysts are colourless or pale-brown and range up to 1 cm in diameter. Exsolution lamellae of Ca-poor pyroxenes are absent and the megacrysts are generally surrounded by a thin rim of pale-mauve clinopyroxene similar in composition to the Ca-rich groundmass phase. Abundant, small (0.05 to 0.1 mm) euhedra of titanomagnetite are characteristically included in the low-pressure rims. Euhedral grains of apatite (0.1

to 0.2 mm diameter) and rounded grains of olivine with similar dimensions are also rare inclusions in clinopyroxene megacrysts.

Pyroxene-rich Cumulates

Cumulate aggregates of orthopyroxene-clinopyroxene, clinopyroxene-plagioclase-titanomagnetite and clinopyroxene-olivine-plagioclase-titanomagnetite-apatite occur sporadically in the hawaiites, trachyandesites and tristanites, whereas occasional aggregates composed of clinopyroxene, anorthoclase and titanomagnetite are found in the mafic trachytes. In several aggregates from the trachyandesites, reaction rims similar to those around pyroxene megacrysts are observed where the cumulate pyroxenes are in contact with the host. In one such orthopyroxene-clinopyroxene aggregate the clinopyroxenes display narrow exsolution lamellae and these indicate some subsolidus reequilibration.

Low-pressure Ca-rich Pyroxene Phenocrysts

Euhedral to subhedral phenocrysts (1 to 3 mm diameter) and microphenocrysts (0.2 to 0.5 mm diameter) of Ca-rich clinopyroxene occur in all rock types except the most evolved comendites and rhyolites. Pyroxene is generally less abundant than olivine as a phenocryst phase in the hawaiites and it is subordinate to plagioclase and anorthoclase phenocrysts in trachyandesites and trachytes, respectively. Many of the clinopyroxene phenocrysts, especially those in the trachyandesites and tristanites, exhibit some evidence of resorption, although reaction rims are absent.

Groundmass Clinopyroxenes

Groundmass Ca-rich pyroxenes are prismatic to granular in the more mafic rock types. The acmitic pyroxenes, on the other hand, are invariably interstitial to interlocking laths of sanidine and anorthoclase in some peralkaline trachytes and comendities, and this indicates late-stage crystallization. Rare occurrences of Na-rich pyroxenes projecting into vesicles of mafic trachyte 49097 indicate that they have crystallized from a late-stage volatile-rich fluid phase.

Compositional Variation

Representative analyses and structural formulae of orthopyroxenes

TABLE 4.2

Analyses of Orthopyroxene megacrysts

Rock Number	49005 Incl.	49008 MC	49008 MC	49008 MC	49009 MC
SiO_2	53.03	52.31	51.45	50.79	51.76
TiO_2	0.15	0.45	0.64	-	0.47
Al_2O_3	4.16	4.55	5.27	4.22	4.27
FeO*	14.14	12.30	15.29	19.13	15.46
MnO	0.19	0.40	0.19	0.11	0.19
MgO	27.04	27.92	25.39	24.44	26.28
CaO	1.31	1.69	1.49	0.88	1.41
Total	100.02	99.62	99.72	99.57	99.83
Fe_2O_3[1]	0.71	1.85	0.59	3.52	2.19
FeO[1]	13.50	10.63	14.76	15.96	13.49
Total[2]	100.09	99.80	99.78	99.92	100.05
Structural Formulae on the Basis of 6 Oxygen Atoms					
Si	1.898	1.867	1.862	1.860	1.867
Al^{iv}	0.102	0.133	0.138	0.140	0.133
Al^{vi}	0.074	0.059	0.087	0.042	0.048
Ti	0.004	0.012	0.017	-	0.013
Fe^{3+}	0.019	0.050	0.016	0.097	0.059
Fe^{2+}	0.404	0.318	0.447	0.489	0.407
Mn	0.006	0.012	0.006	0.003	0.006
Mg	1.443	1.486	1.370	1.334	1.413
Ca	0.050	0.065	0.058	0.035	0.055
X+Y	2.000	2.002	2.001	2.000	2.001
$100Mg/Mg+Fe^{2+}$	78.1	82.4	75.4	73.2	77.6
Mg	75.1	77.0	72.2	68.1	72.9
Fe	22.3	19.6	24.7	30.1	24.3
Ca	2.6	3.4	3.1	1.8	2.8

* - Total Fe as FeO

[1] - Calculated following Papike *et al.* (1974)

[2] - Recalculated using calculated Fe_2O_3 and FeO values

MC - Megacryst core

Incl. - Orthopyroxene from websterite inclusion in trachyandesite

TABLE 4.3

Analyses of Clinopyroxenes

	Hawaiites													
Rock Number	49000 PC	49000 PR	49000 G	49001 PC	49001 PR	49001 G	49002 MPC	49002 MPR	49002 G	49002 Inc.	49003 G	49004 PC	49004 PR	49004 C
SiO_2	48.47	49.06	50.93	47.30	48.99	50.68	50.40	50.14	50.63	40.92	50.86	48.49	49.55	48.05
TiO_2	1.84	2.04	1.34	2.45	1.62	1.57	1.55	1.79	1.68	5.15	1.41	1.99	1.35	1.78
Al_2O_3	5.18	3.79	2.47	6.76	4.68	2.27	3.26	2.90	2.77	13.28	2.14	5.76	3.47	7.66
Cr_2O_3	0.41	0.21	-	0.30	0.61	-	0.34	0.16	-	0.08	-	0.10	0.10	-
FeO*	7.74	8.10	8.95	7.64	6.92	8.85	7.23	8.06	8.40	8.49	10.38	9.48	10.91	9.23
MnO	-	0.14	-	-	-	0.19	0.15	-	0.09	0.11	0.12	0.20	0.28	0.14
MgO	14.03	14.13	14.19	13.54	14.48	14.16	15.45	14.58	14.19	9.25	14.24	13.63	13.05	13.52
CaO	21.41	21.81	21.62	21.56	21.64	21.50	20.79	21.38	21.52	21.47	20.28	20.06	20.30	18.48
Na_2O	0.37	0.42	0.42	0.46	0.31	0.35	0.45	0.51	0.47	0.61	0.26	0.61	0.51	1.08
Total	99.45	99.70	99.92	100.01	99.25	99.57	99.62	99.52	99.75	99.36	99.69	100.32	99.52	99.94
Fe_2O_3[1]	2.51	2.79	1.96	3.04	2.04	1.32	2.18	2.17	1.63	2.05	1.06	3.00	2.60	3.40
FeO[1]	5.49	5.59	7.18	4.91	5.09	7.66	5.27	6.11	6.93	6.65	9.43	6.78	8.57	6.17
Total[2]	99.70	99.98	100.12	100.31	99.45	99.70	99.84	99.74	99.91	99.56	99.80	100.62	99.78	100.28
Structural Formulae on the Basis of 6 Oxygen Atoms														
Si	1.808	1.830	1.896	1.755	1.828	1.897	1.868	1.870	1.886	1.549	1.907	1.797	1.865	1.775
Al^{iv}	0.192	0.167	0.104	0.245	0.172	0.100	0.132	0.127	0.114	0.451	0.093	0.203	0.135	0.225
Al^{vi}	0.036	-	0.004	0.050	0.034	-	0.010	-	0.008	0.142	0.002	0.049	0.019	0.108
Ti	0.052	0.057	0.038	0.068	0.046	0.044	0.043	0.050	0.047	0.147	0.040	0.056	0.038	0.049
Cr	0.008	0.004	-	0.006	0.012	-	0.007	0.003	-	0.002	-	0.002	0.002	-
Fe^{3+}	0.070	0.078	0.055	0.085	0.057	0.037	0.061	0.061	0.046	0.058	0.030	0.084	0.074	0.095
Fe^{2+}	0.171	0.174	0.224	0.152	0.159	0.240	0.163	0.191	0.216	0.211	0.296	0.210	0.270	0.191
Mn	-	0.004	-	-	-	0.006	0.005	-	0.003	0.004	0.004	0.006	0.009	0.004
Mg	0.780	0.786	0.787	0.749	0.806	0.790	0.854	0.810	0.788	0.522	0.796	0.753	0.732	0.745
Ca	0.856	0.872	0.862	0.857	0.865	0.862	0.826	0.854	0.859	0.871	0.815	0.797	0.819	0.731
Na	0.027	0.030	0.030	0.033	0.022	0.025	0.032	0.037	0.034	0.045	0.019	0.044	0.037	0.077
X+Y	2.000	2.005	2.000	2.000	2.001	2.004	2.001	2.006	2.001	2.002	2.002	2.001	2.000	2.000
$100Mg/Mg+Fe^{2+}$	82.0	81.8	77.9	83.1	83.5	76.7	83.9	81.0	78.5	71.3	72.9	78.2	73.1	79.6
Mg	43.2	42.9	42.0	42.6	44.0	41.8	46.3	43.7	42.3	32.5	41.7	42.8	40.2	44.7
Fe^{2+}	9.4	9.5	12.0	8.6	8.7	12.7	8.9	10.3	11.6	13.2	15.5	11.9	14.8	11.5
Ca	47.4	47.6	46.0	48.8	47.3	45.5	44.8	46.0	46.1	54.3	42.8	45.3	45.0	43.8

	Trachyandesites													
Rock Number	49005 MC	49005 MR	49005 G	49005 Inc.	49007 PC	49007 PR	49008 MC	49008 MR	49008 G	49009 MC	49009 G	49010 PC	49010 PR	49012 PC
SiO_2	50.48	49.32	49.17	49.99	50.13	49.85	49.21	48.78	47.94	49.14	50.90	49.13	49.88	49.09
TiO_2	0.82	2.03	2.27	1.00	1.31	1.55	1.36	1.75	3.71	1.43	0.81	1.58	1.46	1.79
Al_2O_3	5.92	3.63	3.85	6.53	3.20	4.28	7.73	7.33	4.29	6.47	1.37	4.72	4.01	4.66
Cr_2O_3	0.40	-	0.12	0.32	-	-	0.18	-	-	-	-	-	-	-
FeO*	7.53	8.62	9.30	7.21	9.12	9.21	7.74	9.21	10.77	9.21	14.82	10.54	9.78	9.31
MnO	-	-	0.20	-	0.43	0.25	-	0.17	0.23	-	0.57	0.20	0.17	0.25
MgO	14.31	13.72	13.25	13.72	14.10	13.69	15.21	13.94	11.36	15.12	11.10	12.76	13.60	14.15
CaO	19.22	22.17	20.96	19.32	20.71	20.22	18.49	18.40	21.49	17.70	20.16	20.32	20.78	19.92
Na_2O	1.33	0.49	0.44	1.20	0.50	0.44	0.56	0.74	0.66	1.11	0.46	0.53	0.63	0.48
Total	100.01	99.98	99.56	99.29	99.50	99.49	100.48	100.32	100.45	100.17	100.19	99.78	100.31	99.65
Fe_2O_3[1]	3.00	2.89	1.26	1.44	2.66	0.87	1.15	1.46	1.00	4.36	1.71	1.99	3.05	2.51
FeO[1]	4.83	6.02	8.16	5.92	6.73	8.43	6.71	7.89	9.87	5.29	13.28	8.75	7.03	7.05
Total[2]	100.31	100.27	99.69	99.43	99.77	99.58	100.60	100.46	100.55	100.61	100.36	99.98	100.62	99.85
Structural Formulae on the Basis of 6 Oxygen Atoms														
Si	1.851	1.837	1.847	1.850	1.873	1.865	1.798	1.798	1.807	1.800	1.938	1.842	1.851	1.829
Al^{iv}	0.149	0.159	0.153	0.150	0.127	0.135	0.202	0.202	0.191	0.200	0.062	0.158	0.149	0.171
Al^{vi}	0.107	-	0.018	0.134	0.014	0.054	0.131	0.117	-	0.079	-	0.051	0.027	0.034
Ti	0.023	0.057	0.064	0.028	0.037	0.044	0.037	0.049	0.105	0.039	0.023	0.045	0.041	0.050
Cr	0.008	-	0.002	0.006	-	-	0.004	-	-	-	-	-	-	-
Fe^{3+}	0.083	0.081	0.036	0.040	0.075	0.024	0.032	0.041	0.029	0.120	0.049	0.056	0.085	0.070
Fe^{2+}	0.148	0.188	0.257	0.183	0.210	0.264	0.205	0.243	0.311	0.162	0.423	0.274	0.218	0.220
Mn	-	-	0.006	-	0.014	0.008	-	0.005	0.007	-	0.018	0.006	0.005	0.008
Mg	0.782	0.762	0.742	0.757	0.785	0.764	0.829	0.766	0.638	0.826	0.630	0.713	0.753	0.787
Ca	0.755	0.885	0.844	0.766	0.829	0.811	0.724	0.727	0.868	0.695	0.823	0.816	0.826	0.796
Na	0.095	0.035	0.032	0.086	0.036	0.032	0.040	0.053	0.048	0.079	0.034	0.039	0.045	0.035
X+Y	2.001	2.008	2.001	2.000	2.000	2.001	2.002	2.001	2.006	2.000	2.000	2.000	2.000	2.000
$100Mg/Mg+Fe^{2+}$	84.1	80.2	74.3	80.5	78.9	74.3	80.2	75.9	67.2	83.6	59.8	72.2	77.5	78.1
Mg	46.9	41.5	40.3	44.4	43.0	41.5	47.2	44.1	35.1	49.1	33.6	39.5	41.9	43.6
Fe^{2+}	8.8	10.3	13.9	10.7	11.5	14.4	11.6	14.0	17.1	9.6	22.5	15.2	12.1	12.2
Ca	45.3	48.2	45.8	44.9	45.5	44.1	41.2	41.9	47.8	41.3	43.9	45.3	46.0	44.2

TABLE 4.3 (continued)

Analyses of Clinopyroxenes

	Trachyandesites				Monzonite	Tristanites								
Rock Number	49012 PR	49012 G	49056 PC	49056 G	49070 G	49074 MC	49074 G	49074 Inc.	49075 MPC	49076 MPC	49076 G	49077 MPC	49077 G	49078 MPC
SiO_2	48.47	50.18	48.90	50.69	51.51	47.17	50.08	48.85	50.56	50.33	47.00	49.99	46.63	51.26
TiO_2	2.00	1.67	1.74	1.14	0.26	1.93	0.81	1.75	0.82	1.18	2.45	1.25	2.58	0.65
Al_2O_3	5.36	2.65	4.43	2.41	0.85	8.67	0.93	4.54	2.31	2.95	5.03	2.89	5.10	1.45
FeO*	9.45	10.50	9.90	10.28	14.41	8.67	17.55	11.11	10.36	11.18	13.72	11.31	13.59	12.75
MnO	0.22	0.31	0.25	0.29	0.51	0.13	0.71	0.24	0.30	0.30	0.38	0.33	0.25	0.54
MgO	13.55	12.84	13.14	14.12	11.36	13.63	8.26	12.17	13.19	13.09	10.60	13.19	10.52	13.65
CaO	19.74	21.08	21.22	20.25	20.25	18.47	19.92	20.60	20.97	20.34	20.16	20.09	20.22	18.80
Na_2O	0.58	0.37	0.69	0.37	0.65	0.90	0.86	0.75	0.55	0.55	0.47	0.61	0.55	0.38
Total	99.37	99.60	100.27	99.55	99.80	99.57	99.12	100.01	99.06	99.92	99.81	99.66	99.44	99.48
Fe_2O_3[1]	2.25	0.99	4.34	1.94	2.49	3.07	2.05	3.22	2.63	2.40	2.86	3.10	3.26	1.76
FeO[1]	7.43	9.61	5.99	8.54	12.17	5.91	15.70	8.21	7.99	9.02	11.15	8.52	10.65	11.17
Total[2]	99.59	99.70	100.71	99.74	100.05	99.88	99.33	100.33	99.32	100.16	100.10	99.97	99.76	99.66
Structural Formulae on the Basis of 6 Oxygen Atoms														
Si	1.815	1.893	1.818	1.901	1.961	1.746	1.957	1.832	1.908	1.887	1.793	1.879	1.784	1.938
Al^{iv}	0.185	0.107	0.182	0.099	0.038	0.254	0.043	0.168	0.092	0.113	0.207	0.121	0.216	0.062
Al^{vi}	0.051	0.011	0.012	0.007	-	0.125	-	0.033	0.011	0.018	0.019	0.007	0.014	0.003
Ti_{3+}	0.056	0.047	0.049	0.032	0.007	0.054	0.024	0.049	0.023	0.033	0.070	0.035	0.074	0.019
Fe_{2+}	0.063	0.028	0.122	0.055	0.071	0.086	0.060	0.091	0.075	0.068	0.082	0.088	0.094	0.050
Fe	0.233	0.303	0.186	0.268	0.388	0.183	0.513	0.258	0.252	0.283	0.356	0.268	0.341	0.353
Mn	0.007	0.010	0.008	0.009	0.016	0.004	0.024	0.008	0.010	0.010	0.012	0.011	0.008	0.017
Mg	0.756	0.722	0.728	0.789	0.645	0.752	0.481	0.680	0.742	0.732	0.603	0.739	0.600	0.769
Ca	0.792	0.852	0.845	0.813	0.826	0.733	0.834	0.828	0.848	0.817	0.824	0.809	0.829	0.762
Na	0.042	0.027	0.050	0.027	0.048	0.065	0.065	0.055	0.040	0.040	0.035	0.044	0.041	0.028
X+Y	2.000	2.000	2.000	2.000	2.001	2.002	2.001	2.002	2.001	2.001	2.001	2.001	2.001	2.001
$100Mg/Mg+Fe^{2+}$	76.5	70.4	79.6	74.7	62.5	80.4	48.4	72.5	74.6	72.1	62.9	73.4	63.8	68.5
Mg_{2+}	42.4	38.5	41.4	42.2	34.7	45.1	26.3	38.5	40.3	40.0	33.8	40.7	33.9	40.8
Fe^{2+}	13.1	16.1	10.6	14.3	20.9	11.0	28.1	14.6	13.7	15.4	20.0	14.8	19.3	18.7
Ca	44.5	45.4	48.0	43.5	44.4	43.9	45.6	46.9	46.0	44.6	46.2	44.5	46.8	40.5

	Tristanite		Trachytes											
Rock Number	49081 MPC	49081 G	49082 MPC	49082 G	49083 G	49084 MPC	49084 MPR	49085 MPC	49085 G	49086 MPC	49086 G	49088 MPC	49088 G	49089 MPC
SiO_2	50.71	47.31	49.58	50.65	49.52	48.53	50.40	50.07	49.98	50.24	50.62	50.69	48.34	50.02
TiO_2	0.65	2.26	1.30	0.60	0.88	1.31	0.50	0.52	0.54	0.57	0.51	0.59	0.60	0.51
Al_2O_3	1.76	5.09	3.34	1.08	1.91	4.37	1.67	1.13	0.95	1.59	1.18	1.20	0.89	1.05
FeO*	12.92	12.26	10.08	16.67	16.32	11.86	16.52	16.76	20.83	16.40	17.84	17.07	25.44	18.15
MnO	0.39	0.35	0.25	0.57	0.47	0.39	0.61	0.59	0.83	0.52	0.74	0.69	0.90	0.69
MgO	12.15	11.84	13.01	9.69	9.66	12.11	9.60	8.77	6.41	9.12	8.60	9.30	4.12	8.06
CaO	20.50	19.99	21.34	20.17	20.32	19.91	19.94	21.53	19.90	21.05	20.22	20.60	18.68	21.20
Na_2O	0.37	0.50	0.40	0.57	0.56	0.65	0.52	0.35	0.79	0.53	0.75	0.41	0.99	0.48
Total	99.45	99.60	99.30	100.00	99.64	99.13	99.76	99.72	100.23	100.02	100.46	100.55	99.96	100.16
Fe_2O_3[1]	1.90	3.34	2.49	1.96	2.68	3.47	1.64	1.63	2.20	2.22	2.54	1.64	2.75	1.86
FeO[1]	11.21	9.25	7.84	14.91	13.91	8.74	15.04	15.29	18.85	14.40	15.55	15.59	22.97	16.47
Total[2]	99.64	99.94	99.55	100.20	99.91	99.48	99.92	99.88	100.45	100.24	100.71	100.71	100.24	100.35
Structural Formulae on the Basis of 6 Oxygen Atoms														
Si	1.928	1.792	1.868	1.950	1.911	1.839	1.943	1.944	1.959	1.935	1.949	1.947	1.942	1.945
Al^{iv}	0.072	0.208	0.132	0.049	0.087	0.161	0.057	0.052	0.041	0.065	0.051	0.053	0.042	0.048
Al^{vi}	0.007	0.020	0.016	-	-	0.034	0.019	-	0.003	0.007	0.003	0.001	-	-
Ti_{3+}	0.019	0.064	0.037	0.017	0.026	0.037	0.015	0.015	0.016	0.017	0.015	0.017	0.018	0.015
Fe_{2+}	0.054	0.095	0.071	0.057	0.078	0.099	0.048	0.048	0.065	0.064	0.074	0.048	0.083	0.055
Fe	0.356	0.293	0.247	0.480	0.449	0.277	0.485	0.497	0.618	0.464	0.501	0.501	0.772	0.536
Mn	0.013	0.011	0.008	0.019	0.015	0.013	0.020	0.019	0.028	0.017	0.024	0.022	0.031	0.023
Mg	0.689	0.669	0.731	0.556	0.556	0.684	0.552	0.508	0.375	0.524	0.494	0.533	0.247	0.467
Ca	0.835	0.811	0.862	0.832	0.840	0.808	0.824	0.896	0.836	0.869	0.834	0.848	0.804	0.883
Na	0.027	0.037	0.029	0.043	0.042	0.048	0.039	0.026	0.060	0.040	0.056	0.031	0.077	0.036
X+Y	2.000	2.000	2.001	2.004	2.006	2.000	2.002	2.009	2.001	2.002	2.001	2.001	2.032	2.015
$100Mg/Mg+Fe^{2+}$	65.9	69.5	74.7	53.7	55.3	71.2	53.2	50.6	37.7	53.0	49.6	51.6	24.2	46.6
Mg_{2+}	36.7	37.7	39.7	29.8	30.1	38.7	29.7	26.7	20.5	28.2	27.0	28.3	13.5	24.8
Fe^{2+}	18.9	16.5	13.4	25.7	24.4	15.6	26.0	26.2	33.8	25.0	27.4	26.6	42.4	28.4
Ca	44.4	45.8	46.9	44.5	45.5	45.7	44.3	47.1	45.7	46.8	45.6	45.1	44.1	46.8

TABLE 4.3 (continued)

Analyses of Clinopyroxenes

	Trachytes													
Rock Number	49089 MPR	49090 MPC	49097 MPC	49097 G	49097 G	49098 G	49098 G	49098 G	49099 G	49099 G	49099 G	49099 G	49101 G	49102 MPC
SiO_2	49.79	49.22	50.32	52.15	52.24	48.11	49.29	50.63	48.31	49.69	50.09	50.47	52.67	49.77
TiO_2	0.48	0.52	1.31	0.99	1.13	0.47	1.07	1.43	0.88	0.50	0.93	0.89	0.42	0.52
Al_2O_3	1.13	0.92	3.09	2.31	0.56	0.67	0.64	0.56	1.47	0.74	2.61	0.54	0.93	0.99
FeO*	19.36	22.57	9.20	14.52	27.04	29.03	29.44	29.14	28.58	27.45	28.53	26.95	30.14	18.84
MnO	0.68	0.87	0.17	0.48	0.86	1.18	0.84	0.45	0.99	1.04	0.55	0.64	0.13	0.88
MgO	7.11	4.98	13.81	10.36	2.51	0.85	0.35	-	0.90	0.79	1.63	0.45	0.30	7.30
CaO	20.90	21.05	21.50	17.01	3.15	18.09	13.28	7.80	14.42	15.16	10.43	11.63	-	20.61
Na_2O	0.52	0.53	0.33	1.90	10.67	1.49	4.77	8.43	3.18	3.52	3.96	6.32	13.20	0.50
Total	99.97	100.66	99.73	99.72	98.16	99.89	99.68	98.44	98.73	98.89	98.73	97.89	97.79	99.41
Fe_2O_3[1]	2.13	1.77	1.89	0.89	24.89	3.95	11.15	18.70	6.48	6.91	4.26	13.66	31.80	1.63
FeO[1]	17.44	20.98	7.50	13.72	4.64	25.48	19.40	12.31	22.75	21.23	24.70	14.66	1.53	17.37
Total[2]	100.18	100.84	99.92	99.81	100.65	100.29	100.80	100.31	99.38	99.58	99.16	99.26	100.98	99.57
Structural Formulae on the Basis of 6 Oxygen Atoms														
Si	1.948	1.948	1.880	1.977	1.992	1.964	1.969	1.989	1.964	2.005	2.009	2.009	1.998	1.956
Al^{iv}	0.052	0.043	0.120	0.023	0.008	0.032	0.030	0.011	0.036	-	-	-	0.002	0.044
Al^{vi}	-	-	0.017	0.080	0.017	-	-	0.015	0.034	0.035	0.123	0.025	0.040	0.002
Ti^{3+}	0.014	0.016	0.037	0.028	0.032	0.014	0.032	0.042	0.027	0.015	0.028	0.027	0.012	0.015
Fe^{3+}	0.063	0.053	0.053	0.025	0.714	0.121	0.335	0.553	0.198	0.210	0.129	0.409	0.908	0.048
Fe^{2+}	0.571	0.694	0.235	0.435	0.148	0.870	0.648	0.405	0.774	0.717	0.829	0.488	0.048	0.571
Mn	0.023	0.029	0.005	0.015	0.028	0.041	0.028	0.015	0.034	0.036	0.019	0.022	0.004	0.029
Mg	0.415	0.294	0.769	0.586	0.143	0.052	0.021	-	0.055	0.048	0.098	0.027	0.017	0.428
Ca	0.876	0.893	0.861	0.691	0.129	0.791	0.568	0.328	0.628	0.655	0.448	0.496	-	0.368
Na	0.039	0.041	0.024	0.140	0.789	0.118	0.369	0.642	0.251	0.275	0.308	0.488	0.971	0.038
X+Y	2.001	2.020	2.001	2.000	2.000	2.007	2.001	2.000	2.001	1.991	1.982	1.982	2.000	1.999
Mg_{2+}	22.3	15.6	41.2	34.2	34.0	3.0	1.7	0.0	3.8	3.3	7.1	2.6	25.9	22.9
Fe^{2+}	30.6	36.9	12.6	25.4	35.2	50.8	52.4	55.2	53.1	50.5	60.3	48.3	74.1	30.6
Ca	47.1	47.5	46.2	40.4	30.7	46.2	45.9	44.8	43.1	46.2	32.6	49.1	0.0	46.5
Mg_{2+}	38.7	27.5	72.4	49.8	12.9	4.8	2.0	0.0	4.9	4.4	7.8	2.6	1.6	39.8
Fe^{2+}+Mn	57.6	68.7	25.3	38.3	15.9	84.3	63.4	39.5	72.6	70.0	67.6	49.8	5.1	56.7
Na	3.7	3.8	2.3	11.9	71.2	10.9	34.6	60.5	22.5	25.6	24.6	47.6	93.3	3.5

	Trachytes							Comendites						
Rock Number	49103 MPC	49103 G	49104 G	49104 G	49108 G	49108 G	49108 G	49160 MPC	49160 G	49161 MPC	49161 MPR	49163 G	49163 G	49164 G
SiO_2	49.36	49.17	52.36	49.82	51.88	52.21	51.69	47.58	47.22	47.94	47.30	51.03	50.16	50.98
ZrO_2	-	-	1.09	0.32	1.14	1.51	2.34	-	-	0.21	0.23	1.09	1.68	0.99
TiO_2	0.64	0.49	0.43	0.32	1.62	3.48	1.71	0.50	0.59	0.47	0.28	1.20	3.04	0.44
Al_2O_3	0.98	0.87	0.51	0.89	0.56	0.72	0.65	1.44	0.77	0.77	0.51	0.62	2.73	0.64
FeO*	21.73	21.71	29.04	32.76	28.42	25.94	26.74	26.86	29.00	25.98	28.68	28.45	25.46	28.61
MnO	0.70	0.79	0.34	0.74	0.38	0.51	0.31	1.01	1.22	1.12	1.40	0.33	0.20	0.63
MgO	5.72	5.78	-	-	-	-	-	2.18	0.65	2.51	0.84	-	0.16	-
CaO	20.75	20.23	2.02	0.55	0.85	0.31	0.41	19.47	19.00	19.88	19.53	4.39	1.09	3.55
Na_2O	0.50	0.79	12.07	11.87	12.66	13.30	13.29	0.63	0.80	0.58	0.49	10.84	12.24	11.06
Total	100.38	99.83	97.86	97.27	97.51	97.98	97.14	99.67	99.25	99.46	99.26	97.95	96.76	96.90
Fe_2O_3[1]	1.54	2.42	29.44	31.34	29.34	27.43	29.72	2.52	2.09	1.76	1.50	26.48	25.31	28.92
FeO[1]	20.34	19.53	2.55	4.56	2.02	1.26	0.00	24.59	27.12	24.40	27.33	4.63	2.69	2.58
Total[2]	100.53	100.07	100.81	100.41	100.45	100.73	100.12	99.92	99.46	99.64	99.41	100.60	99.18	100.11
Structural Formulae on the Basis of 6 Oxygen Atoms														
Si	1.948	1.949	2.003	1.942	1.988	1.982	1.982	1.936	1.956	1.955	1.964	1.972	1.935	1.975
Al^{iv}	0.046	0.041	-	0.041	0.012	0.018	0.018	0.064	0.038	0.037	0.025	0.028	0.065	0.025
Al^{vi}	-	-	0.023	-	0.013	0.014	0.011	0.005	-	-	-	-	0.060	0.004
Zr	-	-	0.020	0.006	0.021	0.028	0.044	-	-	0.004	0.005	0.021	0.032	0.019
Ti^{3+}	0.019	0.015	0.012	0.009	0.047	0.099	0.049	0.015	0.018	0.014	0.009	0.035	0.088	0.013
Fe^{3+}	0.046	0.072	0.848	0.919	0.846	0.784	0.857	0.077	0.065	0.054	0.047	0.770	0.735	0.843
Fe^{2+}	0.672	0.647	0.082	0.149	0.065	0.040	-	0.837	0.940	0.832	0.949	0.150	0.087	0.084
Mn	0.023	0.027	0.011	0.024	0.012	0.016	0.010	0.035	0.043	0.039	0.049	0.011	0.007	0.021
Mg	0.337	0.342	-	-	-	-	-	0.132	0.040	0.153	0.052	-	0.009	-
Ca	0.878	0.859	0.083	0.023	0.035	0.013	0.017	0.849	0.843	0.869	0.869	0.182	0.045	0.150
Na	0.038	0.061	0.895	0.897	0.940	0.979	0.988	0.050	0.064	0.046	0.039	0.812	0.907	0.848
X+Y	2.013	2.023	1.974	2.027	1.979	1.973	1.976	2.000	2.013	2.011	2.019	1.981	1.970	1.982
Mg_{2+}	17.9	18.5	0.0	0.0	0.0	0.0	0.0	7.3	2.2	8.2	2.8	0.0	6.5	0.0
Fe^{2+}	35.6	35.0	49.6	86.6	64.9	76.0	0.0	46.0	51.5	44.9	50.7	45.1	61.5	35.8
Ca	46.5	46.5	50.4	13.4	35.1	24.0	100.0	46.7	46.3	46.9	46.5	54.9	32.0	64.2
Mg_{2+}	31.2	31.4	0.0	0.0	0.0	0.0	0.0	12.2	3.7	14.2	4.7	0.0	0.9	0.0
Fe^{2+}+Mn	65.2	63.0	9.4	17.9	7.6	5.4	1.0	83.2	90.4	81.6	91.7	16.5	9.2	11.0
Na	3.6	5.6	90.6	82.1	92.4	94.6	99.0	4.6	5.9	4.2	3.6	83.5	89.9	89.0

and clinopyroxenes from the Nandewar rocks are listed in Tables 4.2 and 4.3, respectively. Since distinction between ferrous and ferric iron is not possible with the microprobe, estimates of Fe_2O_3 and FeO have been calculated assuming a charge balance in the pyroxenes (Papike *et al.*, 1974). These calculations permit a more realistic estimate of the *M*-values of the pyroxenes for comparison with similar parameters for host rocks and coexisting ferromagnesian phases.

Criticisms of this procedure suggest poor precision (Finger, 1972) and poor correlation with directly determined Fe^{2+} and Fe^{3+}, particularly when the pyroxenes contain a significant jadeite component (Cawthorn and Collerson, 1974; Wood, 1976a; Edwards, 1976). However, comparison of calculated Fe_2O_3 and FeO values (each based on an average of 6 core and rim analyses) with directly analyzed values for FeO on pyroxene phenocrysts separated from two specimens (Table 4.4), indicate that the calculated and analyzed values are in reasonable agreement. None of the Nandewar pyroxenes contains a significant jadeite component, and hence the calculated values for FeO and Fe_2O_3 should adequately reflect 'actual' values.

Table 4.4

Comparison of measured and calculated Fe_2O_3 and FeO values for two pyroxene phenocrysts

Sample	Calculated Fe_2O_3	Calculated FeO	Analyzed FeO
49002	1.99	6.48	6.40
49010	2.44	7.57	8.15

A plot of all low-Na pyroxene analyses in the traditional pyroxene quadrilateral (Fig. 4.2) indicates that they can be largely designated as members of the augite-ferroaugite-ferrohedenbergite series with some overlap into the fields of the more Ca-rich salite-ferrosalite-hedenbergite series. The trend of compositional variation for the Nandewar pyroxenes is comparable to those displayed by other mildly alkaline suites from Oki Dogo (Uchimizu, 1966), Boina and Erta Ale,

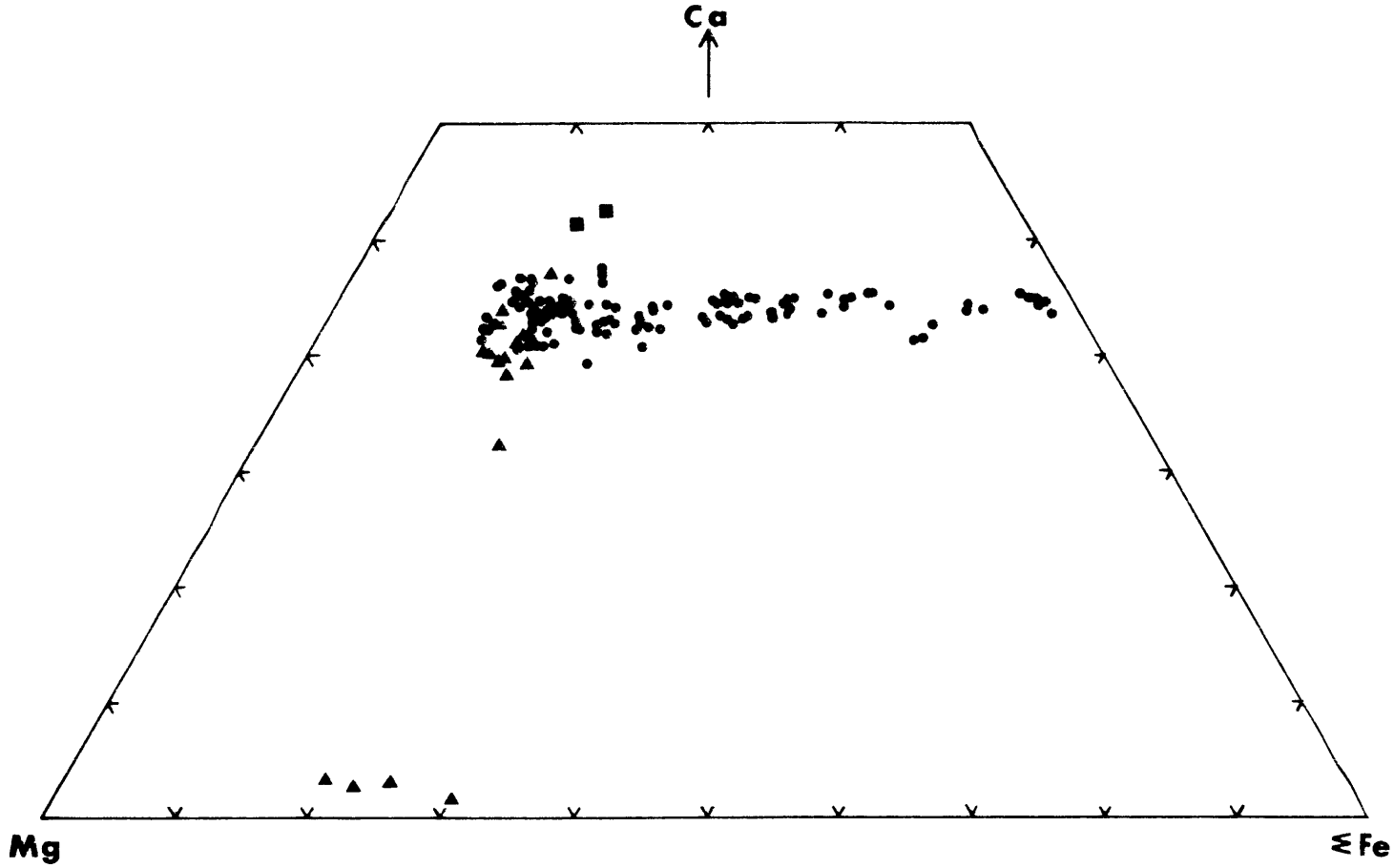

Fig. 4.2: Analyses of Ca-rich and Ca-poor pyroxenes plotted in terms of atom percent Ca, Mg and $\Sigma Fe (Fe^{2+}+Fe^{3+}+Mn)$. Megacrysts (triangles), Ca-rich phenocryst and groundmass pyroxenes (circles), and Al-rich titanaugites included in olivine phenocryst (squares).

Ethiopia (Bizouard *et al.*, 1980) and the Canobolas Volcano, New South Wales (Middlemost, 1981). The essentially continuous variation in composition from augite to ferrohedenbergite reflects the gradually decreasing *M* values of the respective hosts. Variation in Ca content is greatest in the Mg-rich types, the clinopyroxene megacrysts extending the compositional range to low-Ca augites.

Pyroxene Megacrysts

The Nandewar orthopyroxene and clinopyroxene megacrysts are very similar in composition to analogous phases in trachyandesites and hawaiites from Taka-sima (Kuno, 1964) and the Comboyne Province (Knutson and Green, 1975), and a tholeiitic andesite from the Tweed Shield Volcano, north-eastern New South Wales (Duggan and Wilkinson, 1973). The orthopyroxene megacrysts (aluminian bronzites with appreciable Ca contents) are generally unzoned and exhibit moderate Fe^{2+}-Mg substitution (*M* = 73 to 82). There is a greater range in *M* in the megacrysts from one trachyandesite (49008) than between specimens. In general the Nandewar orthopyroxene megacrysts have lower *M* values than those in alkaline volcanics from north-eastern New South Wales (Binns *et al.*, 1970), Nigeria (Frisch and Wright, 1971) and Victoria (Irving, 1974a); however their Al and Ca contents are similar. The very low Cr contents in the Nandewar and Comboyne (Knutson and Green, 1975) orthopyroxene megacrysts (in all cases below the detection limit, 0.08 wt. percent) contrasts with moderately high levels (0.15 to 0.41 wt. percent) in Victorian (Irving, 1974a) and other New South Wales examples (Binns *et al.*, 1970). The low Cr levels in the Nandewar ortho-pyroxene megacrysts reflect the relatively low Cr concentrations in the host melts (85-106 µg/g) and the preferential entry of Cr into coexisting clinopyroxenes (Seward, 1971).

Except for a narrow rim similar to phenocryst rim and groundmass compositions, clinopyroxene megacrysts are unzoned. They characteristically have higher Al, Na, Cr and lower Ca, Ti and Mn than coexisting phenocryst and groundmass phases. In most cases the *M* values of clinopyroxene megacrysts are higher than those of coexisting orthopyroxene megacrysts which is the normal relationship for the low-pressure phases (Hess, 1941; Muir and Tilley, 1958). An orthopyroxene megacryst in trachyandesite 49008 which has a higher *M*-value (*M* =82) than coexisting ortho- and clinopyroxene megacrysts (*M* = 75 and 80 respectively) is most likely

xenocrystal, and could have been derived by disintegration of cumulate inclusions precipitated from a more primitive Mg-rich host. Compared with clinopyroxene megacrysts from a variety of alkaline hosts in New South Wales (Binns *et al.*, 1970) and Victoria (Irving, 1974a) the Nandewar examples are generally lower in Al and Na and higher in Ca.

Pyroxene-rich Cumulates

Clinopyroxenes in inclusions or cumulate aggregates generally have similar compositions to the megacrysts but one rare exception is provided by an aggregate of clinopyroxene included in an olivine phenocryst from hawaiite 49002. The composition of the latter pyroxenes (Table 4.3, No. 49002 Inc.) is characterized by low Si and high Ti and total Al, thereby resulting in high Al^{IV} and Al^{VI}. Ca is high and Na low compared with other pyroxenes with high Al^{VI} which are generally interpreted to be high-pressure in origin.

Low-pressure Ca-rich Pyroxene Phenocrysts and Groundmass Pyroxenes

Phenocryst pyroxenes exhibit only limited compositional zoning which is generally from relatively Mg-rich cores to more Fe-rich rims. Low-Na groundmass pyroxenes usually have compositions which are comparable to those of phenocryst rims. Phenocryst and groundmass pyroxene compositions vary with *M*-value of the host. The most important trend is a decrease in pyroxene *M*-value with the *M*-value of the host. Mn substitution in pyroxenes also increases with decreasing *M* value of the pyroxene and the host, MnO reaching a maximum of 1.40 wt. percent in ferrohedenbergite phenocrysts from several comendites (Table 4.3, No.49161). Mn contents of clinopyroxenes are always lower than those of the coexisting olivines, indicating preferential partitioning of Mn into the latter phase. Although Mn^{2+} is apparently capable of replacing Ca^{2+} and Mg^{2+} as well as Fe^{2+} (Vinokurov, 1966), the strong positive correlation of Fe^{2+} and Mn^{2+} in Fig. 4.3(a) indicates that the substitution is dominantly $Mn^{2+} \rightarrow Fe^{2+}$.

A strong negative correlation is apparent in a plot of Si vs Al (Fig. 4.3b), representing an increase in Si at the expense of Al in the pyroxenes and this coincides with increasing SiO_2 content of the respective hosts. The dependence of clinopyroxene Si content on silica activity of

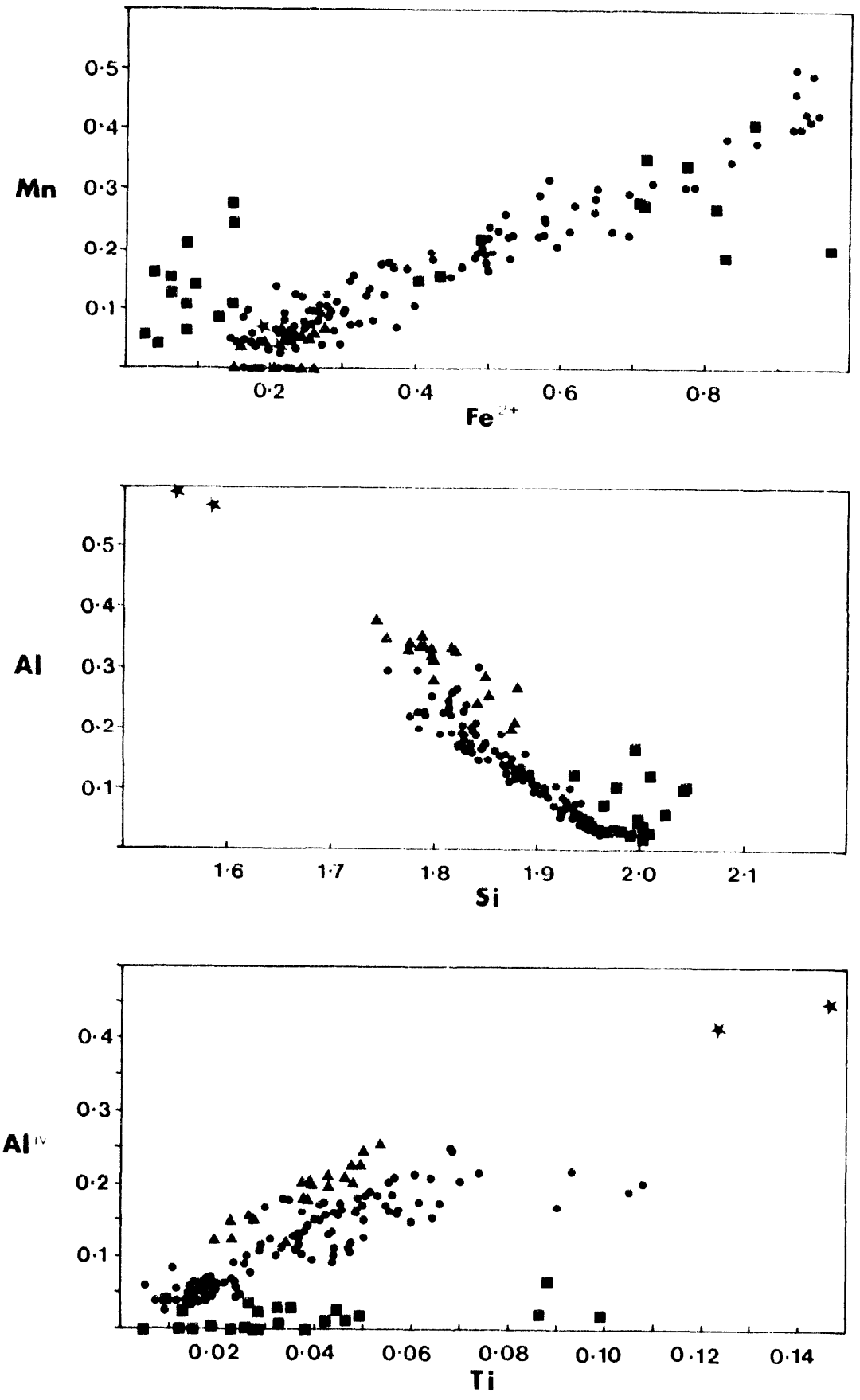

Fig. 4.3: Plots of (a) Fe^{2+} vs Mn (b) Al^{total} vs Si (c) Al^{IV} vs Ti (atoms/formula unit) for the Nandewar clinopyroxenes. Ca-rich pyroxene megacrysts (triangles), Ca-rich phenocryst and groundmass pyroxenes (circles), Na-rich pyroxenes (squares) and Al-rich titanaugites (stars).

the melt has been discussed by Kushiro (1960), Le Bas (1962), Barberi *et al.* (1971) and Gupta *et al.* (1973). Although Al contents of the Nandewar pyroxenes are usually highest in the megacrysts, Al is also very variable in other types. Although many groundmass clinopyroxenes for low Al, others have Al contents that are in fact comparable to megacrysts Al. However, the respective structural states are different. Al in the groundmass pyroxenes is dominantly in tetrahedral coordination, whereas much of the Al in the megacrysts is in octahedral coordination and present as the Ca-Tschermak component ($CaAl_2SiO_6$) (Kushiro, 1962). Wass (1979) noted a similar pattern in the Al contents of coexisting megacryst and groundmass pyroxenes in basaltic rocks from the southern Highlands of New South Wales and the Massif Central, France.

Although the Ti contents of phenocryst and groundmass clinopyroxenes are variable, in general both phases tend to be richer in Ti than coexisting megacrysts. A plot of Al^{IV} versus Ti for phenocrysts and low-Na groundmass pyroxenes (Fig. 4.3c) indicates a good correlation of these variables in the ratio $2Al^{IV}$:Ti. This is often considered as supporting evidence for the substitution of the hypothetical titanopyroxene molecule, $CaTiAl_2O_6$ (Yagi and Onuma, 1967). The observation that the megacrysts plot above the $2Al^{IV}$:Ti line in Fig. 4.3c confirms the importance of the Ca-Tschermaks component in these pyroxenes and consequently they display higher Al^{IV}/Ti ratios than Ca-rich phenocrysts and groundmass phases.

Le Bas (1962) demonstrated that there are significant differences in the Ti contents of clinopyroxenes crystallized from tholeiitic and alkaline magmas, the latter generally being relatively enriched in Ti. High temperatures and relatively high oxygen fugacities were considered by Verhoogen (1962) to favour the concentration of Ti in silicates rather than in Fe-Ti oxides where both phases coexist. However, Kushiro (1960), Carmichael *et al.* (1970) and Gupta *et al.* (1973) concluded that silica activity of the melt was the most important variable controlling the substitution of the $CaTiAl_2O_6$ component in pyroxenes, and the maximum solid solution of $CaTiAl_2O_6$ in diopside takes place at the lowest SiO_2 activities of the melt.

Substitution of Na in the Nandewar pyroxenes is very limited in the compositional range augite to ferrohedenbergite, except in

clinopyroxene megacrysts where it is probably present as the jadeite component ($NaAlSi_2O_6$). Substitution of the type $NaFe^{3+} \rightarrow CaFe^{2+}$ becomes important in groundmass pyroxenes in peralkaline trachytes and comendites. This is illustrated by the ternary plot of acmite, diopside and hedenbergite (Fig. 4.4) which indicates extensive solid solution between hedenbergite and aegirine. This trend is comparable to those of other mildly alkaline volcanic series, including Oki Dôgo, Japan (Uchimizu, 1966), the Comboyne (Knutson, 1975) and Canobolas Provinces, N.S.W. (Middlemost, 1981), as well as the undersaturated nepheline syenites of the Ilimaussaq intrusion, Greenland (Larsen, 1976). Not all mildly alkaline series show this trend. For example, mildly akaline series such as those of Pantelleria (Carmichael, 1962; Nicholls and Carmichael, 1969); Boina and Erta Ale, Ethiopia (Bizouard *et al.* 1980) display only restricted Na-enrichment over an extended range of host rock compositions.

Although the range of compositions of appropriate Nandewar pyroxenes along the hedenbergite-acmite join is restricted, a miscibility gap similar to that proposed by Aoki (1964) is not evident. Complete solid solution between diopside-hedenbergite solid solutions and acmite has been clearly demonstrated by the experimental data (Yagi, 1966; Nolan, 1969) and by data on natural pyroxene assemblages (King, 1965; Tyler and King, 1967; Nash and Wilkinson, 1970; Stephenson, 1972; Larsen, 1976). However, Ferguson (1978) has argued that in individual rock samples a gap is observed between Ca- and Na-rich pyroxenes when amphibole crystallizes and that this gap may be obscured by considering only the pyroxene compositions of a given series as a whole. Comparable gaps are not apparent in individual Nandewar specimens containing co-existing amphiboles and clinopyroxenes, and the range of pyroxene compositions tends to be relatively more restricted in these samples (see Fig. 4.4) than in those described by Ferguson (1978).

Larsen (1976) showed in a comparison of pyroxene crystallization trends from a variety of magmatic associations that there is considerable variation in the stage of Fe^{2+} enrichment in pyroxenes at which significant substitution of Na occurs. To some extent this is evidenced within single samples from the Nanewar suite by the two differing trends of Na-enrichment illustrated in Fig. 4.4.

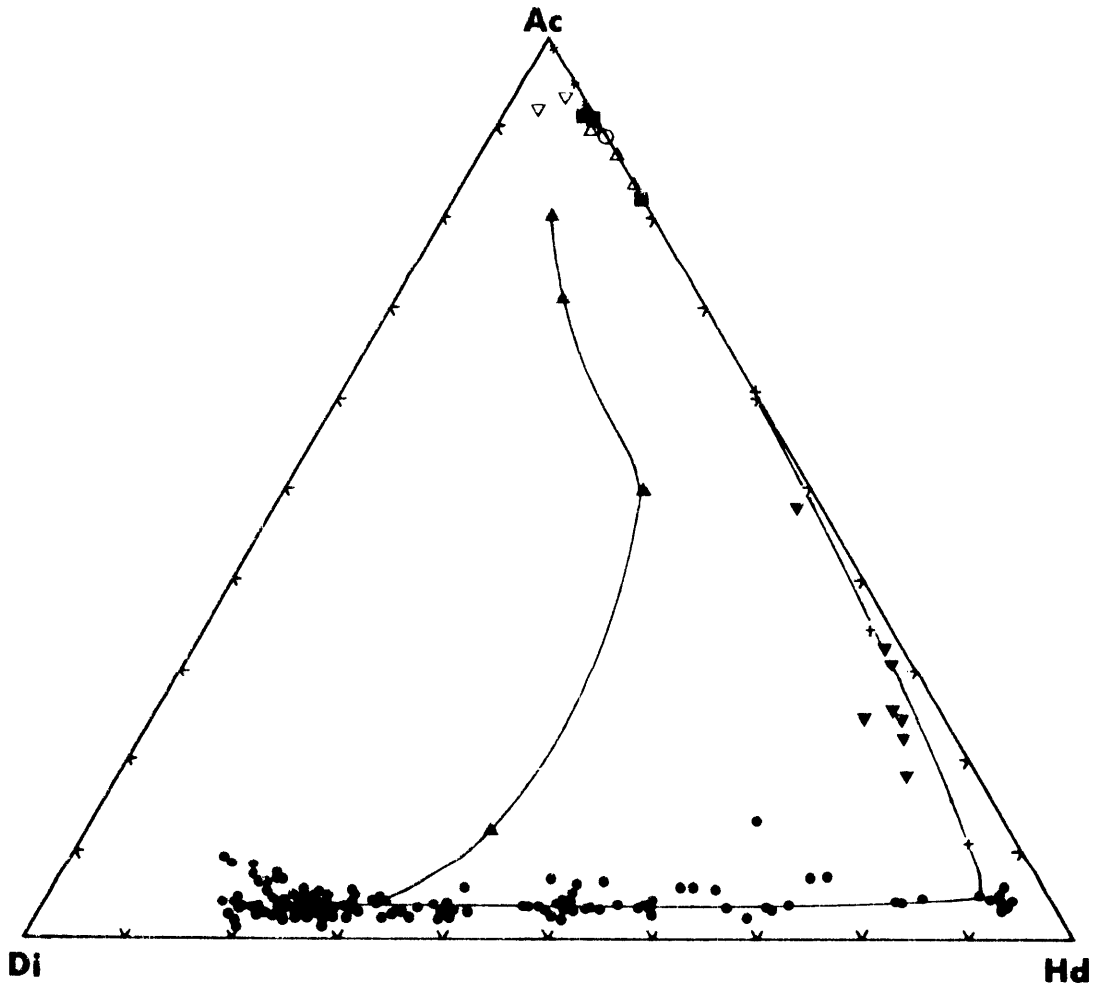

Fig. 4.4: Analyses of Ca-rich and Na-rich pyroxenes plotted in terms of mole percent acmite, diopside and hedenbergite. Ca-rich megacrysts, phenocrysts and groundmass pyroxenes (circles). Other symbols refer to Na-rich pyroxenes from individual samples shown in the key above. Trend lines indicate the various Mg/Fe ratios at which Na enrichment occurs within several different lavas.

The Si contents of the aegirine-hedenbergites (i.e. Mg-poor variants plotting close to the Hd-Ac join; Fig. 4.4) is generally higher than in the ferrohedenbergites. The tetrahedral sites of Na-rich pyroxenes are often completely occupied by Si whereas in several hedenbergites there is insufficient Si and Al to fill this site, the remainder presumably being made up with either Fe^{3+} or Ti^{4+}. Pyroxenes plotting along the acmite-hedenbergite join in Fig. 4.4 also typically have very low Al contents.

Increases in pyroxene Fe^{3+} and Na result in decreasing Mn contents (Fig. 4.3a) and this confirms the coherence of Mn with Fe^{2+}, previously noted for members of the diopside-hedenbergite series. A similar relationship between Fe^{2+} and Mn has been noted from a number of other alkaline associations (Tyler and King, 1967; Nicholls and Carmichael, 1969; Stephenson, 1972; Larsen, 1976).

Zr enrichment in passing from hedenbergite (0.2 wt. percent ZrO_2) to aegirine (maximum 2.3 wt. percent ZrO_2) is comparable with that displayed by analogous pyroxenes from the Ilimaussaq intrusion (Larsen, 1976) and the Gardiner complex, east Greenland (Nielsen, 1979) but substantially less than in the pyroxenes from the Motzfeldt centre, south Greenland (Jones and Peckett, 1980). The latter authors suggested that aegirines with up to 7.0 wt. percent ZrO_2 confirm the existence of a Zr-pyroxene end-member ($Na(Mg,Fe)_{0.5}Zr_{0.5}Si_2O_6$).

The Ti contents of Nandewar pyroxenes plotting along the acmite-hedenbergite join (Fig. 4.4) are variable but generally increase from hedenbergite to aegirine, and TiO_2 attains a maximum of 3.5 wt. percent in groundmass aegirines from several comendites and peralkaline trachytes. The highly variable Ti contents of the Na-rich groundmass pyroxenes are well illustrated by differences of up to 100 percent in the relative Ti abundances in pyroxenes from the same specimen. The Ti contents of aegirines from the Nandewar rocks are comparable to those in aegirines from alkali syenites from Morotu (Grapes *et al.*, 1979), but they are only one half to one third of the abundances reported by Ferguson (1977) and Nielsen (1979) from a variety of other alkaline hosts. Substitution of Ti in aegirine is accompanied by increases in Zr, Na and possibly Mg and Mn, and by a decrease in Fe^{3+}. The preferred model for Ti substitution in aegirines involves the solid solution between $NaFe^{3+}Si_2O_6$ and a

neptunite end-member of the general form

$$R^{+}\ R^{2+}_{0.5}R^{4+}_{0.5}Si_2O_6$$

where R^{+} is Na±Ca±K±Li

R^{2+} is Fe^{2+},Mg,Mn±Zn

R^{4+} is Ti, Zr

as proposed by Pedersen *et al.* (1975), Ferguson (1977) and Nielsen (1979). This model is preferred because alternative models involving substitutions of the form $NaTi(AlSi)O_6$ and $NaTi(Fe^{3+}Si)O_6$ (Flower, 1974), are incapable of maintaining a charge balance for the high Ti contents involved where there is nearly complete occupancy of the tetrahedral sites by Si.

Conditions of Crystallization

Pyroxene Megacrysts

It is now generally accepted that pyroxene megacrysts in alkaline hosts are high-pressure precipitates and this interpretation is based partly on textural evidence, such as well developed crystal faces and low-pressure reaction rims (Binns *et al.*, 1970), and partly on chemical data. The latter indicate the close similarity of pyroxene megacryst compositions with those produced in appropriate high-pressure experimental studies (Green and Hibberson, 1970; Knutson and Green, 1975).

An important characteristic of high-pressure clinopyroxenes (in garnet-free assemblages) is a high Ca-Tschermak's component (Clarke *et al.*, 1962; Kushiro, 1962). Orthopyroxene megacrysts coexisting with aluminian augite or occurring as discrete phases in the same rock are also characterized by moderately high Al^{VI}. Boyd and England (1964) suggested that substitution of Al in orthopyroxene is largely pressure dependent whereas Anastasiou and Seifert (1972), on the basis of experimental data in the system $MgO-Al_2O_3-H_2O$, concluded that temperature is the more important control. Duggan and Wilkinson (1973) observed that in orthopyroxenes crystallizing from complex natural systems under conditions of approximately constant temperature, Al increases with increasing pressure. This suggests that the experimental work of Anastasiou and Seifert (1972) may not be directly applicable to natural systems.

Where appropriate, several geothermometers utilizing the compositions of coexisting clino- and orthopyroxenes (Wood and Banno, 1973; Wells,

1977) and pyroxene/melt equilibria (Nielsen and Drake, 1979) have been applied to obtain estimates of the temperatures at which the Nandewar pyroxenes began to crystallize. Other geothermometers based on olivine-clinopyroxene equilibria (Powell and Powell, 1974) and pyroxene-ilmenite equilibria (Bishop, 1980) are of questionable value (Wood, 1976b; D'arco and Maury, 1981). Calculated pyroxene crystallization temperatures for a number of specimens are presented in Table 4.5. These can be compared with temperatures calculated for the same rocks using coexisting Fe-Ti oxides (Buddington and Lindsley, 1964; Spencer and Lindsley, 1981) and plagioclase/liquid data (Kudo and Weill, 1970) and listed in Tables 4.9 and 4.11, respectively.

Application of a two-pyroxene geothermometer is not strictly justified for coexisting orthopyroxene and clinopyroxene megacrysts, because the two phases may not necessarily have been in equilibrium. This constraint is particularly relevant for one of the orthopyroxene megacrysts in specimen 49008 which was previously interpreted on composition grounds (i.e. higher *M*-value than coexisting orthopyroxene megacrysts) to be xenocrystal. The calculated temperature for this analysis using the Wood-Banno method is ~50^{o}C higher than those for the more Fe-rich coexisting orthopyroxene megacrysts. However, temperatures calculated for the same analyses using the data of Wells (1977) display much less variation (cf. Table 4.5). The calculated temperature for a websterite inclusion in trachyandesite 49005 (1000^{o}C) is probably a subsolidus temperature and this is supported by the presence of exsolution lamellae in the clino-pyroxene.

In general pyroxene crystallization temperatures based on the data of Wells (1977) are in quite good agreement with plagioclase/liquid temperatures calculated following Kudo and Weill (1970) for P_{H_2O} = 0.5 kb, and with experimentally-determined pyroxene crystallization temperatures on rocks with similar composition to the Nandewar trachyandesites (Knutson and Green, 1975). D'arco and Maury (1981) found closer agreement between temperatures calculated using the Wood-Banno method and those based on coexisting Fe-Ti oxides (Buddington and Lindsley, 1964) compared with those calculated according to Wells (1977). However, some experimental data on rocks of similar composition (Knutson and Green, 1975) indicate that at reasonable water contents and moderate pressures, clinopyroxene

Table 4.5

Calculated crystallization temperatures (^{o}C) of coexisting pyroxenes and from pyroxene/melt equilibria (Nielsen and Drake, 1979)

Sample No.	Wood and Banno (1973)	Wells (1977)	Nielsen and Drake (1979) Opx/Liq	Cpx/Liq
49005 (cumulate)	1002	993		
49008	1115	1110		
49008	1063	1101	1104	1116
49008	1061	1117		
49009	1068	1088	1107	1184
49000				1161
49001				1180
49002				1145
49003				1160
49004				1122
49005				1122
49007				1112
49011				1099
49012				1095
49013				1095
49070				1097
49076				1091
49077				1102
49078				1212
49079				1259
49081				1099

may be the liquidus phase, followed by olivine and later by plagioclase and Fe-Ti oxides at some 50 to 100°C below the liquidus. It is evident that comparison of crystallization temperatures based on various mineral/liquid or mineral pairs should be made with some caution because of the dependence of mineral crystallization temperatures on bulk composition, P and a_{H_2O}.

Temperatures estimated from pyroxene/liquid equilibria (Nielsen and Drake, 1979) are comparable to, or usually a little higher than the plagioclase/liquid temperatures (Kudo and Weill, 1970), and reflect the slightly earlier precipitation of clinopyroxene from these liquids.

The duplication of megacryst assemblages and compositions via experimental studies provides strong evidence that the megacrysts have precipitated from their hosts and hence are cognate. The megacryst-bearing Nandewar rocks and megacryst compositions most closely resemble those described by Knutson and Green (1975) from the Comboyne province, N.S.W. An Auckland Island basalt (Green and Hibberson, 1970) has a higher *M* value (*M* = 66) and its clinopyroxene megacrysts, which are considered to have crystallized at about 1200°C and pressures of 14-16 kb, are considerably less calcic ($Ca_{33}Mg_{56}Fe_{11}$) than the Nandewar clinopyroxene megacrysts ($Ca_{41}Mg_{47}Fe_{12}$).

By analogy with the experimental data of Knutson and Green (1975) and the geothermometric data, the Nandewar pyroxene megacryst assemblages probably precipitated from their hosts at temperatures of 1100 to 1150°C and pressures of 6 to 7 kb from melts containing approximately 2 wt. percent H_2O. The good correlation between experimental and natural megacryst compositions and appropriate host rock conditions provides strong support for a cognate relationship. However, some megacryst assemblages may represent a random sample of phases precipitated from either the host magma and/or derivative and/or parental magmas (Irving, 1974a; Stuckless and Irving, 1976).

Low-pressure Pyroxenes

Most clinopyroxene phenocrysts and microphenocrysts probably crystallized under relatively low-pressure conditions, suggested by low Al^{VI} contents, and precipitation possibly occurred during residence in a high-level magma chamber or conduit prior to extrusion. The groundmass

pyroxenes plotting along the diopside-ferrohedenbergite join (Fig. 4.2) probably represent quench products following extrusion of the magma. Although the more sodic groundmass phases are only rarely observed protruding into vesicles, some may be precipitates from a late-stage volatile-rich phase (Ferguson, 1978).

Substitution of $NaFe^{3+}$ for $Ca(Mg,Fe^{2+})$ in pyroxenes from undersaturated volcanic series and intrusive complexes occurs at an earlier stage of Fe-enrichment than in oversaturated volcanic series, the exception being the Ilimaussaq intrusion, south Greenland (Larsen, 1976) which has a pyroxene trend closely comparable with the Nandewar series. Larsen (1976) considered that this trend resulted from crystallization of the Ilimaussaq syenites under lower oxygen fugacities than most other undersaturated rock series described. Differing trends of Na-enrichment in pyroxenes from different portions of the Shonkin Sag laccolith were attributed by Nash and Wilkinson (1970) to slightly different T and fO_2 conditions during crystallization resulting from changes in the nature of the 'internal buffer' assemblage and presumably bulk composition.

Experimental data have indicated that the stability of acmite (Bailey, 1969; Gilbert, 1969) is sensitive to fluctuations in oxygen fugacity, although relatively insensitive to changes in total pressure. In synthetic systems acmite is stable under very low oxygen fugacities, in equilibrium with a fayalite-magnetite-quartz (FMQ) assemblage and iron metal, respectively (Bailey, 1969; Gilbert, 1969). However, in natural assemblages aegirine does not necessarily appear to crystallize under such highly reduced conditions. In pantellerites from Pantelleria (Carmichael, 1962; Nicholls and Carmichael, 1969) and Ethiopia (Bizouard *et al.*, 1980) the pyroxene phenocrysts interpreted to have crystallized under fO_2 conditions equal to or slightly less than those defined by the FMQ buffer, are sodic ferrohedenbergites. Olivine is absent from Nandewar rocks which contain aegirine, and in rocks where titanomagnetite or ilmenite occur as microphenocrysts, these phases are rimmed by aenigmatite. This suggests that in the natural systems, crystallization of aegirine occurs under oxygen fugacities not controlled by the FMQ buffer and also supports the concept of a 'no-oxide' field in T-fO_2 space suggested by Nicholls and Carmichael (1969). Nash and Wilkinson (1970) noted that the appearance of Na-rich pyroxenes in the Shonkin Sag

intrusion coincided with the disappearance of olivine and relatively enhanced fO_2 of the magma subsequently buffered by the assemblage annite-magnetite-alkali feldspar.

Although the stability of aegirine is clearly sensitive to fluctuations in fO_2, it is difficult to estimate the relative importance of controls such as liquid composition, T and fO_2 on the development of the four major mafic groundmass assemblages in the Nandewar peralkaline rhyolites and trachytes. These assemblages are:

1) Na-rich pyroxene + aenigmatite + arfvedsonite
2) aegirine + arfvedsonite
3) aenigmatite + arfvedsonite
4) arfvedsonite.

The coexistence of Na-rich pyroxenes with aenigmatite and arfvedsonite (the latter two phases are considered to be unstable at oxygen fugacities significantly greater than those of the FMQ buffer (Bailey, 1969; Lindsley, 1971) suggests that liquid composition may also be important in controlling the stability of these assemblages. For example, Bailey (1969) concluded that acmite only crystallizes from liquids containing excess Na_2SiO_3, given that T and fO_2 are appropriate. Increases in the Fe^{3+}/Fe^{2+} ratio of the liquids accompany increases in alkali content (Paul and Douglas, 1965; Carmichael and Nicholls, 1967; Kogarko, 1974) and this, together with an increase in the Na/Fe^{2+} ratio of the liquid, may assist in stabilizing aegirine together with arfvedsonite and aenigmatite under oxygen fugacity conditions which are possibly not the most favourable for the crystallization of aegirine alone. Lower Na/Fe^{2+} ratios and high P_{F_2} and P_{H_2O} conditions would favour the precipitation of arfvedsonite (Ernst, 1968). The effect of high P_{F_2}, an accepted feature of peralkaline acid liquids (Kogarko, 1974), is to decrease the oxygen fugacity.

The coexistence of aegirine and arfvedsonite (devoid of a reaction relationship) in the groundmass of peralkaline lavas supports the suggestion of Nash and Wilkinson (1970) that they are stable over a narrow T-fO_2 and perhaps compositional range.

Occurrence of groundmass Na-rich pyroxenes which protrude into

vesicles in mafic trachyte 49097, a significantly less evolved (non-peralkaline) liquid than the other aegirine-bearing rocks, suggests a different control on its formation. Growth into vesicles together with evidence of late-magmatic oxidation effects suggests that the aegirine precipitated from a Na, Fe, H_2O-rich phase during degassing of the lava. The absence of coexisting F-rich amphiboles indicates that P_{F_2} was low, compared with the peralkaline lavas and oxidation may have occurred as a result of selective hydrogen loss in a gaseous phase following dissociation of H_2O (Sato, 1978).

AMPHIBOLES

Occurrence

Sodic-calcic and sodic amphiboles occur in the groundmass of Nandewar volcanics ranging in composition from trachyandesite to comendite.

Several trachyandesites have minor edenitic amphibole anhedra occurring interstitially to groundmass feldspar laths. Amphibole of similar composition also occurs in inclusions of trachyandesite within tristanite 49081.

Although amphibole has not been observed in the tristanites, it is relatively abundant as reaction rims on augite in a monzonitic pluton, which is probably the intrusive equivalent of the tristanite lavas.

Most of the mafic and peralkaline trachytes contain one or two species of amphibole as a groundmass phase interstitial to laths of alkali feldspar and associated with aegirine-hedenbergite, aegirine, or aenigmatite.

The alkali rhyolites are largely devoid of mafic minerals except in a few instances where minor amphibole occurs in the groundmass. Amphibole is the dominant mafic constituent of the comendites where it is occasionally accompanied by minor aegirine.

Compositional Variation

Representative amphibole analyses are presented in Table 4.6 with structural formulae calculated on the basis of 23 oxygens anhydrous. An

TABLE 4.6

Analyses of Amphiboles

	Trachyandesites		Monzonite		Tristanite	Trachytes					
Rock Number	49009 E	49009 E	49070 C F-E	49070 R F-A	49081 Inc. E	49082 R	49082 F-R	49083 F-R	49084 E	49084Inc. E	49085 F-R
SiO_2	46.57	46.66	46.18	46.77	47.69	50.22	51.04	51.44	49.22	47.73	49.55
TiO_2	1.24	1.31	1.08	-	1.24	1.95	2.17	1.64	0.63	0.93	1.91
Al_2O_3	6.72	5.46	5.36	3.13	4.98	1.27	1.14	1.17	4.04	5.79	1.28
FeO*	16.07	17.15	21.49	36.04	16.17	18.11	21.43	20.46	16.74	17.53	27.66
MnO	0.36	0.40	0.47	1.27	0.26	0.48	0.41	0.52	0.37	0.53	0.65
MgO	13.12	13.06	10.07	0.26	13.78	11.30	8.98	10.20	12.69	11.63	4.88
CaO	9.87	10.21	10.02	10.01	9.90	6.11	5.38	5.83	9.62	9.62	5.48
Na_2O	3.31	2.95	2.22	0.79	3.07	5.74	6.09	5.62	2.87	2.93	5.98
K_2O	1.04	1.08	1.04	0.29	1.00	1.20	1.35	1.42	1.07	1.27	1.41
Total	98.30	98.28	97.93	98.56	98.09	96.38	97.99	98.30	97.25	97.96	98.80
Structural Formulae on the Basis of 23 Oxygen Atoms											
Si	6.927	6.988	7.062	7.557	7.097	7.665	7.747	7.745	7.374	7.153	7.713
Al^{iv}	1.073	0.964	0.938	0.443	0.874	0.228	0.204	0.208	0.626	0.847	0.235
Al^{vi}	0.105	-	0.029	0.153	-	-	-	-	0.088	0.176	-
Ti	0.139	0.148	0.124	-	0.139	0.224	0.248	0.186	0.071	0.105	0.224
Fe^{2+}	1.999	2.148	2.749	4.870	2.013	2.309	2.720	2.576	2.097	2.197	3.601
Mn	0.045	0.051	0.061	0.174	0.033	0.062	0.053	0.066	0.047	0.067	0.086
Mg	2.908	2.915	2.295	0.063	3.056	2.567	2.031	2.289	2.833	2.597	1.132
Ca	1.573	1.638	1.642	1.733	1.579	0.998	0.875	0.941	1.544	1.544	0.914
Na	0.955	0.857	0.658	0.248	0.886	1.697	1.792	1.641	0.834	0.851	1.805
K	0.197	0.206	0.203	0.060	0.190	0.233	0.261	0.273	0.205	0.243	0.280
Z	8.000	7.952	8.000	8.000	7.971	7.893	7.951	7.953	8.000	8.000	7.948
Y	5.196	5.262	5.258	5.259	5.241	5.161	5.052	5.117	5.136	5.140	5.043
X	2.725	2.701	2.503	2.041	2.655	2.928	2.928	2.855	2.583	2.638	2.999
$100Mg/Mg+Fe^{2+}$	59.3	57.6	45.5	1.3	60.3	52.7	42.8	47.1	57.5	54.2	23.9

	Trachytes										
Rock Number	49088 K	49088 A	49089 A	49090 A	49098 A	49099 A	49100 A	49101 A-K	49101 A	49102 F-R	49102 A
SiO_2	45.40	48.18	48.90	49.79	49.27	50.59	49.32	47.52	49.92	49.37	52.82
TiO_2	3.05	2.68	2.98	0.32	1.50	0.45	0.23	0.68	-	1.75	1.54
Al_2O_3	6.10	1.68	0.71	0.47	0.81	0.75	0.58	12.45	0.56	1.06	5.97
FeO*	30.27	32.57	33.46	35.11	34.02	32.69	34.66	25.09	35.32	30.04	24.20
MnO	0.62	0.76	0.84	1.36	0.79	1.14	1.23	0.55	1.31	0.83	0.59
MgO	1.27	1.05	0.82	0.28	0.48	0.57	0.32	0.20	-	2.70	1.17
CaO	4.25	3.62	2.86	1.02	2.67	2.59	2.99	4.83	2.31	4.25	2.51
Na_2O	5.90	6.55	7.11	8.01	7.20	7.76	7.47	5.64	7.43	5.95	6.92
K_2O	1.37	1.48	1.39	1.65	1.46	1.60	1.40	0.85	1.36	1.57	2.70
Total	98.23	98.57	99.07	98.01	98.20	98.14	98.20	97.81	98.21	97.52	98.42
Structural Formulae on the Basis of 23 Oxygen Atoms											
Si	7.199	7.696	7.794	8.080	7.934	8.099	7.997	7.238	8.084	7.863	7.986
Al^{iv}	0.801	0.304	0.133	-	0.066	-	0.003	0.762	-	0.137	0.014
Al^{vi}	0.339	0.013	-	0.090	0.087	0.142	0.108	1.473	0.107	0.062	1.051
Ti	0.364	0.322	0.357	0.039	0.182	0.054	0.028	0.078	-	0.210	0.175
Fe^{2+}	4.014	4.351	4.460	4.765	4.581	4.377	4.700	3.196	4.784	4.001	3.060
Mn	0.083	0.103	0.113	0.187	0.108	0.155	0.169	0.071	0.180	0.112	0.076
Mg	0.300	0.250	0.195	0.068	0.115	0.136	0.077	0.045	-	0.641	0.264
Ca	0.722	0.620	0.489	0.177	0.461	0.444	0.520	0.788	0.401	0.725	0.407
Na	1.814	2.029	2.197	2.520	2.248	2.409	2.348	1.666	2.333	1.837	2.029
K	0.277	0.302	0.283	0.342	0.300	0.327	0.290	0.165	0.281	0.319	0.521
Z	8.000	8.000	7.928	8.080	8.000	8.099	8.000	8.000	8.084	8.000	8.000
Y	5.100	5.039	5.126	5.149	5.073	4.864	5.082	4.863	5.071	5.025	4.625
X	2.813	2.951	2.969	3.039	3.009	3.180	3.158	2.619	3.015	2.881	2.957
$100Mg/Mg+Fe^{2+}$	7.0	5.4	4.2	1.4	2.5	3.0	1.6	1.4	0.0	13.8	7.9

* - Total Fe as FeO

C - Core

R - Rim

Inc. - Occurring within inclusion

E - Edenite

F-E - Ferro-edenite

F-A - Ferro-actinolite

R - Richterite

F-R - Ferro-richterite

K - Kataphorite

A-K - Alumino-kataphorite

A - Arfvedsonite

TABLE 4.6 (continued)

Analyses of Amphiboles

	Trachytes						Comendites			
Rock No.	49103 F-R	49104 A	49104 A	49107 A	49108 A	49108 A	49129 A	49129 A	49163 A	49164 A
SiO_2	48.45	49.74	50.51	49.30	48.24	50.34	49.10	49.95	50.46	50.32
TiO_2	2.52	0.60	0.20	2.55	2.48	0.54	0.66	0.39	1.08	0.35
Al_2O_3	1.45	0.75	0.73	0.76	0.99	0.63	0.79	0.63	0.76	0.78
Fe_2O_3	-	-	-	-	-	-	8.75	-	-	-
FeO*	32.21	33.90	35.52	32.71	34.14	34.01	26.55†	33.99	34.38	32.26
MnO	0.72	1.13	1.26	0.78	1.00	1.12	1.21	1.40	0.82	1.72
MgO	1.34	0.60	-	1.30	0.28	-	0.52	-	-	-
CaO	4.09	2.22	0.80	3.14	3.07	0.77	1.87	2.04	0.96	0.98
Na_2O	6.53	7.58	8.17	6.73	6.46	8.13	7.38	7.69	8.85	8.55
K_2O	1.55	1.44	1.38	1.52	1.24	1.67	1.39	1.43	1.40	1.51
H_2O	-	-	-	-	-	-	0.67	-	-	-
Total	98.86	97.96	98.57	98.79	97.90	97.21	98.89	97.52	98.71	96.47
	Structural Formulae on the Basis of 23 Oxygen Atoms									
Si	7.712	8.025	8.122	7.842	7.807	8.167	7.814	8.104	8.069	8.192
Al^{iv}	0.272	-	-	0.143	0.189	-	0.148	-	-	-
Al^{vi}	-	0.143	0.138	-	-	0.121	-	0.121	0.143	0.150
Ti	0.302	0.073	0.024	0.305	0.302	0.066	0.079	0.048	0.130	0.043
Fe^{3+}	-	-	-	-	-	-	1.049	-	-	-
Fe^{2+}	4.288	4.574	4.777	4.352	4.621	4.615	3.534	4.612	4.598	4.392
Mn	0.097	0.154	0.172	0.105	0.137	0.154	0.163	0.192	0.111	0.237
Mg	0.318	0.144	-	0.308	0.068	-	0.123	-	-	-
Ca	0.698	0.384	0.138	0.535	0.532	0.134	0.319	0.355	0.165	0.171
Na	2.015	2.371	2.547	2.076	2.027	2.557	2.277	2.419	2.744	2.699
K	0.315	0.296	0.283	0.309	0.256	0.346	0.282	0.296	0.286	0.314
Z	7.984	8.025	8.122	7.985	7.996	8.167	7.962	8.104	8.069	8.192
Y	5.005	5.088	5.111	5.070	5.128	4.802	4.948	4.973	4.982	4.822
X	3.028	3.051	2.968	2.920	2.815	3.037	2.878	3.070	3.195	3.184

* - Total Fe as FeO
† - Measured FeO, analysis by XRF and wet chemical techniques
F-R - Ferro-richterite
A - Arfvedsonite

attempt was made to calculate Fe_2O_3 values using a charge balance equation (Papike *et al.*, 1974), but poor agreement between the calculated and analyzed Fe_2O_3 contents of an arfvedsonite separated from alkali rhyolite 49129 indicated that this method is not applicable, at least to amphiboles of that composition. A further comparison of calculated with analyzed Fe_2O_3 values on a range of sodic-calcic and sodic amphiboles tabulated by Deer *et al.* (1962a) supported this conclusion.

The classification scheme proposed by Leake (1978) was adopted for amphibole nomenclature, even though some knowledge of Fe^{3+} is necessary to distinguish some types. For the amphiboles under discussion the only ambiguity concerned the distinction between arfvedsonite and ferro-eckermannite which is based on the $Fe^{3+}/(Fe^{3+}+Al^{VI})$ ratio. In the majority of cases the very low Al contents of these amphiboles (even with the apparently low calculated Fe_2O_3 values) indicated they are arfvedsonites (i.e. $Fe^{3+}/(Fe^{3+}+Al^{VI}) > 0.5$). In several instances where the calculated Fe_2O_3 value was zero, even with low Al^{VI} contents the amphiboles strictly classify as ferro-eckermannites. However, in view of the likelihood that the calculated Fe_2O_3 values have been considerably under-estimated, these amphiboles are probably best described as arfvedsonites.

The calciferous amphiboles in the trachyandesites (e.g. Table 4.6, No. 49009) are edenites (approximately $NaCa_2Mg_3Fe_2^{2+}Si_7AlO_{22}(OH)_2$), whereas slightly more Fe-rich ferro-edenites occur in the monzonite. The latter are often strongly zoned (Mg_{46} core to Mg_1 rim, Table 4.6, No. 49070) to rims of ferro-actinolite ($Ca_2Fe_5^{2+}Si_8O_{22}(OH)_2$), indicating that the coupled substitution $Si \rightleftarrows NaAl$ has been the dominant substitution in the amphibole crystallizing in the monzonite.

Substitution of the type $NaSi \rightleftarrows CaAl$ in edenite gives rise to the richterites ($NaCaNaMg_5Si_8O_{22}(OH)_2$; e.g. Table 4.6 No. 49082) and ferro-richterites ($NaCaNaFe_5^{2+}Si_8O_{22}(OH)_2$; e.g. Table 4.6, No. 49083) that are characteristic of the mafic trachytes. Arfvedsonite (e.g. Table 4.6, No. 49088) and katophorite ($NaCaNaFe_4^{2+}Fe^{3+}Si_7AlO_{22}(OH)_2$; e.g. Table 4.6, No. 49088) are occasionally associated with ferro-richterite in these rocks.

Arfvedsonite is the principal variety of amphibole in the peralkaline trachytes (e.g. Table 4.6, No. 49098) and comendites

(e.g. Table 4.6, No. 49163), although a little alumino-katophorite ($NaCaNaFe_4^{2+}AlSi_7AlO_{22}(OH)_2$ also occurs in one peralkaline trachyte (Table 4.6, No.49101).

Increasing Na contents with corresponding decrease in Ca and Al in the transition from edenite to arfvedsonite compositions are illustrated in Figs 4.5a and b. A ternary plot of Na-Mg-Ca (Fig. 4.6a), regarded by Larsen (1976) as analogous to the Ac-Di-Hd plot for pyroxenes (Ca ~ Fe^{2+}+Mn for Mg-poor Ca-rich pyroxenes), indicates a different trend of amphibole compositional variation than for the pyroxenes. The most noteable difference between the amphibole and pyroxene trends relates to the consistently higher Mg content of the amphiboles at a given Na/Ca ratio. Mg content of the amphibole decreases consistently from the edenites to the arfvedsonites with decreasing Mg content of the host. This diagram also illustrates the essentially continuous compositional variation between the ferro-richterites and arfvedsonites. This contrasts with the marked gaps between the edenites, richterites and ferro-richterites.

The Nandewar amphiboles are comparable to those of many other alkaline volcanic associations. In particular, ferro-richterites and arfvedsonites are common constituenets of both oversaturated and undersaturated salic rocks (cf. Borley, 1963; de Keyser, 1966; Frisch, 1970; Stull, 1973; Neumann, 1976; Larsen, 1976; Thompson, 1976; Grapes *et al.*, 1979), but edenite appears to be a relatively rare constituent in alkaline hosts. Members of the more Al-rich magnesio-hastingsite-hastingsite series tend to be the characteristic calciferous amphibole in miascitic syenites and nepheline syenites (cf. Frisch, 1970; Stull, 1973; Neumann, 1976; Larsen, 1976).

With the exception of the edenites and katophorites, the Al content of the Nandewar amphiboles is generally low and most is located in tetrahedral sites. Occasionally in the richterites there is insufficient Si and Al to fill the tetrahedral sites, indicating that a small amount of Fe^{3+} may also occur in that position (up to 0.1 atoms/formula unit). The arfvedsonites usually have sufficient Si alone to fill the tetrahedral sites, and indeed there may be a slight excess of Si. Most of this apparent excess would disappear if Fe^{3+} were taken into account in the structural formula calculation.

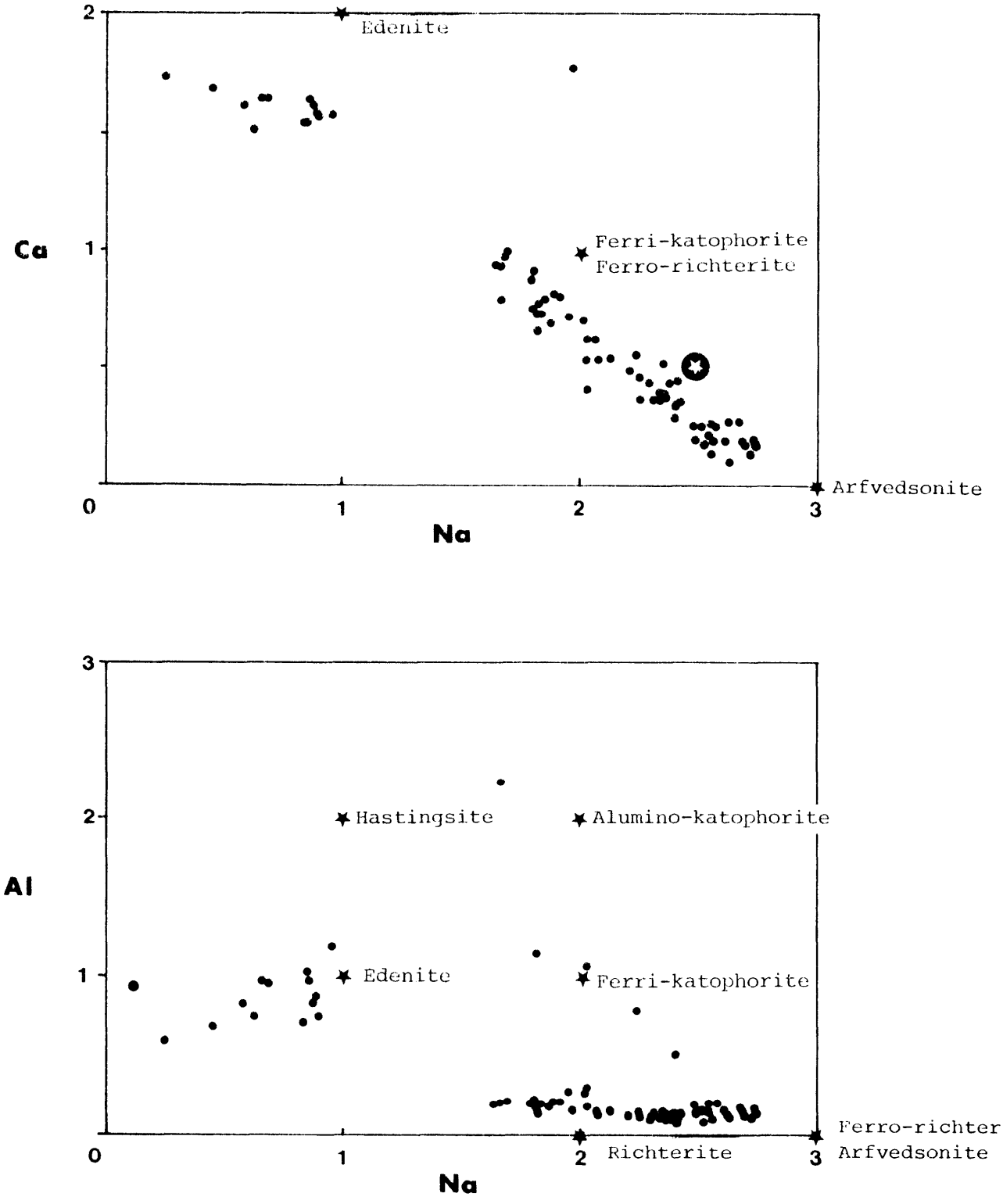

Fig. 4.5: Plot of (a) Ca versus Na and (b) Al versus Na for the Nandewar amphiboles showing the positions of the various end-member species and the composition of natural arfvedsonites (asterisk in circle) given by Miyashiro (1957). Scales are cations per 23 oxygens.

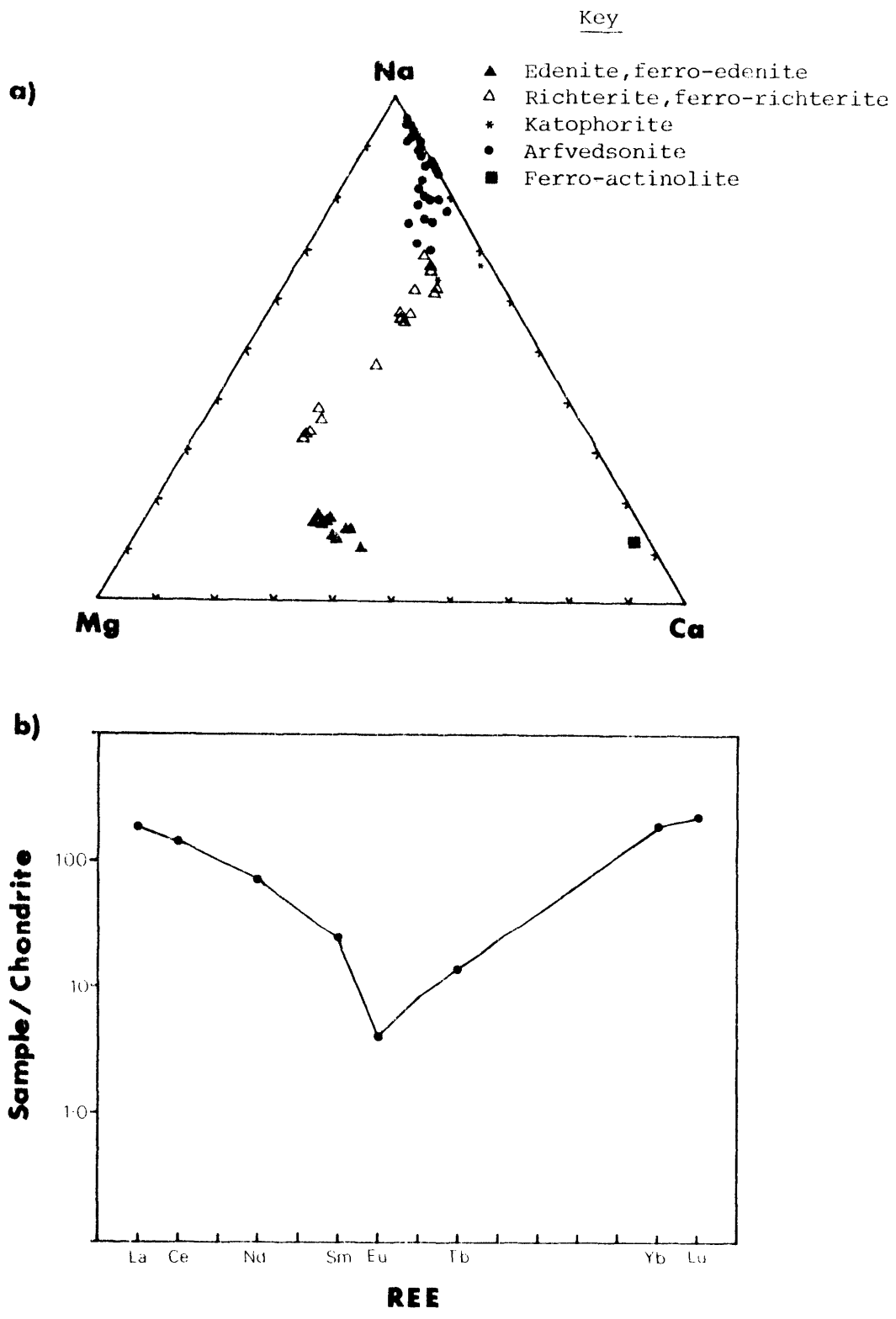

Fig. 4.6 (a) Plot of Na-Mg-Ca (atom percent) for amphiboles from trachyandesites, trachytes and comendites.

(b) Chondrite-normalized plot of REE for arfvedsonite separated from sample 49129.

The Y-sites of most edenites, ferro-edenites, richterites and ferro-richterites contain the 'ideal' 5 atoms or a slight excess, whereas many of the arfvedsonites contain less than the 5 atoms/formula unit. A survey of sodic amphiboles from the literature (Hawthorne, 1976) has indicated that this is a common phenomenon. Hawthorne (*loc. cit.*) observed an inverse correlation between X-group and Y-group sums of these amphiboles and suggested, since vacancies are unlikely to occur in Y-sites, that Ca, normally allocated only to M4 sites, may also substitute to a limited extent in octahedral sites.

In general the Mn content of the amphiboles increases in the transition from edenite to arfvedsonite compositions. Substitution of Mn in the ferro-richterites and arfvedsonites appears to depend, at least in part, on the composition of the coexisting pyroxene. Amphiboles coexisting with ferrohedenbergite contain about the same or a little less Mn than the coexisting pyroxene. However, the Mn content of amphiboles is considerably higher than that of coexisting Na-rich pyroxenes.

Substitution of Zr in the amphiboles is less extensive than in the sodic pyroxenes. Although Zr (0.28 wt. percent ZrO_2) was determined on only one arfvedsonite separated from an alkali rhyolite (49129), visual inspection of microprobe spectra indicated similar or lower levels in the majority of analyzed amphiboles. These observations are broadly in agreement with those of Larsen (1976) who found that Zr was preferentially concentrated in Na-rich pyroxenes relative to coexisting alkali amphiboles.

Trace element data on the separated arfvedsonite and its host are presented in Table 4.7 for comparison. This amphibole is often found projecting into vesicles and apparently it has crystallized from a volatile-rich liquid phase.

The most noteable features of Table 4.7 are extremely high concentrations of Li, Zn, Zr and Nb in the amphibole compared to the host, and the concentration of HREE in the amphibole. This latter feature is well illustrated by the chondrite-normalized REE plot for the amphibole (Fig. 4.6b). These data indicate that Li, Zn, Zr, Nb and the REE were relatively concentrated in the interstitial liquid phase as crystallization proceeded and ultimately concentrated in the

Table 4.7

Trace element (μg/g) in arfvedsonite (49129) and its host alkali rhyolite

	Arfvedsonite	Host
Li	765	18
Sc	3.6	-
V	n.d.	2
Cr	n.d.	n.d.
Ni	n.d.	8
Cu	9	4
Zn	1360	75
Rb	21	187
Sr	n.d.	n.d.
Y	66	95
Zr	2048	833
Nb	577	151
Ba	n.d.	7
La	59	142
Ce	116	214
Nd	43	109
Sm	4.9	-
Eu	0.30	-
Tb	0.69	-
Yb	39.7	-
Lu	7.4	-
Hf	41	-
Ta	11.2	-
Pb	16	21
Th	2.1	21
U	1.2	-

n.d. - not detected
- - not determined

latest crystallizing phase (amphibole). The LREE and Rb show a relative depletion in the amphibole with respect to the host reflecting their partitioning into the liquid/volatile phase. If indeed these elements were concentrated in the liquid phase from which the amphibole precipitated, which appears reasonable from their accepted geochemical behaviour, then assuming that the amphibole was the last phase to crystallize, it seems likely that a proportion of these elements have since been lost from the system.

Discussion

Experimental data on the stability relations of richterite-ferro-richterite solid solutions (Charles, 1975,1977), indicated that their maximum temperature stability is strongly dependent on composition and oxygen fugacity. The Mg end-member (richterite) is stable to 1030°C at 1 kb P_{total} for a wide range of oxygen fugacities. However, ferro-richterite on the IW buffer is stable to only 715°C at 1 kb P_{total}, and with increasing oxygen fugacity the maximum temperature stability of ferro-richterite decreases (525°C at 1 kb and the FMQ buffer). These data indicate that the Nandewar ferro-richterites precipitated at temperatures between approximately 650° and 750°C under low to moderate oxygen fugacities (probably between the MW and FMQ buffers). This is in agreement with conclusions based on experimentally determined stability relations of pyroxenes and aenigmatite from the same host rocks.

Charles (1975) suggested that the appearance of richterite was favoured by melts characterized by normative *qz* and metasilicate, high volatile content, and low fO_2 for iron-rich varieties. The general restriction of richterite and ferro-richterite to mafic trachytes of the Nandewar suite contrasts with the dominance of arfvedsonite in more evolved peralkaline lavas, while the transitional alkaline and peralkaline varieties may have ferro-richterite coexisting with arfvedsonite or katophorite. This apparent host rock control on the paragenesis of these phases probably reflects the decreasing melt Ca contents in passing from mafic to peralkaline trachytes.

Charles (1975) also suggested a reaction relationship between aegirine-hedenbergite pyroxenes and fayalite, magnetite, quartz and vapour to give ferro-richterite with decreasing oxygen fugacities; with

an analogous relationship between acmite and arfvedsonite. The co-existence of aegirine-hedenbergite and arfvedsonite in the groundmass of specimens 49098 and 49099, and the absence of ferro-richterite, suggests that arfvedsonite may be stable to higher oxygen fugacities than ferro-richterite at comparable temperatures.

Experimental studies on the stability of riebeckite-arfvedsonite solid solutions (Ernst, 1957,1959,1962,1968) indicate that arfvedsonite is stable to lower temperatures than ferro-richterite, although the high temperature stability limit of the former is extended in the presence of a F-rich volatile phase. Ernst (1962) determined that riebeckite-arfvedsonite is stable up to 655°C at 250 bars P_{fluid} and 712°C at 2000 bars P_{fluid} with oxygen fugacities defined by the IW buffer.

These mineralogical and experimental data confirm suggestions that crystallization of the Nandewar lavas ranging in composition from mafic trachyte to comendite generally proceeded under conditions of decreasing temperature and oxygen fugacity. However, the latter parameter may have been subject to irregular fluctuations in the peralkaline trachytes and comendites in which oxygen buffering was probably controlled by a discrete volatile phase as opposed to the solid-solid buffering that evidently was operative in lavas containing the common solid buffer assemblage fayalite-magnetite-quartz.

IRON-TITANIUM OXIDES

Occurrence

Titanomagnetite is the dominant Fe-Ti oxide phase throughout the Nandewar volcanic series. The hawaiites and trachyandesites contain occasional phenocrysts of titanomagnetite and rarely ilmenite, together with abundant euhedra of titanomagnetite±ilmenite dispersed in the groundmass. Several trachyandesites which exhibit widespread evidence of subsolidus oxidation contain phenocrysts of titanomagnetite with a network of narrow lamellae of exsolved ilmenite parallel to (111) planes. These were probably exsolved originally as ulvöspinel and subsequently were oxidized to ilmenite (Buddington and Lindsley, 1964). Some of the titanomagnetite phenocrysts in the trachyandesites may be of high-pressure origin as indicated by marginal resorption effects and similarity of

composition (i.e. relatively high Al, Mg and Cr) with those occurring in aggregates with aluminous clinopyroxenes of inferred high-pressure origin.

Partially resorbed microphenocrysts of titanomagnetite are common in the tristanites, often occurring in aggregates with apatite microphenocrysts. Titanomagnetite is relatively abundant in the groundmass and hence it is only rarely accompanied by ilmenite.

Titanomagnetite occurs as a phenocryst and groundmass phase in the mafic trachytes, whereas it generally forms microphenocrysts in the peralkaline trachytes which are usually rimmed with aenigmatite. Ilmenite is only a very rare phase in the trachytes and it is absent from the rhyolites and comendites. Rare microphenocrysts of ilmenite in peralkaline trachytes are also rimmed with aenigmatite.

Primary titanomagnetite has been eliminated from many of the alkali rhyolites because of late-stage oxidation to titanhematite. The most evolved comendites are apparently devoid of any primary Fe-Ti oxide phase.

Compositional Variation

Representative analyses of homogeneous titanomagnetites and ilmenites and their respective structural formulae are presented in Tables 4.8 and 4.9. The analyses have been recalculated using the method of Carmichael (1967) which assumes stoichiometry to permit estimation of the Fe_2O_3 content.

Small amounts of SiO_2 (0.1-0.5 wt. percent) systematically appeared in the titanomagnetite and ilmenite analyses. This was suspected as being an artifact of the data reduction technique and was therefore ignored. Although Deer *et al.* (1962b) suggested that a small amount of SiO_2 may substitute in the spinel structure, the possible effects of this constituent can be regarded as negligible for the purposes of this discussion.

Throughout the volcanic series the titanomagnetites display a considerable range in ulvöspinel content, the highest values occurring in spinels from the comendites and tristanites. This general trend of increasing ulvöspinel content with SiO_2 content of the host contrasts

TABLE 4.8

Analyses of Titanomagnetites

	Hawaiites					Trachyandesites							
Rock Number	49000 G	49002 PC	49002 G	49003 G	49004 PC	49005 PC	49005 G	49006 PC	49007 MC	49008 MC	49008 G	49009 PC	49009 C
TiO_2	24.85	24.19	24.58	23.26	26.88	24.85	25.41	17.48	19.50	21.09	26.17	24.61	19.93
Al_2O_3	1.42	3.29	1.86	1.46	1.82	1.78	2.82	1.55	4.15	4.51	0.97	1.68	4.91
V_2O_3	0.35	0.79	0.53	0.37	0.43	0.27	0.27	0.19	0.30	0.25	0.18	0.28	0.41
Cr_2O_3	0.17	1.15	0.51	-	0.52	0.19	0.24	0.43	0.14	0.10	0.41	-	-
FeO*	68.27	64.11	66.55	70.93	64.99	67.31	66.31	73.35	68.05	65.79	66.67	69.27	65.61
MnO	0.52	0.44	0.37	0.87	0.94	0.53	0.56	0.29	0.67	0.37	0.65	0.83	0.62
MgO	2.27	4.19	2.52	1.48	2.51	2.67	2.74	2.68	4.05	4.85	2.59	1.12	5.19
CaO	0.13	-	-	0.21	-	0.18	-	-	-	-	-	-	-
Total	97.98	98.16	96.92	98.58	98.09	97.78	98.35	95.97	96.86	96.96	97.64	97.79	96.67
$Fe_2O_3^1$	20.06	18.74	18.83	23.47	15.08	19.77	17.66	33.79	27.97	24.85	17.73	19.66	26.66
FeO^1	50.22	47.25	49.61	49.81	51.43	49.52	50.42	42.94	42.88	43.43	50.72	51.58	41.62
Total[2]	99.99	100.04	98.81	100.93	99.61	99.76	100.12	99.35	99.67	99.45	99.42	99.76	99.34
Structural Formulae on the Basis of 32 Oxygen Atoms													
Ti	5.480	5.207	5.461	5.121	5.916	5.465	5.535	3.892	4.218	4.530	5.798	5.482	4.271
Al	0.491	1.110	0.648	0.503	0.628	0.614	0.963	0.540	1.407	1.518	0.337	0.587	1.648
V	0.082	0.181	0.126	0.087	0.101	0.063	0.063	0.044	0.069	0.057	0.043	0.067	0.093
Cr	0.039	0.260	0.119	-	0.120	0.044	0.055	0.101	0.032	0.023	0.096	-	-
Fe^{3+}	4.428	4.036	4.187	5.169	3.321	4.351	3.851	7.532	6.056	5.343	3.930	4.384	5.716
Fe^{2+}	12.317	11.312	12.258	12.193	12.587	12.113	12.214	10.635	10.318	10.375	12.498	12.779	9.919
Mn	0.129	0.107	0.093	0.215	0.233	0.131	0.137	0.072	0.163	0.090	0.162	0.208	0.150
Mg	0.993	1.788	1.110	0.646	1.095	1.164	1.183	1.184	1.737	2.065	1.138	0.495	2.204
Ca	0.041	-	-	0.067	-	0.056	-	-	-	-	-	-	-
Sum	24.000	24.001	24.002	24.001	24.001	24.001	24.001	24.000	24.000	24.001	24.002	24.002	24.001
Mol. % Usp.	69.7	68.8	70.4	65.5	76.4	69.9	72.4	47.2	53.7	58.2	72.6	70.5	54.2

	Trachyandesites					Monzonite	Tristanites						
Rock Number	49010 MC	49011 PC	49012 PC	49013 G	49014 Inc.	49070 G	49075 PC	49076 PC	49076 G	49077 PC	49078 MPC	49078 G	49079 G
TiO_2	13.03	21.44	21.37	27.51	16.36	20.72	24.74	24.89	23.79	22.27	23.62	29.73	27.57
Al_2O_3	6.08	2.83	3.98	1.91	7.53	1.33	1.26	2.08	1.02	2.23	2.91	0.44	1.58
V_2O_3	0.59	0.26	0.53	0.13	0.48	-	-	0.23	-	-	0.13	0.26	0.34
Cr_2O_3	0.95	-	-	0.14	1.29	-	-	-	-	-	-	-	-
FeO*	71.71	70.02	69.00	65.57	64.89	73.82	70.42	67.78	71.11	70.71	68.56	66.96	65.98
MnO	0.47	0.51	0.45	0.87	0.28	0.91	0.73	0.79	0.92	0.81	0.76	0.74	0.88
MgO	3.47	2.40	3.00	2.55	6.39	-	0.83	1.71	0.41	1.55	2.45	0.99	1.88
CaO	-	-	-	-	0.24	-	-	-	0.16	-	-	-	0.11
Total	96.30	97.46	98.33	98.68	97.46	96.78	97.98	97.48	97.41	97.57	98.43	99.12	98.34
$Fe_2O_3^1$	37.00	25.30	24.69	14.86	30.61	27.10	20.20	18.74	21.85	24.21	21.57	11.56	14.44
FeO^1	38.43	47.26	46.79	52.20	37.35	49.45	52.24	50.92	51.46	48.93	49.15	56.57	52.99
Total[2]	100.02	100.00	100.81	100.17	100.53	99.51	100.00	99.36	99.61	100.00	100.59	100.29	99.79
Structural Formulae on the Basis of 32 Oxygen Atoms													
Ti	2.808	4.705	4.605	6.016	3.399	4.694	5.523	5.528	5.358	4.931	5.140	6.608	6.091
Al	2.054	0.973	1.344	0.655	2.452	0.471	0.441	0.724	0.360	0.774	0.993	0.154	0.547
V	0.136	0.061	0.122	0.030	0.106	-	-	0.055	-	-	0.030	0.061	0.081
Cr	0.215	-	-	0.032	0.282	-	-	-	-	-	-	-	-
Fe^{3+}	7.980	5.557	5.325	3.252	6.364	6.143	4.514	4.166	4.924	5.365	4.698	2.570	3.192
Fe^{2+}	9.211	11.534	11.214	12.696	8.630	12.461	12.972	12.577	12.890	12.048	11.896	13.985	13.015
Mn	0.114	0.126	0.109	0.214	0.066	0.232	0.184	0.198	0.233	0.202	0.186	0.186	0.218
Mg	1.483	1.044	1.282	1.105	2.632	-	0.367	0.753	0.183	0.680	1.057	0.436	0.823
Ca	-	-	-	-	0.071	-	-	-	0.051	-	-	-	0.034
Sum	24.001	24.000	24.001	24.000	24.002	24.001	24.001	24.001	23.999	24.000	24.000	24.000	24.001
Mol. % Usp.	37.3	60.7	60.9	77.1	44.4	60.3	70.2	71.3	68.4	63.3	66.6	83.1	78.4

TABLE 4.8 (continued)

Analyses of Titanomagnetites

	Tristanite	Trachytes											
Rock Number	49081 MPC	49082 MPC	49082 G	49083 MPC	49084 MPC	49084 G	49084 Inc.	49085 MPC	49086 MPC	49086 G	49087 MPC	49088 MPC	49089 MPC
TiO_2	20.31	25.12	24.15	23.13	20.34	23.98	28.62	25.77	23.28	24.55	11.50	26.50	22.71
Al_2O_3	1.72	-	-	1.29	-	1.06	0.73	0.25	0.82	0.36	0.99	0.49	0.40
V_2O_3	0.19	-	-	-	0.75	-	-	-	-	-	-	-	-
Cr_2O_3	-	-	-	-	0.36	-	-	-	-	-	-	-	-
FeO*	73.93	71.56	70.61	71.83	73.46	72.40	68.22	71.39	72.75	72.55	82.36	70.21	73.25
MnO	0.72	0.92	2.55	0.76	1.38	0.76	1.05	0.98	0.84	0.93	0.97	0.97	0.94
MgO	0.67	0.17	-	0.67	-	-	0.52	-	-	0.11	0.19	-	-
Total	97.54	97.77	97.31	97.68	96.29	98.20	99.14	98.39	97.69	98.50	96.01	98.17	97.30
Fe_2O_3[1]	28.18	20.47	22.05	23.19	27.98	21.73	13.51	19.17	23.09	21.71	46.17	17.19	24.52
FeO[1]	48.58	53.14	50.78	50.97	48.29	52.86	56.07	54.15	51.98	52.92	40.83	54.75	51.19
Total[2]	100.37	99.82	99.53	100.01	99.10	100.39	100.50	100.32	100.01	100.57	100.65	99.90	99.76
Structural Formulae on the Basis of 32 Oxygen Atoms													
Ti	4.531	5.683	5.492	5.177	4.659	5.377	6.369	5.798	5.250	5.502	2.601	5.975	5.148
Al	0.601	-	-	0.453	-	0.372	0.256	0.088	0.290	0.127	0.350	0.173	0.142
V	0.045	-	-	-	0.183	-	-	-	-	-	-	-	-
Cr	-	-	-	-	0.087	-	-	-	-	-	-	-	-
Fe^{3+}	6.292	4.635	5.017	5.194	6.413	4.876	3.007	4.316	5.211	4.869	10.449	3.878	5.562
Fe^{2+}	12.053	13.372	12.841	12.688	12.302	13.184	13.876	13.549	13.036	13.218	10.268	13.728	12.908
Mn	0.181	0.234	0.650	0.192	0.356	0.193	0.262	0.248	0.213	0.234	0.246	0.246	0.240
Mg	0.296	0.076	-	0.297	-	-	0.231	-	-	0.049	0.086	-	-
Sum	23.999	24.000	24.000	24.001	24.000	24.002	24.001	23.999	24.000	23.999	24.000	24.000	24.000
Mol. % Usp.	58.3	70.5	67.3	65.9	58.3	66.8	80.4	72.0	65.2	68.9	32.0	74.3	63.8

	Trachytes										Comendites	
Rock Number	49090 MPC	49092 MPC	49097 MPC	49099 MPC	49101 MPC	49101 G	49102 MPC	49103 MPC	49104 G	49107 G	49124 MPC	49160 G	49161 MPC
TiO_2	24.36	22.98	28.08	27.18	23.36	26.23	22.86	23.74	22.77	24.11	21.11	31.59	23.44
Al_2O_3	0.25	0.77	1.42	0.33	0.21	0.96	0.15	0.37	0.93	0.38	1.02	-	0.31
V_2O_3	-	-	0.33	-	-	-	-	-	-	-	-	-	-
Cr_2O_3	-	-	0.17	-	-	-	-	-	-	-	-	-	-
FeO*	72.20	72.01	67.99	69.09	70.76	67.18	72.58	72.09	71.89	71.60	73.95	64.38	71.26
MnO	1.02	1.25	0.53	1.30	2.45	3.46	1.02	1.12	1.43	1.05	0.56	2.14	1.40
MgO	-	-	0.87	0.17	-	0.10	-	-	0.13	0.17	-	-	0.14
ZnO	n.d.	n.d.	n.d.	n.d.	n.d.	n.d.	n.d.	n.d.	n.d.	n.d.	n.d.	n.d.	1.25
Total	97.83	97.01	99.39	98.07	96.78	97.93	96.61	97.32	97.15	97.31	96.64	98.11	97.80
Fe_2O_3[1]	21.68	23.29	13.58	16.02	23.04	17.06	24.08	22.43	23.70	21.74	26.55	7.20	23.42
FeO[1]	52.70	51.06	55.77	54.69	50.03	51.83	50.90	51.91	50.57	52.04	50.07	57.87	50.19
Total[2]	100.01	99.35	100.75	99.69	99.09	99.64	99.01	99.57	99.53	99.49	99.31	98.80	100.15
Structural Formulae on the Basis of 32 Oxygen Atoms													
Ti	5.505	5.218	6.196	6.134	5.332	5.908	5.216	5.387	5.153	5.466	4.798	7.181	5.295
Al	0.089	0.272	0.491	0.116	0.075	0.339	0.054	0.132	0.329	0.135	0.364	-	0.110
V	-	-	0.078	-	-	-	-	-	-	-	-	-	-
Cr	-	-	0.040	-	-	-	-	-	-	-	-	-	-
Fe^{3+}	4.902	5.292	2.999	3.616	5.262	3.845	5.515	5.095	5.366	4.934	6.040	1.639	5.295
Fe^{2+}	13.245	12.897	13.684	13.728	12.701	12.985	12.950	13.100	12.728	13.121	12.655	14.632	12.609
Mn	0.260	0.320	0.133	0.329	0.630	0.878	0.265	0.286	0.364	0.268	0.142	0.549	0.356
Mg	-	-	0.379	0.076	-	0.045	-	-	0.060	0.076	-	-	0.063
Zn	-	-	-	-	-	-	-	-	-	-	-	-	0.278
Sum	24.001	23.999	24.000	23.999	24.000	24.000	24.000	24.000	24.000	24.000	23.999	24.001	24.002
Mol. % Usp.	68.3	64.5	80.1	76.7	65.3	73.0	64.7	66.7	64.3	68.3	59.6	89.4	66.6

* - Total Fe as FeO

[1] - Calculated using the method of Carmichael (1967)

[2] - Recalculated using calculated Fe_2O_3 and FeO values

MC - Megacryst core

PC - Phenocryst core

MPC - Microphenocryst core

G - Groundmass

Inc. - Occurring within inclusion

C - Occurring within cumulate aggregate

n.d. - not determined

TABLE 4.9

Analyses of Ilmenites

	Hawaiites				Trachyandesites			Monzonite		Tristanite	Trachytes	
Rock Number	49000 G	49002 G	49003 G	49004 PC	49007 PC	49010 MPC	49013 G	49070 G	49070 GS	49079 G	49097 G	49100 MPC
TiO_2	51.57	51.06	49.58	51.18	49.39	48.02	51.78	49.77	49.35	43.31	51.18	51.46
Al_2O_3	-	0.09	0.27	0.27	0.24	0.88	0.18	0.11	0.24	0.54	0.34	-
V_2O_3	-	0.32	0.23	0.29	0.22	-	-	-	-	-	-	-
Cr_2O_3	-	0.15	-	-	0.09	-	-	0.15	-	-	-	-
FeO*	44.74	43.55	47.42	42.29	43.49	45.19	43.94	48.40	45.40	48.74	45.99	46.76
MnO	0.57	0.64	0.70	0.51	0.76	0.41	0.84	0.72	3.81	1.46	1.92	2.17
MgO	3.49	3.10	1.01	4.93	4.43	4.80	3.09	0.27	-	3.41	0.94	-
CaO	0.11	-	0.35	-	-	-	-	-	-	-	-	-
Total	100.48	98.91	99.56	99.47	98.62	99.30	99.83	99.42	98.80	97.46	100.37	100.39
Fe_2O_3[1]	5.90	4.24	6.44	6.20	8.61	12.14	4.16	5.40	5.43	19.29	3.99	2.99
FeO[1]	39.43	39.74	41.61	36.71	35.74	34.03	40.20	43.54	40.51	31.38	42.40	44.07
Total[2]	101.07	99.33	100.19	100.09	99.48	100.28	100.25	99.96	99.34	99.39	100.77	100.69
Structural Formulae on the Basis of 6 Oxygen Atoms												
Ti	1.892	1.909	1.866	1.873	1.829	1.752	1.918	1.891	1.889	1.623	1.915	1.944
Al	-	0.005	0.016	0.016	0.014	0.050	0.010	0.007	0.014	0.032	0.020	-
V	-	0.013	0.009	0.011	0.009	-	-	-	-	-	-	-
Cr	-	0.006	-	-	-	-	-	0.006	-	-	-	-
Fe^{3+}	0.217	0.159	0.243	0.227	0.319	0.446	0.154	0.205	0.208	0.723	0.150	0.113
Fe^{2+}	1.609	1.652	1.742	1.494	1.472	1.388	1.656	1.840	1.725	1.308	1.765	1.851
Mn	0.024	0.027	0.030	0.021	0.032	0.017	0.035	0.031	0.164	0.062	0.081	0.092
Mg	0.254	0.230	0.076	0.358	0.325	0.347	0.227	0.020	-	0.253	0.070	-
Ca	0.006	-	0.019	-	-	-	-	-	-	-	-	-
Sum	4.002	4.001	4.001	4.000	4.000	4.000	4.000	4.000	4.000	4.001	4.001	4.000
Mol. % Hm[3]	6.3	4.6	6.5	7.1	9.8	13.8	4.4	5.3	5.7	21.7	4.1	3.0
Estimated Temperature (°C)												
Buddington and Lindsley (1964)	1020	970	990	(1080)	(970)	(880)	1030	920	-	-	1080	-
Spencer and Lindsley (1981)	940	870	910	(1030)	(940)	(910)	880	830	-	-	910	-
Estimated Oxygen Fugacities ($-\log_{10} fo_2$)												
Buddington and Lindsley (1964)	11.0	12.0	11.5	(10.1)	(11.2)	(12.0)	11.0	12.6	-	-	10.3	-
Spencer and Lindsley (1981)	12.7	14.5	13.1	(11.2)	(11.8)	(11.5)	14.4	14.9	-	-	14.1	-

* - Total Fe as FeO

[1] - Calculated using the method of Carmichael (1967)

[2] - Recalculated using calculated Fe_2O_3 and FeO values

[3] - Calculated using the method of Anderson (1968)

PC - Phenocryst core

MPC - Microphenocryst core

G - Groundmass

GS - Groundmass constituent of schlieren

with observations of Price and Taylor (1980), who noted the reverse trend in lavas from the Banks Peninsula, New Zealand.

Although individual titanomagnetite and ilmenite phenocrysts display little or no zoning, there are generally distinct compositional differences between phenocryst and groundmass titanomagnetites. Groundmass spinels are usually enriched in the ulvöspinel component relative to the associated phenocrysts and this is consistent with the generalized ulvöspinel trend throughout the host rock series. Prévot and Mergoil (1973) observed a similar relationship in alkali basalts from St Clement, France, whereas Wass (1973) noted the reverse trend in alkali basalts and basanites from southern New South Wales.

Megacryst, cumulate, and to a lesser extent, phenocryst spinels are characterized by higher MgO, Al_2O_3, Cr_2O_3 and V_2O_3 than the groundmass phases. Maximum MgO and Al_2O_3 contents of cumulate titanomagnetites are 6.4 and 7.5 wt. percent respectively (cf. Table 4.8, No.49014). Comparable MgO and Al_2O_3 contents in spinels have been reported from Japanese trachyandesites (Aoki, 1966) and N.S.W. basalts (Wass, 1973). Wass (*loc. cit.*) suggested that increased substitution of MgO and Al_2O_3 into the spinel structure is pressure dependent, but there are apparently no experimental data to confirm this suggestion.

Phenocrysts of ilmenite, some which may be high-pressure megacrysts, are characterized by moderately high MgO contents (up to 4.9 wt. percent MgO, Table 4.9, No. 49004). Unfortunately, the relative scarcity of the rhombohedral phase in these rocks does not permit an evaluation of changes in R_2O_3 content and minor element components with progressive crystallization of the hosts.

Where titanomagnetite and ilmenite coexist either as phenocrysts or groundmass phases the trivalent elements Al, Cr and V are concentrated in the spinel phase, whereas Mg tends to be higher in the rhombohedral phase that has probably crystallized in equilibrium with the spinel. Schuiling and Feenstra (1980) demonstrated the clear preference of V for the spinel structure in a literature survey of coexisting titanomagnetite-ilmenite pairs. The MgO preferentially concentrated in the ilmenites is presumably present as the geikielite component ($MgTiO_3$).

Mn appears to be approximately equally distributed between

coexisting titanomagnetite and ilmenite and it increases in the titanomagnetites with increasing SiO_2 of the host, reaching a maximum of 3.5 wt. percent MnO in the groundmass phase of a peralkaline trachyte (49101).

Zn was not determined on the majority of titanomagnetites, but substitution of this element is clearly quite significant in spinels in the comendites (e.g. 1.25 wt. percent ZnO, Table 4.8, No. 49161). Visual inspection of microprobe spectra of spinels from many of the peralkaline trachytes indicated significant Zn contents, and this is reflected in the consistently low totals of many of these analyses. The increase in MnO and ZnO coincides with the general increase in Fe^{2+}/Fe^{3+} ratios and ulvöspinel contents of the spinels with increasing SiO_2 content of the hosts.

Conditions of Crystallization

Coexisting homogeneous titanomagnetite and ilmenite permit estimations of the temperature and oxygen fugacity conditions at the time of their crystallization, employing the technique of Buddington and Lindsley (1964). Temperature and oxygen fugacity estimates are valid where:

1. Ideally the compositions of the natural phases do not depart significantly from ulvöspinel-magnetite and ilmenite-hematite solid solutions upon which the experimental data are based.
2. Equilibrium was achieved between the Fe-Ti oxide phases during crystallization.
3. The compositions of the phases have not been affected by unmixing or subsequent low temperature oxidation.

Attainment of equilibrium between the Fe-Ti oxides in the various rock types is strongly supported by limited compositional variation between groundmass grains. Estimates of temperature and oxygen fugacity have been provided for coexisting titanomagnetite and ilmenite phenocrysts (Table 4.9, in brackets). There is some doubt whether these are in fact equilibrium pairs, and these data must therefore be regarded with some caution. Temperature estimates derived from compositions of

groundmass phases are interpreted as quench temperatures, following soon after eruption.

Where there is significant departure in composition from 'ideal' ulvöspinel-magnetite and ilmenite-hematite solid solutions, the precise role of the minor components is poorly understood. Experimental work by Speidel (1970) and Mazzullo *et al.* (1975) indicated better consistency in T-fO_2 estimates using the Buddington and Lindsley (1964) technique if MgO and MnO are taken into account during calculation of the end-member components. The method of Anderson (1968) has been considered to cater more adequately for these minor components than that of Carmichael (1967). However, calculation of end-members using both methods in this study indicated only minor differences in calculated T and fO_2. A literature survey of a large number of coexisting titanomagnetite-ilmenite pairs from a variety of hosts (D'arco and Maury, 1981) has also shown that there is close agreement (pairs usually differ by less than 30^{o}C) between temperatures calculated using both methods. the data presented here were calculated following Anderson (1968), to permit direct comparison with previous studies on alkaline rocks.

Recently several refinements have been made to the data of Buddington and Lindsley (1964). Powell and Powell (1977) fitted a solution model to the NNO and FMQ experiments of Lindsley (1962,1963), and although estimated temperature and fO_2 values are consistent with those obtained using the Buddington and Lindsley (1964) curves, large uncertainties (±80^{o}C) are indicated where MgO and Al_2O_3 are significant constituents (i.e. 3-4 wt. percent in the spinel and rhombohedral phases). Spencer and Lindsley (1981) fitted a solution model to the original data together with data obtained from experiments over an extended range of oxygen fugacities. This model was used to completely revise the Fe-Ti oxide geothermometer-oxybarometer.

Temperatures and oxygen fugacity estimates for the Nandewar rocks (Table 4.9) have been obtained using both the Buddington and Lindsley (1964) and Spencer and Lindsley (1981) curves. The obvous differences between the two determinative curves are both disappointing and disconcerting, considering that the Fe-Ti oxide geothermometer has often been regarded as the 'standard' for comparing and testing other geothermometers.

Comparison of these data with temperatures calculated using the plagioclase geothermometer of Kudo and Weill (1970) and Mathez (1973) (Table 4.11), indicate closest agreement between temperatures determined using the methods of Buddington and Lindsley (1964) and Kudo and Weill (1970). The temperatures obtained using the curves of Spencer and Lindsley (1981) are consistently lower than Buddington-Lindsley estimates by 30 to 170°C, and the fO_2 estimates are consistently lower by 0.5 to 3.8 orders of magnitude.

In view of the apparently imprecise nature of these estimates it is probably best to discuss only general trends in the T-fO_2 data, although the Buddington and Lindsley (1964) estimates can be directly compared with previous estimates for alkaline rocks. These data for alkaline rocks (e.g. Anderson, 1968; Wass, 1973; Prévot and Mergoil, 1973; Bizouard *et al.*, 1980) and also many tholeiitic rocks (Carmichael, 1967; Anderson and Wright, 1972; Thompson, 1975) cluster about the FMQ buffer curve in a plot of T versus fO_2 and exhibit a trend of decreasing T with decreasing fO_2. A comparable plot for the Nandewar data (Fig. 4.7) indicates a similar trend, with most of the points plotting parallel to and just below the FMQ buffer curve. The presence of ilmenite microphenocrysts in peralkaline trachyte 49100 with a very low R_2O_3 content (3.0 mole percent Fe_2O_3), although unaccompanied by a spinel phase, can be regarded as indicating extension of this trend to lower temperature and fO_2 conditions for at least some of the salic rock types of the series. Close correspondence of this trend with the synthetic buffer curves supports the contention of Carmichael and Nicholls (1967), that magmas are 'internally buffered', at least for part of their cooling history, or alternatively, the composition of the vapour phase is controlled by the crystallizing phases. In 'externally buffered' magmas a higher vapour pressure ensures that the gas phase controls the composition of the crystallizing phases.

Direct measurements of temperatures and fO_2 on volcanic gases from tholeiitic and alkaline volcanoes (Heald *et al.*, 1963; Sato and Wright, 1966; Sato and Moore, 1973) indicate a similar positive correlation of temperature with fO_2. Measured fO_2 values in these cases are usually slightly higher than those derived from studies of coexisting Fe-Ti oxides, and this is usually attributed to air contamination during

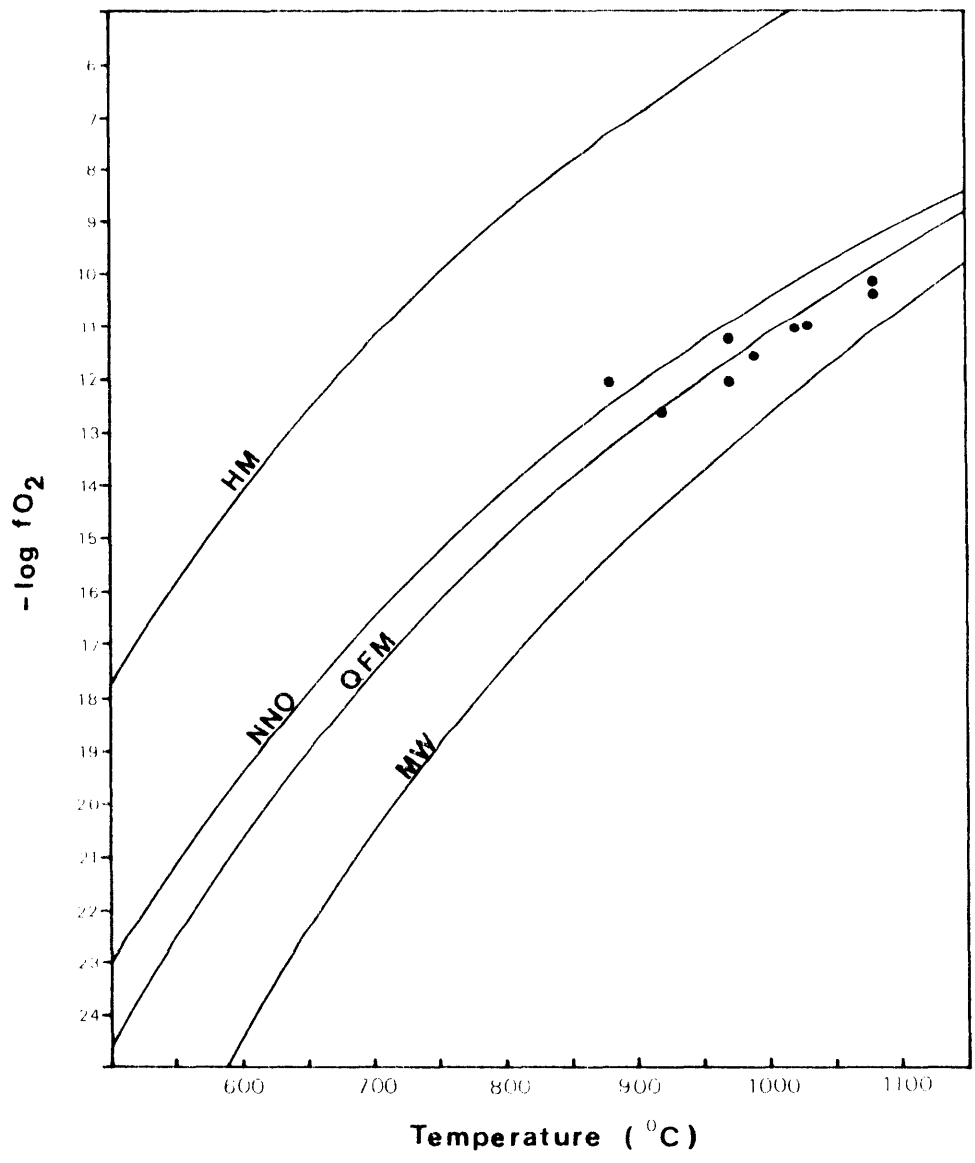

Fig. 4.7: Plot of -log fO_2 versus temperature deduced from coexisting Fe-Ti oxide pairs from rocks of the Nandewar series. The synthetic buffer curves have been reproduced from Buddington and Lindsley (1964) for comparison.

measurement.

The various controls on the oxygen fugacity of a magma have been discussed by Carmichael and Nicholls (1967), Anderson (1968), and Wass (1973). The dominant controls include: 1. The composition and extent of melting of phases at the site of magma generation; 2. Variations in temperature and pressure during migration of the magma from the source region to the site of crystallization; and 3. Variations in melt composition resulting from additions to and losses from the magma prior to crystallization and solidification.

If the various members of a suite of lavas are related solely through fractional crystallization in a high-level magma chamber, variations in their oxygen fugacities will be controlled by changes in temperature and variations in melt composition resulting from fractionation of crystalline phases. The available T-fO_2 data for the Nandewar suite which show close coherence with the synthetic FMQ buffer can be interpreted as indicating temperature has been the dominant control on fO_2 (Wass, 1973), and changes in Fe^{3+}/Fe^{2+} and O^{2-} resulting from fractionation of solid phases were apparently minimal.

In the more evolved lavas lack of specific fO_2 data precludes a precise evaluation of changes in this parameter. The phase relationships in the trachytes and peralkaline trachytes, including the presence of coexisting quartz, fayalite and titanomagnetite (the natural analogue of the synthetic FMQ buffer) and the various ferromagnesian assemblages, support the notion that many of these magmas were also internally buffered.

However, extensive alteration of the ferromagnesian silicates and original titanomagnetite in the older alkali rhyolites indicates pervasive late-stage oxidation of these lavas. The fO_2 of these magmas was clearly much higher than in the comendites which contain arfvedsonite and aenigmatite as groundmass constituents. If indeed the alkali rhyolites are comagmatic with the rest of the suite, special circumstances or conditions are required to explain the quite different degrees of oxidation displayed by them. The pervasive vesiculation of the alkali rhyolites indicates significant loss of a volatile phase, a feature not apparent in the extrusive comendites. Selective loss of

H_2, following thermal dissociation of H_2O (Sato, 1978; Haggerty, 1978), may provide a mechanism for the oxidation of these lavas. One of the implications of this model is that the alkali rhyolite magmas were considerably enriched in volatile constituents (principally H_2O) compared with the comendites. This seems inconsistent with a model of closed-system fractional crystallization and is discussed in more detail in Chapter 7.

In summary, crystallization of the Nandewar lavas appears to have occurred under conditions of decreasing fO_2 and temperature through the operation of internal mineralogical buffer reactions. Departures from this trend are evident for an important group of salic lavas (the older alkali rhyolites) in which separation of a gaseous phase probably provided the dominant control on oxygen fugacity.

FELDSPARS

Occurrence

Feldspars are the most abundant phenocryst phases in most of the porphyritic rocks of the Nandewar series and an understanding of the compositional relations of this mineral group is critical in evaluating possible liquid lines of descent and genetic relationships amongst members of the suite (Chapter 7).

Plagioclase is a relatively uncommon phenocryst phase in the hawaiites in which it is subordinate in this role to olivine, whereas it is the dominant phenocryst species in the trachyandesites and tristanites. Plagioclase phenocrysts are typically free of inclusions and occur as subhedral partially corroded crystals with large optically homogeneous cores and narrow zoned rims. The cores of plagioclase phenocrysts may take on a sieved appearance due to the presence of abundant tiny clinopyroxene and opaque inclusions. Plagioclase phenocrysts in the tristanites occasionally contain euhedral inclusions of apatite.

Cumulate aggregates of plagioclase, clinopyroxene and olivine occur in several trachyandesites, whereas in the tristanites plagioclase tends to be more commonly associated with clinopyroxene, titanomagnetite and apatite. A cumulate inclusion of inferred high-pressure origin (as

indicated by pyroxene compositional data), features clinopyroxene euhedra poikilitically enclosed in plagioclase.

Plagioclase is only a sparse phenocryst phase in the mafic trachytes, and where present it typically has a narrow rim of untwinned alkali feldspar. Rocks more evolved than the mafic trachytes (including the peralkaline trachytes, alkali rhyolites and comendites) are devoid of plagioclase.

The peralkaline trachytes and rhyolitic rocks commonly contain euhedral to subhedral, partially corroded crystals of anorthoclase or sanidine as their sole phenocryst phase. These phenocrysts exhibit either fine cross-hatched twinning or simple twinning, are free of inclusions, and in some specimens occur in glomeroporphyritic aggregates. In some phenocrysts incipient exsolution is visible in thin section but most alkali feldspars are probably cryptoperthites.

Alkali feldspar is a minor groundmass constituent in the hawaiites. It becomes increasingly abundant in the trachyandesites, tristanites and mafic trachytes, being the dominant groundmass phase in the latter two rock types.

Compositional Variation

Representative analyses of phenocryst and groundmass feldspars from the Nandewar rocks are presented in Table 4.10. Structural formulae have not been tabulated, although it may be noted that Σ cations for formulae calculated on the basis of 32 oxygens give sums which range from 19.92 to 20.14, with most in the range 20.00 ± 0.04.

Feldspar analyses for the suite as a whole and for specific rock groups are plotted (Figs 4.8 and 4.9 respectively) in terms of mole percent Ab, An and Or, and these indicate the compositional variation in feldspars within the Nandewar rocks.

Normal zoning characterizes the majority of plagioclase phenocrysts in the hawaiites (An_{63-46}) and trachyandesites (An_{54-39}). However, the rare sieved phenocrysts, and quite a significant proportion of unsieved phenocrysts in several specimens, exhibit reverse zoning ranging from An_{47-56} in the hawaiites and An_{39-42} and An_{53-61} for two trachyandesites (49008 and 49010 respectively) of different composition. In some eruptives

TABLE 4.10

Analyses of Feldspars

	Hawaiites										
Rock No.	49000 PC	49000 PR	49000 G	49001 MPC	49001 G	49001 G	49002 PC	49002 PR	49003 PC	49003 PR	49003 G
SiO_2	52.84	53.92	52.48	54.69	56.15	63.98	53.61	53.82	56.14	53.94	52.59
Al_2O_3	29.82	29.26	29.89	28.12	27.30	20.19	29.17	28.90	27.78	28.73	29.14
Fe_2O_3*	0.34	0.46	0.52	0.56	0.67	0.58	0.36	0.57	0.26	0.61	0.37
CaO	12.38	11.52	12.65	10.66	9.24	1.44	11.68	11.29	9.72	11.58	12.22
Na_2O	4.18	4.80	4.27	5.15	5.93	6.30	4.71	4.87	5.87	4.32	4.38
K_2O	0.37	0.47	0.36	0.50	0.53	6.99	0.42	0.51	0.41	0.30	0.32
Total	99.93	100.43	100.17	99.68	99.82	99.48	99.95	99.96	100.18	99.98	99.52
Ab	37.1	41.8	37.1	45.3	52.1	53.9	41.2	42.6	51.0	42.2	38.6
An	60.7	55.5	60.8	51.8	44.8	6.8	56.4	54.5	46.7	56.1	59.5
Or	2.2	2.7	2.1	2.9	3.1	39.3	2.4	2.9	2.3	1.7	1.9

	Hawaiite			Trachyandesites							
Rock No.	49004 PC	49004 PR	49004 G	49005 G	49005 G	49005 G	49007 PC	49007 PR	49008 PC	49008 PR	49008 G
SiO_2	52.27	55.85	53.11	56.20	63.79	64.30	54.28	55.43	57.83	57.39	55.22
Al_2O_3	30.18	27.16	29.29	27.09	21.79	20.85	28.40	27.94	26.24	26.64	27.21
Fe_2O_3*	0.54	0.69	0.98	1.00	0.63	0.43	0.56	0.57	0.27	0.28	0.79
CaO	12.75	9.53	12.19	9.21	2.95	1.78	11.02	10.19	8.01	8.62	9.96
Na_2O	3.96	5.72	4.47	5.98	7.41	5.83	5.07	5.39	6.56	6.07	5.75
K_2O	0.26	0.60	0.27	0.62	3.67	6.86	0.34	0.44	0.77	0.80	0.54
Total	99.96	99.55	100.31	100.10	100.24	100.05	99.67	99.96	99.68	99.80	99.47
Ab	35.4	50.2	39.3	52.1	64.7	51.5	44.6	47.6	57.1	53.5	49.5
An	63.1	46.3	59.2	44.3	14.2	8.7	53.5	49.8	38.5	41.9	47.4
Or	1.5	3.5	1.5	3.6	21.1	39.8	1.9	2.6	4.4	4.6	3.1

	Trachyandesites										
Rock No.	49009 PC	49009 PR	49009 G	49010 PC	49010 PR	49010 G	49011 PC	49011 PR	49011 G	49012 G	49012 G
SiO_2	57.10	57.51	66.27	54.33	52.44	54.14	54.23	57.14	60.33	63.78	65.48
Al_2O_3	27.18	26.11	19.78	28.43	29.72	28.07	28.68	26.66	24.71	21.82	19.95
Fe_2O_3*	0.38	0.63	0.58	0.66	0.51	1.09	0.64	0.57	0.89	0.42	0.46
CaO	8.71	7.95	0.86	10.97	12.63	10.78	11.02	8.82	6.24	2.98	0.93
Na_2O	6.16	6.35	6.88	4.98	4.23	5.01	5.14	5.97	7.51	7.40	5.37
K_2O	0.71	0.80	6.36	0.47	0.39	0.61	0.43	0.72	0.79	3.53	7.36
Total	100.24	99.35	100.73	99.84	99.92	99.70	100.14	99.88	100.47	99.93	100.55
Ab	53.8	56.4	59.6	43.9	36.9	44.1	44.6	52.7	65.5	65.1	50.8
An	42.1	39.0	4.1	53.4	60.9	52.4	52.9	43.1	30.0	14.5	4.4
Or	4.1	4.6	36.3	2.7	2.2	3.5	2.5	4.2	4.5	20.4	44.8

TABLE 4.10 (continued)

Analyses of Feldspars

	Trachyandesites						Monzonite		Tristanite		
Rock No.	49013 G	49013 G	49014 Inc.	49056 PC	49056 PR	49056 G	49070 G	49070 G	49074 PC	49074 PR	49074 PC
SiO_2	58.81	64.10	55.61	54.60	55.04	65.35	59.41	65.41	59.51	64.89	65.07
Al_2O_3	25.16	21.39	27.77	28.33	27.75	20.64	25.48	18.89	25.59	19.85	20.01
Fe_2O_3*	0.69	0.38	0.53	0.54	0.66	0.59	0.11	-	0.52	0.26	0.42
BaO	-	-	-	-	-	-	-	-	-	-	0.31
CaO	7.14	2.42	9.68	10.57	9.90	1.36	7.02	0.10	7.03	0.92	0.87
Na_2O	7.34	7.30	5.66	5.35	5.45	7.27	7.18	2.96	6.85	6.04	5.22
K_2O	0.62	4.34	0.62	0.54	0.62	5.31	0.70	12.40	1.19	7.43	8.86
Total	99.76	99.93	99.87	99.93	99.42	100.52	99.90	99.76	100.69	99.39	100.76
Ab	62.8	63.5	49.6	46.3	48.1	63.1	62.3	26.5	59.5	52.8	45.0
An	33.7	11.6	46.8	50.6	48.3	6.5	33.7	0.5	33.7	4.4	4.2
Or	3.5	24.9	3.6	3.1	3.6	30.4	4.0	73.0	6.8	42.8	50.8

	Tristanites										
Rock No.	49075 PC	49075 PR	49075 G	49076 PC	49076 PR	49076 G	49076 G	49077 PC	49077 PR	49077 G	49078 PC
SiO_2	56.24	56.76	64.24	56.28	57.39	61.44	64.72	55.90	56.66	62.61	55.99
Al_2O_3	27.10	26.90	21.12	27.24	26.58	24.19	21.63	27.47	26.77	22.66	27.23
Fe_2O_3*	0.41	0.38	0.54	0.57	0.54	0.60	0.56	0.52	0.41	0.71	0.67
CaO	9.08	8.77	2.19	9.54	8.35	5.60	2.12	9.77	8.87	4.08	9.37
Na_2O	5.95	5.99	7.73	5.82	6.23	7.51	7.86	5.62	5.96	8.18	5.93
K_2O	0.63	0.71	3.64	0.60	0.71	1.28	3.65	0.57	0.60	1.66	0.51
Total	99.41	99.51	99.46	100.05	99.80	100.62	100.54	99.85	99.27	99.90	99.70
Ab	52.3	53.0	68.2	50.7	55.1	65.6	68.8	49.3	53.0	71.0	51.8
An	44.1	42.9	10.7	45.9	40.8	27.0	10.2	47.4	43.5	19.5	45.3
Or	3.6	4.1	21.1	3.4	4.1	7.4	21.0	3.3	3.5	9.5	2.9

	Tristanites									Trachyte	
Rock No.	49078 PR	49078 G	49078 G	49079 PC	49079 PR	49079 G	49081 PC	49081 G	49081 Inc.	49082 PC	49082 PC
SiO_2	57.01	65.35	66.61	54.61	56.46	59.68	59.26	64.19	54.97	53.65	65.57
Al_2O_3	26.76	20.33	18.24	28.17	27.62	24.77	25.21	21.17	27.94	29.18	19.97
Fe_2O_3*	0.43	0.43	1.26	0.64	0.66	1.00	0.44	0.74	0.50	0.49	0.22
CaO	8.61	2.08	0.14	10.57	9.03	6.64	6.86	2.23	10.29	11.65	1.00
Na_2O	6.57	7.82	6.14	5.31	6.06	7.27	6.84	7.81	5.41	4.59	6.94
K_2O	0.54	4.64	7.65	0.45	0.42	0.96	1.12	3.57	0.56	0.37	6.01
Total	99.92	100.65	100.04	99.75	100.25	100.32	99.73	99.71	99.67	99.93	99.71
Ab	56.2	65.0	54.6	46.4	53.5	62.8	60.2	68.6	47.2	40.7	60.6
An	40.7	9.6	0.7	51.0	44.1	31.7	33.3	10.8	49.6	57.1	4.8
Or	3.1	25.4	44.7	2.6	2.4	5.5	6.5	20.6	3.2	2.2	34.6

TABLE 4.10 (continued)

Analyses of Feldspars

Rock No.	Trachytes										
	49083 MPC	49083 MPR	49083 MPC	49084 PC	49084 PC	49084 Inc.	49085 PC	49085 PC	49086 PC	49086 PR	49086 G
SiO_2	61.09	65.21	62.96	62.20	65.15	57.96	65.26	65.74	63.15	64.61	65.51
Al_2O_3	24.25	20.38	22.69	23.05	20.16	26.51	20.74	19.55	21.74	20.12	18.92
Fe_2O_3*	0.38	0.48	0.44	0.18	0.46	0.81	0.21	0.54	0.23	0.20	0.66
BaO	-	-	-	0.69	0.35	-	-	0.44	1.65	0.59	0.50
CaO	5.42	1.15	2.81	4.16	1.07	7.63	1.33	0.53	2.00	1.11	0.11
Na_2O	7.41	5.51	7.19	7.31	6.44	6.71	7.55	7.04	7.25	6.99	5.71
K_2O	1.47	6.81	4.16	2.78	6.44	0.72	4.61	5.75	4.13	5.94	8.41
Total	100.02	100.53	100.25	100.37	100.07	100.34	99.70	99.59	100.15	99.56	99.82
Ab	65.2	55.9	62.6	63.1	56.8	58.9	66.7	62.8	63.6	60.1	50.1
An	26.3	5.5	13.5	19.9	5.2	37.0	6.5	2.6	9.7	5.2	0.5
Or	8.5	38.6	23.9	17.0	38.0	4.1	26.8	34.6	26.7	34.7	49.4

Rock No.	Trachytes										
	49087 PC	49087 PR	49088 PC	49088 PR	49089 PC	49089 G	49090 PC	49090 G	49097 PC	49097 PC	49097 G
SiO_2	65.13	66.00	63.61	65.51	63.75	66.51	66.19	66.02	53.93	65.83	65.90
Al_2O_3	20.49	19.07	21.63	19.46	20.99	19.65	19.84	19.47	28.40	19.54	19.84
Fe_2O_3*	0.18	0.57	0.38	0.46	0.16	0.58	0.28	0.48	0.58	-	0.31
BaO	-	-	1.78	0.46	1.19	-	-	-	-	-	0.23
CaO	1.29	0.14	2.20	0.43	2.20	0.41	0.66	0.27	11.06	0.77	0.67
Na_2O	7.23	6.62	6.92	6.75	7.11	7.38	7.26	7.00	4.90	6.44	7.17
K_2O	5.23	7.00	4.37	6.38	4.43	6.17	5.90	6.89	0.46	6.85	6.02
Total	99.55	99.40	100.89	99.45	99.83	100.70	100.13	100.13	99.33	99.43	100.14
Ab	63.5	58.6	60.9	59.8	61.9	63.3	63.1	59.9	43.3	56.6	62.1
An	6.3	0.7	10.7	2.1	10.6	1.9	3.2	1.3	54.0	3.8	3.2
Or	30.2	40.7	28.4	38.1	27.5	34.8	33.7	38.8	2.7	39.6	34.7

Rock No.	Trachytes										
	49098 PC	49098 PR	49099 PC	49099 G	49100 PC	49100 G	49101 PC	49101 G	49102 PC	49102 PC	49102 G
SiO_2	66.04	66.85	66.45	66.25	66.68	65.89	66.00	66.06	63.82	65.62	66.75
Al_2O_3	19.61	19.16	19.31	19.43	19.54	19.43	19.34	19.16	22.49	20.26	18.85
Fe_2O_3*	0.21	0.50	0.18	0.50	0.26	0.59	0.47	0.63	0.20	0.28	0.61
CaO	0.40	-	-	0.16	0.19	0.40	0.39	0.33	2.97	0.94	-
Na_2O	6.46	7.26	7.60	7.97	7.49	7.60	7.18	7.91	8.12	7.88	6.47
K_2O	7.61	6.33	6.27	5.49	6.03	5.30	6.54	5.53	2.96	4.92	7.74
Total	100.33	100.10	99.81	99.80	100.19	99.21	99.92	99.62	100.56	99.90	100.42
Ab	52.3	63.5	64.8	68.3	64.8	67.2	61.4	67.4	69.4	67.7	56.0
An	1.9	-	-	0.8	0.9	2.0	1.8	1.6	14.0	4.5	-
Or	42.8	36.5	35.2	30.9	34.3	30.8	36.8	31.0	16.6	27.8	44.0

TABLE 4.10 (continued)

Analyses of Feldspars

	Trachytes										
Rock No.	49103 PC	49103 G	49103 G	49104 PC	49104 G	49105 PC	49106 PC	49107 PC	49108 PC	49108 G	49119 PC
SiO_2	65.66	65.72	66.23	66.46	65.45	66.52	65.74	65.85	65.77	66.61	65.39
Al_2O_3	20.28	20.40	18.68	19.37	20.19	19.14	19.87	19.61	20.31	19.43	20.03
Fe_2O_3*	0.21	0.38	0.79	-	0.60	0.24	0.14	0.24	0.22	0.43	0.43
BaO	0.96	-	-	-	-	-	-	-	-	-	0.59
CaO	0.68	0.82	-	0.45	1.08	-	0.76	0.48	0.22	0.36	0.86
Na_2O	6.78	7.61	5.62	6.70	7.53	6.58	6.95	7.02	7.05	8.32	6.79
K_2O	6.46	5.11	8.94	6.90	4.96	6.77	6.34	6.32	6.33	4.47	6.23
Total	101.03	100.04	100.26	99.88	99.81	99.52	99.80	99.52	99.90	99.62	100.32
Ab	58.5	66.6	48.9	58.3	66.1	60.6	60.2	61.4	62.2	72.6	59.1
An	3.2	4.0	-	2.2	5.2	-	3.6	2.3	1.1	1.7	4.1
Or	38.3	29.4	51.1	39.5	28.7	39.4	36.2	36.3	36.7	25.7	36.8

	Rhyolites										
Rock No.	49120 PC	49121 PC	49121 G	49122 PC	49123 PC	49124 PC	49125 PC	49126 PC	49127 PC	49128 G	49129 PC
SiO_2	65.65	65.88	68.44	66.75	66.68	66.61	65.72	65.93	66.57	66.32	66.50
Al_2O_3	19.50	19.45	19.94	19.29	19.54	19.55	19.96	19.67	19.38	18.92	19.10
Fe_2O_3*	-	0.18	0.16	0.21	0.32	0.27	0.14	-	0.24	0.80	0.24
CaO	0.44	0.52	-	0.16	0.19	0.29	0.21	0.60	0.23	0.16	0.31
Na_2O	6.37	6.89	11.54	6.81	6.77	6.91	6.42	6.92	6.77	7.48	7.08
K_2O	7.17	6.91	0.24	7.20	7.08	6.94	7.31	6.24	7.13	6.30	6.67
Total	99.13	99.84	100.32	100.42	100.58	100.57	99.76	99.36	100.32	99.98	99.90
Ab	56.2	58.8	98.6	58.5	58.7	59.4	56.6	60.9	58.4	63.9	60.8
An	2.2	2.4	-	0.8	0.9	1.4	1.0	2.9	1.1	0.7	1.5
Or	41.6	38.8	1.4	40.7	40.4	39.2	42.4	36.2	40.5	35.4	37.7

	Rhyolites			Comendites							
Rock No.	49129 G	49130 PC	49131 PC	49160 PC	49161 PC	49162 PC	49163 PC	49163 G	49164 PC	49164 G	49165 PC
SiO_2	67.02	66.33	65.90	65.91	66.13	66.43	66.58	66.50	66.33	66.31	66.71
Al_2O_3	18.85	19.03	19.30	19.25	19.60	19.21	18.23	18.54	19.25	19.72	18.91
Fe_2O_3*	0.61	0.18	0.18	0.34	0.17	0.23	1.23	0.96	-	0.17	0.46
CaO	0.10	-	0.22	0.28	0.26	0.25	-	0.10	0.19	0.45	-
Na_2O	6.05	7.31	6.29	6.93	7.44	6.86	7.23	8.44	7.26	8.48	6.67
K_2O	7.93	6.45	7.59	6.67	6.29	6.78	6.65	4.96	6.85	4.74	6.98
Total	100.56	99.30	99.48	99.38	99.89	99.76	100.02	99.50	99.88	99.87	99.73
Ab	59.1	63.2	55.1	60.4	63.5	59.9	62.3	71.8	61.1	71.6	59.2
An	0.4	-	1.1	1.3	1.2	1.2	-	0.5	0.9	2.1	-
Or	40.5	36.8	43.8	38.3	35.3	38.9	37.7	27.7	38.0	26.3	40.8

* - Total Fe as Fe_2O_3

PC - Phenocryst core

PR - Phenocryst rim

MPC - Microphenocryst core

MPR - Microphenocryst rim

G - Groundmass

Inc. - Occurring with inclusion

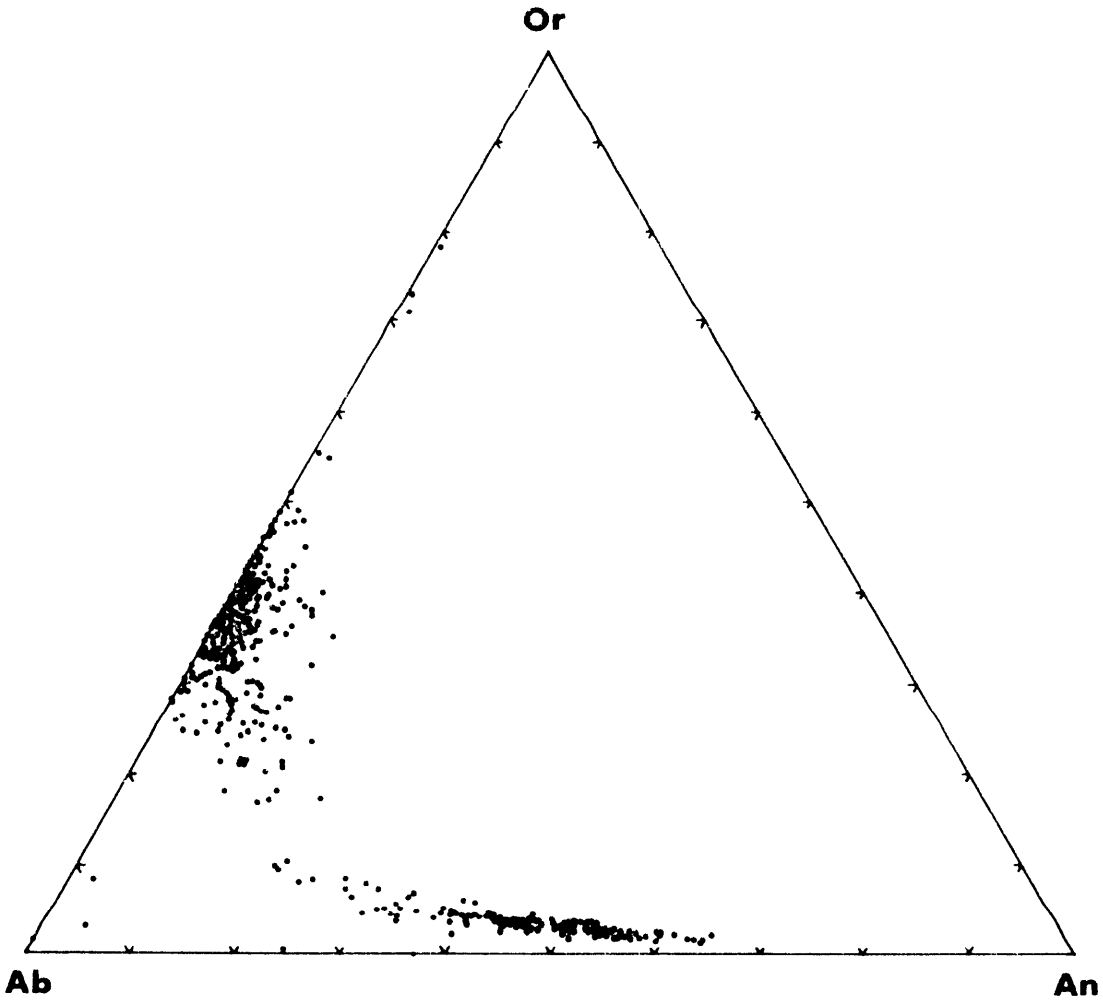

Fig. 4.8: Plot of all feldspar analyses from Nandewar rocks (mole percent).

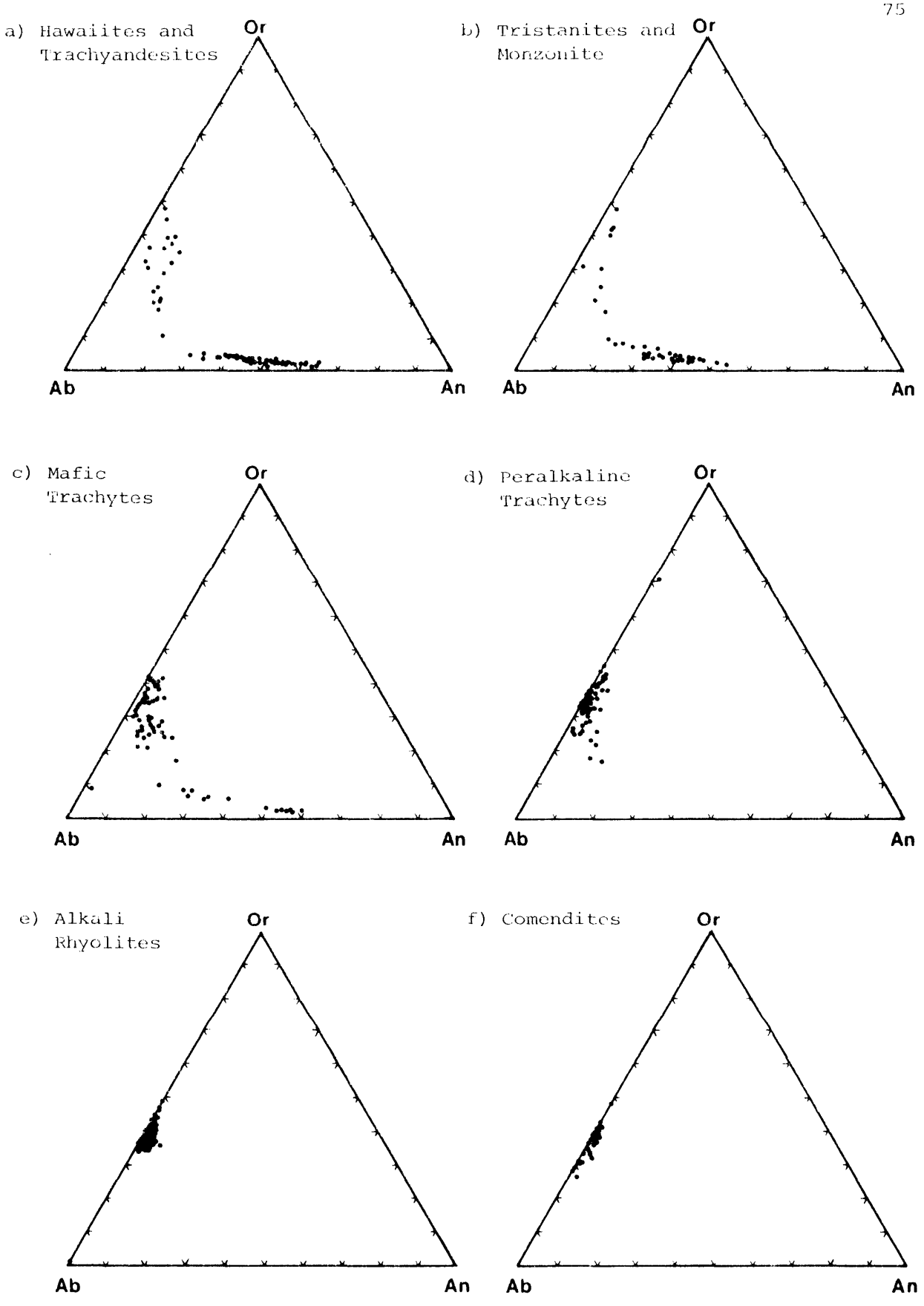

Fig. 4.9: Plot of feldspar analyses (mole percent) from:
a) hawaiites and trachyandesites b) tristanites
c) mafic trachytes d) peralkaline trachytes
e) alkali rhyolites and f) comendites.

these plagioclases coexist with tschermakitic clinopyroxene. Similar sieved and unsieved phenocrysts of andesine and oligoclase in alkaline and tholeiitic lavas from a number of localities (Vitaliano and Harvey, 1965; Wright, 1968a; Binns *et al.*, 1970; Aoki, 1970; Frisch and Wright, 1971; Hoffer and Hoffer, 1973; Duggan and Wilkinson, 1973; Laughlin *et al.*, 1974; Knutson and Green, 1975) have been termed megacrysts, and are often interpreted as high-pressure cognate precipitates.

Compositions of groundmass plagioclases in the hawaiites and trachyandesites are usually comparable to coexisting phenocryst rim compositions indicating that they were in equilibrium with the host liquid at the time of eruption. Groundmass alkali feldspars in the hawaiites and trachyandesites range in composition from anorthoclase ($Or_{20}Ab_{65}An_{15}$) to sanidine ($Or_{45}Ab_{51}An_4$).

Plagioclase phenocrysts in the tristanites exhibit normal zoning in the range An_{51-44}, whereas groundmass plagioclase laths are relatively sodic (An_{32-20}) and coexist with either sanidine ($Or_{45}Ab_{55}An_1$) or lime anorthoclase ($Or_{21}Ab_{68}An_{11}$ to $Or_{25}Ab_{65}An_{10}$).

Several of the mafic trachytes are notable for the presence of reverse-zoned calcic plagioclase phenocrysts (An_{50-57}) which in turn are rimmed with anorthoclase ($Or_{35}Ab_{60}An_5$). These crystals are probably xenocrystal because plagioclase core compositions in these rocks are more commonly in the range An_{25-30}. Coexisting alkali feldspar phenocrysts in these lavas are characterized by zoning from calcic anorthoclase ($Or_{27}Ab_{63}An_{10}$) to rims of more Ca-poor anorthoclase ($Or_{35}Ab_{60}An_5$) or sanidine ($Or_{41}Ab_{58}An_1$). Depletion in Ca from core to rim in the anorthoclase phenocrysts and the low Ca contents of groundmass anorthoclases reflect the relatively low levels of Ca in these rocks and preferential partitioning of Ca into coexisting ferrohedenbergite microphenocrysts.

The anorthoclase and sanidine occurring as phenocryst and groundmass constituents of the peralkaline trachytes, alkali rhyolites and comendites (Figs 4.9e,f) exhibit quite a restricted range of compositions (Or_{26-49}) with a concentration of analyses between Or_{34} and Or_{42}. These compositions correspond with the feldspar composition range of the minimum in the alkali feldspar solid solution series (Tuttle and Bowen, 1958).

There appear to be systematic differences between the Or contents of alkali feldspar phenocryst and groundmass phases in the mafic trachytes and the peralkaline rocks. Zoning of phenocrysts in the former group is from Ab-rich to more Or-rich rims, a trend extended by the groundmass feldspar compositions. The peralkaline rock types generally exhibit the reverse trend with Or-rich phenocryst cores and more Ab-rich rim and groundmass compositions. This is depicted in histograms (Fig. 4.10a,b) of Or contents for groundmass and phenocryst core compositions in both groups of rocks. These data contrast with those of Nicholls and Carmichael (1969) on peralkaline lavas from Pantelleria and New Zealand, for which the compositional zoning of the feldspars is in the opposite sense (i.e. from Ab-rich cores to Or-rich rims). However, the data on the Nandewar feldspars are consistent with the general conclusions of Bailey and Schairer (1964) and Bailey (1974); namely feldspars which separate from peralkaline liquids (and phenocrysts in natural liquids) in general are more potassic than their conjugate liquids. Bailey and Schairer (1964) termed this the 'orthoclase effect' because the separation of such feldspars fractionates K_2O and Al_2O_3 from peralkaline liquids.

Almost without exception, phenocrysts and groundmass alkali feldspars in trachytic and rhyolitic rocks exhibit a stoichiometric excess of Al_2O_3, usually with a complementary depletion in SiO_2. Fractionation of feldspars in which the molecular proportions $Al_2O_3/(Na_2O+K_2O+CaO)>1$, from a liquid with an agpaitic index (mol. prop. $(Na_2O+K_2O)/Al_2O_3$) slightly less than unity can potentially produce a peralkaline residual liquid. This has important implications in evaluation of possible fractionation trends in the volcanic series and will be further discussed in Chapter 7.

The Fe content of the alkali feldspars, although variable, is in general probably a little lower than in the plagioclase. Fe exhibits no correlation with Ca, Na, K or Al in the plagioclases but exhibits a weak correlation with Al in the alkali feldspars from trachytes and rhyolites. This is in accord with the generally accepted substitution of Fe^{3+} for Al in alkali feldspars (Deer *et al.*, 1963; Smith, 1975). The lack of correlation between Fe and Al for the plagioclases probably reflects the presence of some Fe as Fe^{2+} (Smith, 1975).

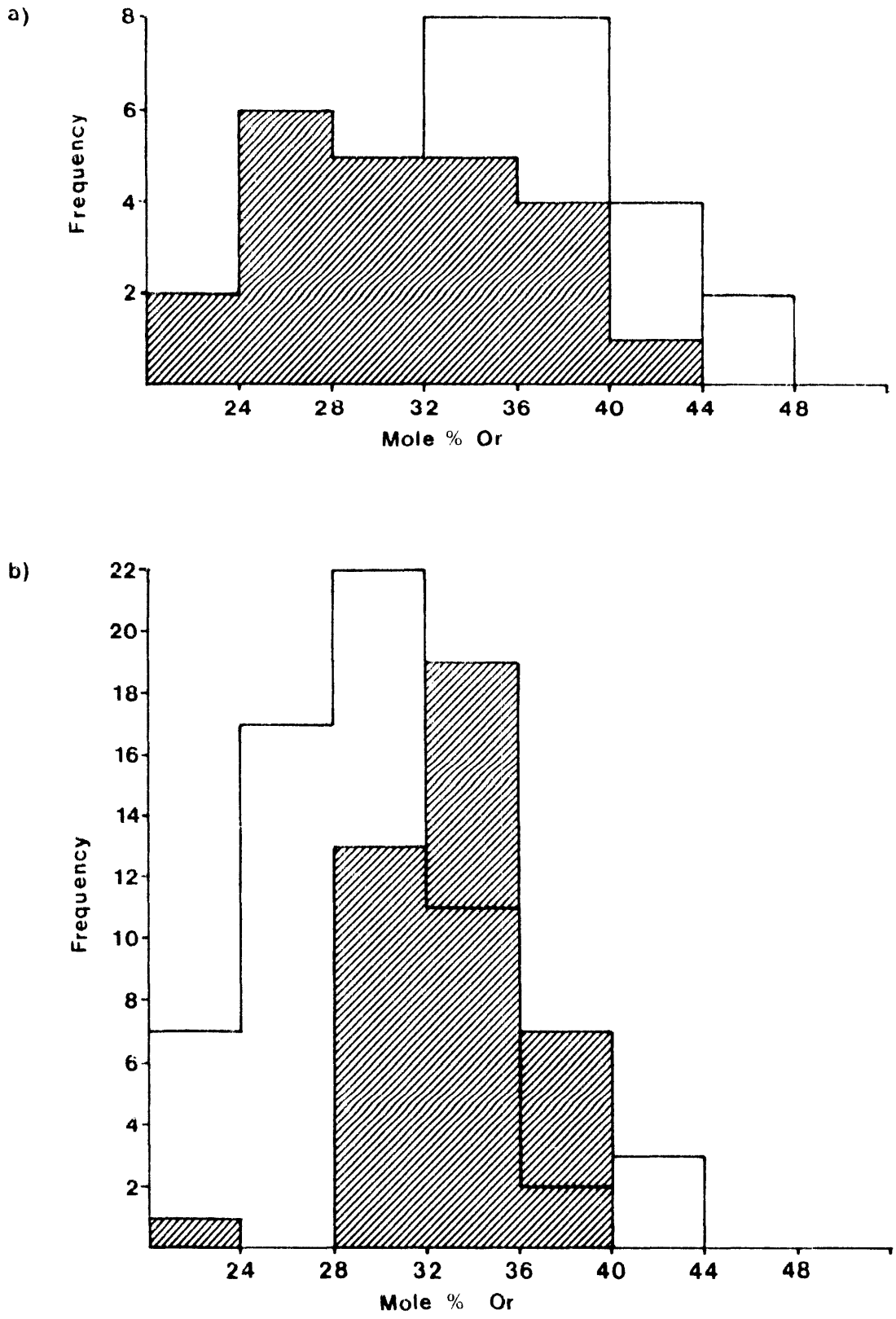

Fig. 4.10: Frequency histograms of Or content (mole percent) in phenocryst cores (shaded) and groundmass alkali feldspars from a) mafic trachytes and b) peralkaline trachytes and comendites.

Fe also exhibits a strong tendency towards concentration in the groundmass phases and phenocryst rims relative to the cores of phenocrysts for plagioclases and alkali feldspars from all rock types. This is shown in histograms (Fig. 4.11a,b) showing Fe content of plagioclase and alkali feldspar phenocryst cores and groundmass phases respectively, from all rock types. Duggan (1974) noted a similar trend in feldspars from eruptives of the Tweed Volcano in north-eastern N.S.W. and suggested that it may be the result of concentration gradients around feldspar crystals during precipitation when the host liquid adjacent to the feldspar crystal is enriched in Fe compared to the bulk liquid. Brown and Carmichael (1971) suggested that a decrease in Fe content with decreasing An content of plagioclase in lavas from the Lake Rudolf Region, East African rift valley, may be due to decreasing temperature and differing volatile pressures during crystallization. The alternative suggestion by Brown and Carmichael (1971), that the iron content is governed by rate of crystallization gains support from Mossbauer studies of Hafner *et al.* (1971), who showed that Fe probably does not occupy regular structural sites in plagioclase but exists at irregular site vacancies and lattice defects. Disorder in feldspars increases with higher temperatures (Stewart, 1975), and more rapid rates of cooling and crystallization (Martin, 1974). Disordering would probably be more pronounced in rapidly crystallized groundmass feldspars and phenocryst rims where cooling has been too rapid to permit structural readjustments. Accordingly, there is a greater potential for Fe substitution into relatively more disordered groundmass feldspars.

Ba is an important minor component in the alkali feldspar phenocrysts of several mafic trachytes, reaching a maximum of approximately 1.8 wt. percent BaO in the core areas. There is a strong depletion of Ba in these phenocrysts from core to rim indicating the strong partitioning of this element into the earliest crystallizing phase and its quite rapid depletion in the melt. The K_2O content of the relatively Ba-rich phenocrysts is considerably lower than in low-Ba types indicating substitution of Ba for K in the lattice.

Conditions of Crystallization

The rare association of plagioclase phenocrysts in aggregates

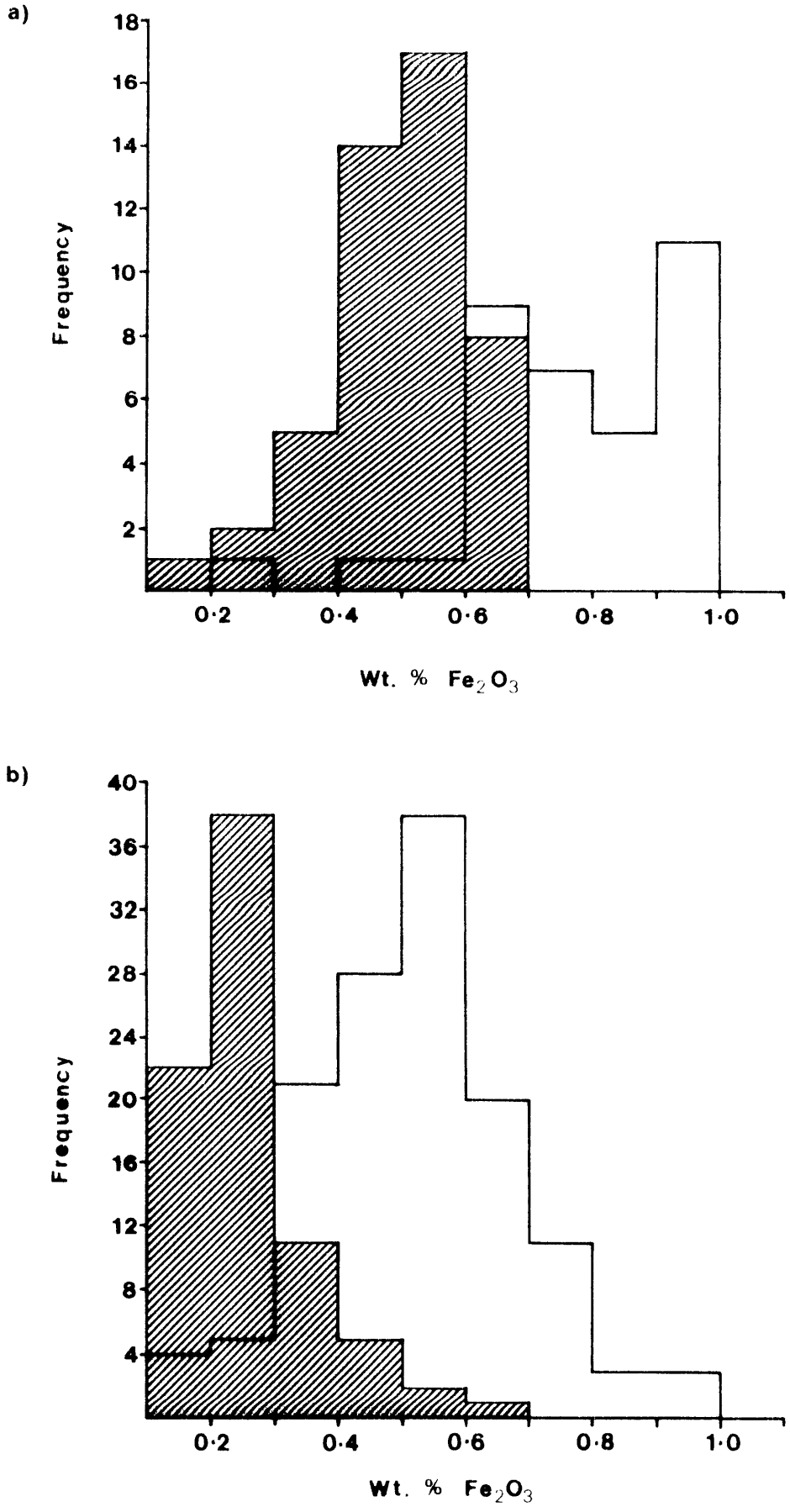

Fig. 4.11: Frequency histograms of Fe_2O_3 content (wt. percent) in phenocryst cores (shaded) and groundmass a) plagioclases and b) alkali feldspars.

and occasional inclusions with aluminous clinopyroxenes of inferred high-pressure origin indicates that some of these feldspars are also high-pressure phases. Discrete reverse-zoned, sieved and unsieved plagioclase phenocrysts coexisting with aluminous clinopyroxene and orthopyroxene megacrysts are also interpreted as megacrysts although their precipitation at elevated pressures is more equivocal.

Plagioclase megacrysts have been recognized at a number of localities in both alkaline and tholeiitic hosts. Oligoclase and andesine megacrysts have been described from alkali basalts in Nigeria (Wright, 1968a,b, 1972; Frisch and Wright, 1971), Japan (Aoki, 1970), Nevada (Vitaliano and Harvey, 1965), New Mexico (Hoffer and Hoffer, 1973), and California (Laughlin *et al.*, 1974). Duggan and Wilkinson (1974) interpreted abundant, large, relatively sodic plagioclase crystals in a tholeiitic andesite from the Tweed Shield Volcano, north-eastern New South Wales, as high-pressure cognate phases.

The relatively sodic nature of the plagioclase megacrysts with respect to low pressure rims and associated more calcic phenocrysts is best explained by rapid transfer of the megacrysts from a high pressure to a lower pressure regime. Experimental studies on melts of basaltic and andesitic compositions (Cohen *et al.*, 1967; Green, 1969; Thompson, 1972a) indicate that under moderately dry conditions, liquidus or near-liquidus plagioclases exhibit systematic increases in Ab content with increasing pressure.

Further support for a high-pressure origin of the plagioclase megacrysts in the Nandewar hawaiites and trachyandesites is provided by experimental data of Knutson and Green (1975) on a hawaiite of similar composition from the Comboyne Volcanic Province, N.S.W. They demonstrated that plagioclase was a liquidus or near-liquidus phase under dry conditions at pressures of 5 to 10 kb, although its appearance was depressed by about 100°C in the 5 kb experiments with the addition of 2 wt. percent H_2O. The suppression of plagioclase crystallization with increased P_{H_2O} is widely supported by experimental data on natural igneous compositions (Green and Ringwood, 1967; Green and Hibberson, 1970; Nesbitt and Hamilton, 1970; Thompson, 1972a).

An alternative interpretation of the origin of the plagioclase

megacrysts is that they are xenocrystal and acquired by their host following mixing of magmas of differing composition. Limited evidence for magma mixing has been suggested for a hawaiite in which very magnesian olivines appear to be xenocrystal. However, the reverse-zoned plagioclase megacrysts occurring in hosts varying in their normative An contents tend to be more sodic in the lower normative An rocks and relatively more calcic in the rocks with higher normative An. This relationship does not support an accidental origin of the plagioclase megacrysts through random magma mixing.

Plagioclase Geothermometry

The plagioclase geothermometer (Kudo and Weill, 1970; Mathez, 1973) has been applied to the Nandewar basic and intermediate rocks to obtain estimates of crystallization temperatures for plagioclase phenocrysts and groundmass feldspar 'quench temperatures'. Calculations based on phenocryst, core and whole-rock compositions should provide estimates of the temperatures at which plagioclase first appeared. These temperatures should approach the liquidus temperatures of many of the trachyandesites and tristanites where plagioclase is the dominant phenocryst phase. The whole-rock composition approximates the groundmass (liquid) composition in equilibrium with the feldspar phenocrysts where these comprise less than 5 to 10 percent of the mode. This condition is met by all the analyzed samples.

Temperatures (Table 4.11) were calculated using the equations of both Kudo and Weill (1970) and Mathez (1973). The Kudo-Weill values were preferred because they were slightly lower for most pressures and generally more consistent with temperature estimates based on other techniques.

Phenocryst core temperatures appear to be consistent with the crystallization of plagioclase close to the liquidi of the various lavas for P_{H_2O} = 0.5 kb. If groundmass Fe-Ti oxide temperatures (Buddington and Lindsley, 1964) are taken as quench temperatures, approaching the solidus, the indicated crystallization intervals of lavas for which these data are available is of the order of 100-250°C. This interval is comparable to crystallization intervals suggested by Yoder and Tilley (1962) for most basaltic lavas (150-200°C) and similarly derived estimates

TABLE 4.11

Crystallization temperatures (°C) of plagioclase calculated using the Kudo-Weill geothermometer

Rock Number	Plagioclase Phenocryst Core/Rock 1 bar	0.5 kb	1.0 kb	Groundmass Plagioclase/Rock 1 bar
49000	1210	1185	1130	1225
49001	1170	1140	1085	1130
49002	1210	1180	1125	1195
49003	1115	1095	1035	1215
49004	1250	1220	1165	1230
49005	-	-	-	1145
49007	1200	1175	1115	-
49008	1130	1110	1050	1170
49009	1145	1125	1065	1130
49011	1180	1160	1095	1130
49013	-	-	-	1090
49070	1130	1120	1045	-
49075	1150	1140	1065	-
49076	1150	1135	1060	1035
49077	1155	1140	1065	1130
49078	1150	1140	1060	-
49079	1185	1165	1095	-
49081	1095	1090	1005	-
49083	1060	1060	970	1060
49084	1070	1070	980	-

of Brown and Carmichael (1971) for alkaline lavas from Kenya (250-300°C).

Temperatures estimated from groundmass plagioclase and whole-rock compositions for 'dry' conditions generally appear to be 60-225°C higher than quench temperatures estimated using the Buddington and Lindsley (1964) geothermometer. This probably indicates that the experimental data on 'dry' systems (Kudo and Weill, 1970) are not directly applicable to the volcanics under discussion.

Uncertainties inherent in the plagioclase geothermometer include: 1. The dependence of plagioclase compositions, and hence temperature estimates, on the P_{H_2O} of the liquid at the time of crystallization; and 2. the effect of higher total load pressure during crystallization prior to extrusion. P_{H_2O} was probably quite low in most of the Nandewar rocks which have plagioclase as a common phenocryst phase, because as mentioned in the preceding section, the appearance of plagioclase is considerably delayed when appreciable water is dissolved in the melt. The effects of significantly higher load pressures are unknown, although a small increase in load pressure probably has a negligible effect (Kudo and Weill, 1970). This factor can be minimized by using only compositions of unsieved, normally zoned phenocrysts which are assumed to have crystallized at relatively low load pressures.

A summary of the geothermometric data for the Nandewar suite is provided in a plot (Fig. 4.12) of calculated plagioclase, pyroxene and Fe-Ti oxide temperatures versus differentiation index (D.I.) of the host (Thornton and Tuttle, 1960). The expected general decrease in crystallization temperatures of plagioclase and pyroxene from hawaiite to trachyte compositions is a result of the decreasing Mg and normative An contents of the host liquids. The trend is in accord with trends in liquidus temperatures for similar rock types (Thompson, 1972a).

Although the temperature data are not sufficiently precise to be unequivocal, in general they are consistent with petrographic data which suggest that clinopyroxene was the earliest crystallizing phase in the trachyandesite and this was closely followed by olivine and plagioclase. Several of the hawaiites differ in the apparently earlier crystallization of olivine and clinopyroxene with a significant delay in the appearance of plagioclase. Petrographic evidence from a nearly completely glassy trachyandesite which is transitional to tristanite,

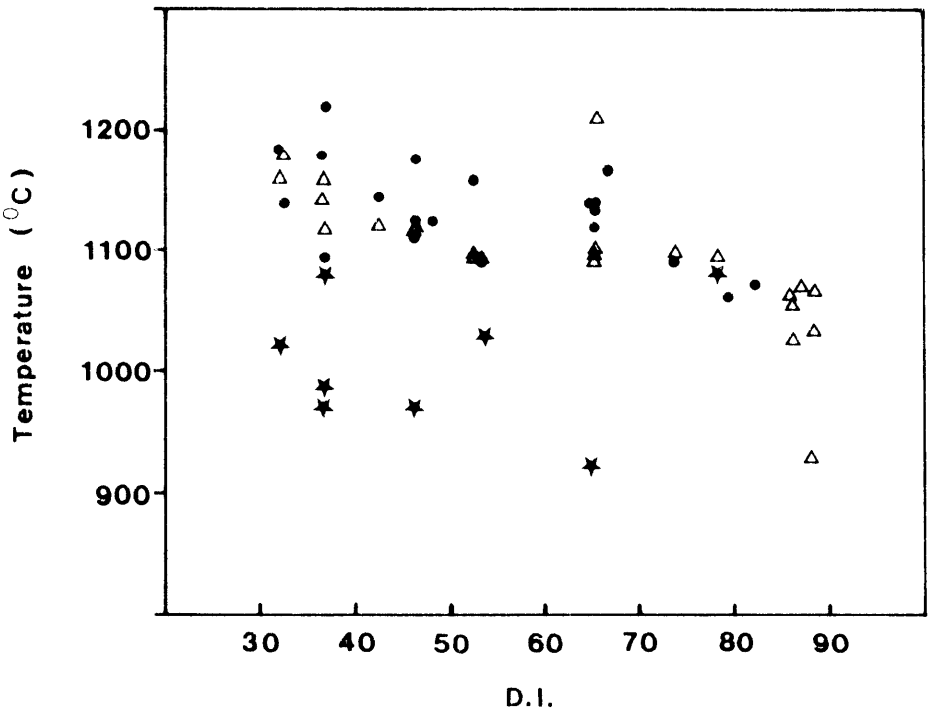

Fig. 4.12: A compilation of all geothermometric data in a plot of temperature (°C) versus differentiation index (D.I.) of the host rock. The various temperatures were estimated using plagioclase (circles), pyroxene (triangles) and Fe-Ti oxide (stars) compositional data, as discussed in the text.

indicates that plagioclase and titanomagnetite were the earliest phases to crystallize from that particular melt.

AENIGMATITE

Occurrence

Aenigmatite occurs solely as a groundmass phase and is restricted to the peralkaline trachytes and comendites. It occurs interstitial to laths of sanidine or anorthoclase in association with arfvedsonite, aegirine-hedenbergite and quartz. Microphenocrysts of titanomagnetite or ilmenite in these rocks commonly exhibit a narrow rim of aenigmatite.

Compositional Variation

Typical analyses of the aenigmatites are presented in Table 4.12 together with structural formulae calculated on the basis of 20 oxygens. Ferric iron was calculated assuming stoichiometry on the basis of 20 anions and 14 cations.

The Nandewar aenigmatites exhibit a very restricted range in composition, and TiO_2 displays the most marked variation (7.33 - 8.57 wt. percent TiO_2). Variation in Ti does not appear to be correlated with changes in Fe_2O_3 as was noted by Hodges and Barker (1973), although this conclusion is tentative because of the large uncertainty of the calculated Fe_2O_3 values (Finger, 1972; Larsen, 1977). The small deficiency of Al necessary to fill the tetrahedral sites may also reflect uncertainties in the calculation procedure. It is possible that some Fe^{3+} is in tetrahedral coordination (Deer *et al.*, 1978).

Aenigmatites from most magmatic associations generally exhibit a restricted range in composition (Nicholls and Carmichael, 1969; Nash *et al.*, 1969; Yagi and Souther, 1974; Borley, 1976). However, significant compositional variations have been noted in aenigmatites from nepheline syenites of the Trans Pecos province, Texas (Hodges and Barker, 1973), and the Ilimaussaq intrusion, south Greenland (Larsen, 1976,1977). The aenigmatites described by Hodges and Barker (1973) were considered to be largely the result of solid solution between 'ideal aenigmatite' ($Na_2Fe_5^{2+}TiSi_6O_{20}$) (Kelsey and McKie, 1964; Cannillo *et al.*, 1971) and Ti-free aenigmatite ($Na_2Fe_4^{2+}Fe_2^{3+}Si_6O_{20}$) of the form synthesized

TABLE 4.12

Analyses of Aenigmatites

	Peralkaline Trachytes							Comendite
Rock No.	49098 G	49099 G	49100 MPR	49102 G	49103 G	49103 G	49107 G	49161 G
SiO_2	40.20	41.87	41.06	40.79	39.39	40.56	40.92	40.71
TiO_2	7.40	7.42	8.18	7.50	8.57	7.33	7.52	7.68
Al_2O_3	0.72	0.91	0.86	0.61	1.11	1.12	0.57	0.93
FeO*	41.64	39.49	39.71	41.86	41.29	42.00	42.79	40.99
MnO	1.20	1.09	1.03	0.88	0.81	0.93	0.71	1.29
MgO	0.17	0.18	0.16	-	0.26	0.12	0.11	-
CaO	0.21	0.28	0.22	0.33	0.65	0.44	0.31	0.34
Na_2O	7.38	7.82	7.92	7.52	7.34	7.53	7.25	7.14
K_2O	0.10	0.15	-	-	0.12	0.18	-	0.28
Total	99.02	99.21	99.14	99.49	99.54	100.21	100.18	99.36
Fe_2O_3[1]	7.19	4.88	5.29	6.35	6.86	7.86	5.75	4.89
FeO[1]	35.17	35.10	34.95	36.14	35.11	34.93	37.61	36.59
Total[2]	99.74	99.70	99.67	100.12	100.22	101.00	100.75	99.85
Structural Formulae on the Basis of 20 Oxygen Atoms								
Si	5.782	5.958	5.859	5.838	5.639	5.751	5.836	5.845
Al^{iv}	0.122	0.042	0.141	0.103	0.187	0.187	0.096	0.155
Al^{vi}	-	0.111	0.004	-	-	-	-	0.003
Ti	0.800	0.794	0.878	0.807	0.923	0.782	0.807	0.829
Fe^{3+}	0.779	0.523	0.569	0.685	0.740	0.839	0.618	0.528
Fe^{2+}	4.231	4.178	4.171	4.327	4.204	4.142	4.487	4.395
Mn	0.146	0.131	0.125	0.107	0.098	0.112	0.086	0.157
Mg	0.037	0.038	0.034	-	0.056	0.025	0.023	-
Ca	0.032	0.043	0.034	0.051	0.100	0.067	0.047	0.052
Na	2.058	2.158	2.191	2.087	2.037	2.070	2.005	1.988
K	0.018	0.027	-	-	0.022	0.033	-	0.051

* - Total Fe as FeO

[1] - Calculated on the basis of 20 anions and 14 cations

[2] - Recalculated using calculated Fe_2O_3 and FeO values

MPR - Microphenocryst rim

G - Groundmass

by Ernst (1962). Coupled substitutions of the type $Fe^{2+}Si \rightleftarrows AlFe^{3+}$ and $Fe^{2+}Ti \rightleftarrows 2Fe^{3+}$ were suggested by Hodges and Barker (1973) to account for Fe^{3+} present in excess of that required to replace Ti^{4+}. Larsen (1976) suggested an additional substitution $CaAl_{(core)} \rightleftarrows NaSi_{(rim)}$ to account for zoning in Ilimaussaq aenigmatites. Marginally higher Al_2O_3 and Fe_2O_3 contents of the aenigmatites from one Nandewar peralkaline trachyte (Table 4.12, No. 49103) are coupled with slightly lower SiO_2 and FeO suggesting limited substitution of the form $Fe^{2+}Si \rightleftarrows AlFe^{3+}$.

Ca and Mg are both low in the Nandewar aenigmatites and this probably reflects the very low levels of these elements in the host peralkaline melts. Mn was preferentially partitioned into aenigmatite relative to the liquid reflecting its generally strong coherence with Fe^{2+}.

Discussion

Investigation of Ti-free aenigmatite (Ernst, 1962) indicated it is stable at very low oxygen fugacities appropriate to the iron-wüstite (IW) and magnetite-wüstite (MW) buffers. Subsequent experimental data on 'ideal' aenigmatite (Lindsley, 1971) indicated that it is stable in the range 400-900°C and at low to moderate oxygen fugacities. At 750°C and 500 bars the stability curve for aenigmatite lies between the nickel-nickel oxide (NNO) and FMQ buffer curves.

A relatively high Ti melt content was suggested by Abbott (1967) and Borley (1976) as an important factor controlling the stability of aenigmatite. Although the influence of Ti on the composition of aenigmatite is clear from the data of Hodges and Barker (1973), low Ti concentrations in the melt evidently do not inhibit its crystallization. Instead, temperature, oxygen fugacity and $Na_2Si_2O_5$ content of the melt appear to be the most important variables controlling aenigmatite stability. Aenigmatite overgrowths on titanomagnetite microphenocrysts, also noted by Abbott (1967), Marsh (1975) and Larsen (1977), suggest a reaction of the type proposed by Marsh (1975):

$$\underset{\text{titanomagnetite}}{2Fe_2TiO_4} + 2Fe_3O_4 + \underset{\text{liquid}}{2Na_2Si_2O_5 + 8SiO_2} \rightleftarrows \underset{\text{aenigmatite}}{2Na_2Fe_5^{2+}TiSi_6O_{20}} + \underset{\text{gas}}{O_2} \qquad (1)$$

Aenigmatite rimming ilmenite also suggests a reaction relationship

between ilmenite microphenocrysts and residual peralkaline liquid, according to the reaction:

$$\underset{\text{ilmenite}}{FeTiO_3} + \underset{\text{liquid}}{Na_2Si_2O_5 + SiO_2} + 2Fe_2O_3 \rightleftarrows \underset{\text{aenigmatite}}{Na_2Fe_5TiSi_6O_{20}} + \underset{\text{gas}}{O_2} \qquad (2)$$

Additional evidence in favour of the reaction is provided by the selective replacement by aenigmatite of ilmenite lamellae in titanomagnetites from pegmatoids in the Picture Gorge Basalt, Washington (Lindsley *et al.*, 1971).

Nicholls and Carmichael (1969) proposed reaction (3) to account for an antipathetic relationship in the relative abundances of ilmenite and aenigmatite in many peralkaline rocks. Reaction (4) has been demonstrated experimentally (Nolan, 1966; Bailey, 1969) but petrographic evidence, which should include aegirine rimming Fe-oxides, is seldom found (Bailey, 1969; Marsh, 1975). This presumably reflects the fact that the common β-phase in alkaline volcanic rocks contains ulvöspinel in solid solution.

$$\underset{\text{aenigmatite}}{Na_2Fe_5TiSi_6O_{20}} + \underset{\text{liquid}}{Na_2Si_2O_5} + \underset{\text{gas}}{O_2} \rightleftarrows \underset{\text{acmite}}{4NaFeSi_2O_6} + \underset{\alpha\text{-phase}}{FeTiO_3} \qquad (3)$$

$$\underset{\beta\text{-phase}}{4Fe_3O_4} + \underset{\text{liquid}}{6Na_2Si_2O_5 + 12SiO_2} + \underset{\text{gas}}{O_2} \rightleftarrows \underset{\text{acmite}}{12NaFeSi_2O_6} \qquad (4)$$

Nicholls and Carmichael (1969) applied reactions (3) and (4) to calculate the position of a no-oxide field in T-fO_2 space for silicic volcanics in which acmite coexists with aenigmatite and Fe-Ti oxides are absent. Support for the existence of a no-oxide field is provided in the present study by the petrographic evidence of aenigmatite rimming titanomagnetite and ilmenite microphenocrysts of some peralkaline trachytes. However, the exact position and extent of the no-oxide field in T-fO_2 space is subject to considerable uncertainty because of effects of solid solutions, and possible errors in the free-energy estimates of aenigmatite and magnetite (Nicholls and Carmichael, 1969).

APATITE

Occurrence

Stumpy prismatic (albeit slightly rounded) apatite microphenocrysts

up to 3 mm are quite common in the tristanites and the most evolved trachyandesite (49018). They are generally absent from the mafic trachyandesites and hawaiites where the highly acicular apatite is confined to the groundmass. Apatite microphenocrysts also occur in several of the more mafic trachytes which are transitional to tristanites, but are absent from the alkaline and peralkaline trachytes and comendites.

The apatites occur as discrete phases and in cumulates composed of olivine, clinopyroxene, plagioclase and titanomagnetite in various proportions. The tendency of apatite microphenocrysts (D = 3.1 - 3.35) to segregate with titanomagnetite (D = 4.5 - 5) and ferromagnesian silicates may have facilitated their removal from the host liquids because of the greater aggregate solid/liquid density contrast. However other factors, such as viscosity and convection, are also likely to be important.

Abundant, oriented, fine needle-like inclusions of an indeterminate brown material in the apatite microphenocrysts impart a pigmented or striated appearance.

Compositional Variation

The composition of apatite microphenocrysts (Table 4.13) from a variety of hosts exhibits a restricted range in CaO and P_2O_5 with relatively constant contents of the minor constituents FeO, Na_2O and Cl. MgO is slightly lower in apatites from the trachytes compared to those from more mafic hosts which indicates a similar trend to that noted by Nash (1972) for the various differentiates of the Shonkin Sag intrusion in Montana. Analyses of apatite 'megacrysts' from Victorian lavas (Irving, 1974a) showed that they contain appreciable F and are therefore classified as fluor-hydroxy apatites. The Nandewar apatites may also contain moderate quantities of F and H_2O as indicated by the consistently low analysis totals (Table 4.13).

Conditions of Crystallization

The occurrence of apatite as relatively large euhedral crystals indicates they were early precipitates from their host liquids. Subsequent magmatic corrosion resulting in slight rounding of the euhedral forms suggests that they were rapidly transported to P/T regimes different

TABLE 4.13

Analyses of Apatites

	Trachyandesites			Tristanites	
Rock Number	49009	49011	49056	49074	49075
FeO*	0.28	0.41	0.30	0.18	0.54
MgO	0.59	0.64	0.60	0.72	0.57
CaO	55.13	55.75	54.65	54.79	54.77
Na_2O	0.56	0.53	0.53	0.95	0.61
P_2O_5	41.75	41.91	41.59	41.62	41.41
Cl	0.21	0.29	0.26	0.22	0.25
Total	98.52	99.53	97.93	98.48	98.15

	Tristanites		Trachytes		
Rock Number	49076	49078	49081	49083	49084
FeO*	0.39	0.58	-	0.33	0.32
MgO	0.72	-	0.55	0.45	0.49
CaO	54.54	54.66	55.60	55.39	56.15
Na_2O	0.64	-	0.64	0.41	0.55
P_2O_5	41.20	42.90	41.67	41.87	41.90
Cl	0.30	0.24	0.07	0.12	0.20
Total	97.79	98.38	98.53	98.57	99.61

* Total Fe as FeO

from those under which they initially precipitated. The presence of apatite microphenocrysts (e.g. Table 4.13, No. 49009) occasionally included in tschermakitic clinopyroxenes of inferred high-pressure origin suggests that some probably crystallized at elevated pressures and perhaps are better termed megacrysts. Experimental duplication of megacryst assemblages (which include apatite) in a hawaiite from the Comboyne volcanic province in New South Wales at 1040°C, 6.5 kbar pressure and with 2 percent H_2O (Knutson and Green, 1975), supports this interpretation.

Apatite is apparently a rather rare megacryst species and has been recognized as discrete crystals and inclusions in other megacrysts at only a few alkali volcanic localities (Wilkinson, 1962; White, 1966; Wise, 1966; Dickey, 1968; Aoki, 1970; Wright, 1970; Irving, 1974a; Wass, 1979) in addition to the Comboyne province.

Although occasional apatites in the more evolved trachyandesites may have crystallized at elevated pressures, the absence of tschermakitic pyroxenes from the tristanites and mafic trachytes suggests that the apatite microphenocrysts in these rocks are probably low-pressure phases.

BIOTITE

Biotite is absent from the volcanic rocks of the Nandewar suite. It is, however, a constituent of a small high-level monzonitic intrusive comparable in composition to several tristanites in the overlying volcanic pile. The biotite occurs as subhedral to anhedral crystals 2-3 mm in diameter in the monzonite and in felsic schlieren developed within it.

Analyses of biotites (probably Mg-biotites in the notation of Foster (1960)) from the host monzonite and schlieren are presented in Table 4.14 together with structural formulae calculated on the basis of 22 oxygens anhydrous. Assuming all Fe is FeO, the calculated formulae indicate insufficient Si and Al to provide the theoretical 8 atoms allocated to the tetrahedral sites. This is in part at least due to calculation of the structural formulae on a Fe^{3+}-free basis which diminishes the amount of Si and Al somewhat. Since some Fe is undoubtedly present as Fe^{3+} the deficiency may only be apparent.

TABLE 4.14

Analyses of Biotites

	Monzonite	Monzonite Schlieren
Rock Number	49070	49070
SiO_2	37.43	37.51
TiO_2	6.16	5.88
Al_2O_3	13.17	13.22
FeO*	19.06	20.40
MgO	12.26	11.50
Na_2O	0.63	0.66
K_2O	9.03	9.33
Total	97.74	98.50
Structural Formulae on the Basis of 22 Oxygen Atoms		
Si	5.564	5.575
Al^{iv}	2.308	2.316
Al^{vi}	-	-
Ti	0.689	0.657
Fe^{2+}	2.369	2.535
Mg	2.716	2.547
Na	0.182	0.190
K	1.712	1.769
Z	7.872	7.891
Y	5.774	5.740
X	1.894	1.959
$100Mg/Mg+Fe^{2+}$	53.4	50.1

* Total Fe as FeO

However, Nockolds (1947) showed that biotites from alkaline rocks often are deficient in Al compared with those from calc-alkaline hosts. This feature is more apparent in biotites from peralkaline types and presumably reflects the decreasing availability of Al in the melt.

Compositional differences between the biotites from the host and schlieren are relatively small (Table 4.14) but a relative decrease in the *mg*-value of the schlieren biotite is consistent with this phase crystallizing from a fractionated residuum.

Crystallization of biotite from the monzonitic magma and its absence in associated volcanic rocks of similar composition indicates that conditions favouring biotite precipitation prevailed during crystallization of the pluton. Experimental work on the stability of biotite (Eugster and Wones, 1962; Wones and Eugster, 1965) showed that increasing P_{H_2O} at constant T and fO_2, favours the formation of annite according to the reaction:

$$\text{sanidine} + \text{magnetite} \rightleftarrows \text{annite}.$$

Enhanced P_{H_2O} conditions during crystallization of the monzonite are also indicated by the common development of amphibole rims on early formed clinopyroxenes.